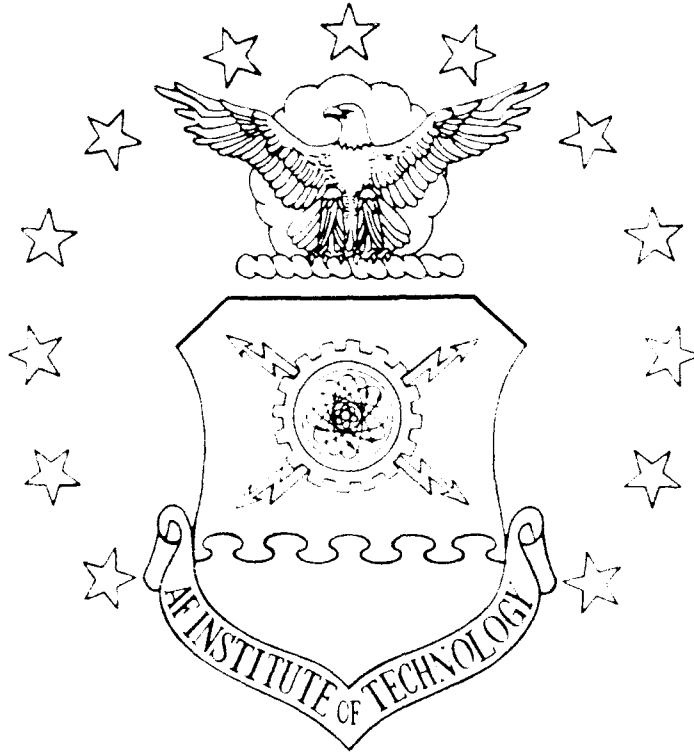


AD-A231 027

1



Fracture Toughness of Unidirectional
 Fiber Reinforced Ceramic Composites in
 Mode II Utilizing Laser Interferometry

THESIS

Joseph W. Truskowski
 Captain, USAF

AFIT/GAE/ENY/90D-31

DTIC
 ELECTE
 JAN 08 1991
 S E D

DEPARTMENT OF THE AIR FORCE
 AIR UNIVERSITY

AIR FORCE INSTITUTE OF TECHNOLOGY

Wright-Patterson Air Force Base, Ohio

DISTRIBUTION STATEMENT A
 Approved for public release
 Distribution Unlimited

91 1 3 082

1

AFIT/GAR/ENY/90D-31

Fracture Toughness of Unidirectional
Fiber Reinforced Ceramic Composites in
Mode II Utilizing Laser Interferometry

THESIS

Joseph W. Truskowski
Captain, USAF

AFIT/GAE/ENY/90D-31

Approved for public release; distribution unlimited

AFIT/GAE/ENY/90D-31

Fracture Toughness of Unidirectional
Fiber Reinforced Ceramic Composites in Mode II
Utilizing Laser Interferometry

THESIS

Presented to the Faculty of the School of Engineering
of the Air Force Institute of Technology
Air University
In Partial Fulfillment of the
Requirements for the Degree of
Master of Science in Aeronautical Engineering

Joseph W. Truskowski, B.S.
Captain, USAF

December 1990

| |
|---------------|
| Accession For |
| NTIS GRA&I |
| DTIC TAB |
| Unannounced |
| Justification |
| By |
| Distrib |
| Avail |
| Dist |

A-1

Approved for public release; distribution unlimited

Acknowledgments

Several individuals have been instrumental in the success of this undertaking. I would first like to thank my thesis advisor, Dr. S. Mall, whose guidance, patience, and technical knowledge made this project possible. His directions and technical insights were superb and kept the efforts clearly focused. I would also like to extend thanks to Dr. Ted Nicholas of the Wright Research and Development Center, whose sponsorship enabled me to use the facilities and technical support of the Metals and Ceramics Division. Mr. Larry Zawada, besides providing the ceramic composite plates, allowed me to observe the fabrication of the plates and supplied substantial information on the mechanical properties of the materials. Dr. Regi Johns provided me with the detailed information on the tabs required for the laser measurements and provided technical assistance on several occasions. I am extremely grateful to Mr. George Hartman who provided the software to run the laser interferometer displacement gauge and supplied a vast array of assistance throughout this undertaking. I also appreciate the fixtures and hardware constructed by Captain Michael Hobbler, who did Mode II testing the year before me. The support of the technicians in the laboratory was exceptional. The willingness to help, often beyond the responsibilities of their jobs, was the norm from Jay Anderson, Mark Derriso and

Andy Pitts. Without their support, this effort would have been limited in scope. To the men of the AFIT shop, I extend my appreciation and respect for the quality of support and expediency in which they delivered. From my rough sketches, they made what I needed and helped me maintain an aggressive schedule.

To my children, Joshua and Jessica, thanks for the understanding and continual love that pulled me through. To my friends, the fellowship and prayers were essential and helped me maintain my proper perspective on life throughout. Final thanks go to my wonderful wife Marsha. The late night cups of tea, the encouragement, the patience, and the emotional support were all needed and very much appreciated. Without her inspiration, this project would not have been possible.

Table of Contents

| | Page |
|--|------|
| Acknowledgments | ii |
| List of Figures | vi |
| List of Tables | ix |
| Abstract | x |
| I. Introduction | 1 |
| Problem | 1 |
| Objective | 2 |
| Approach | 2 |
| II. Background | 5 |
| III. Test Setup | 8 |
| Load Cell | 8 |
| Linear Variable Differential Transformer | 9 |
| Three Point Bend Fixture | 9 |
| Instron TTD Tension/Compression Tester | 10 |
| Laser Interferometer Displacement Gauge | 10 |
| Laser Mounting Fixture | 14 |
| System Integration | 16 |
| IV. Experimental Procedure | 20 |
| Specimen Preparation | 20 |
| Pre-cracking of Specimen | 22 |
| Reflective Tab Preparation | 25 |
| Tab Application to the Specimen | 31 |
| Indentation of Reflective Tabs | 33 |
| Specimen Alignment | 34 |
| Load Application | 37 |
| Post Test Analysis | 39 |
| V. Results and Discussions | 40 |
| Young's Modulus | 40 |
| LVDT Compliance Calculations | 47 |
| Critical Load | 51 |
| Fracture Toughness | 58 |
| LIDG Compliance Calculations | 63 |
| Post-Mortem Examination | 70 |

| | |
|---|----|
| VI. Conclusions and Recommendations | 73 |
| Conclusions | 73 |
| Recommendations | 74 |
| Appendix A: Laser Mounting Fixture | 76 |
| Appendix B: Specimen Dimensions | 86 |
| Appendix C: Polishing Fixtures | 91 |
| Appendix D: LVDT Calibration | 94 |
| Bibliography | 96 |
| Vita | 99 |

List of Figures

| Figure | Page |
|---|------|
| 1. Test Fixture Designed by Hoobler | 11 |
| 2. Modified Three-Point Bend Fixture | 12 |
| 3. Component Layout of the Photo Detector Section of the Laser Interferometer Displacement Gauge System | 13 |
| 4. Laser Fringe Generation | 15 |
| 5. Laser Mounting Fixture | 17 |
| 6. Test System Component Interaction | 19 |
| 7. Microstructure of Composite Specimens | 23 |
| 8. Pre-cracking Jig | 24 |
| 9. Specimen Dimensions | 26 |
| 10. Tab Not Sufficiently Polished for Micro- indentation Magnified 200 Times | 28 |
| 11. Tab Sufficiently Polished for Micro- indentation Magnified 200 Times | 29 |
| 12. Tabs Placed on Aluminum Block in Preparation for Polishing | 30 |
| 13. Teflon Tab Mounting Fixture | 32 |
| 14. Placement of Adhesive on Tabs | 33 |
| 15. Proper Placement and Orientation of a Set of Indents | 35 |
| 16. Load-Displacement Curves of Specimen 713 with No Crack Present | 42 |
| 17. Load-Displacement Curves for Specimen 714 with No Crack Present | 43 |
| 18. Load-Displacement Curves of Nicalon Test Sample Used to Determine Machine Test Setup Compliance . | 44 |
| 19. Comparison of Theoretical and Experimental Compliance for Plate 90C07 | 48 |

| | | |
|-----|--|----|
| 20. | Comparison of Russell's Beam Theory Model and Carlsson's Extension with Actual Test Data | 52 |
| 21. | Critical Load Determined from Only LVDT Load Displacement Curve on an X-Y Recorder | 54 |
| 22. | Typical Data from a Test Run | 55 |
| 23. | Second Example of Typical Test Run Data | 56 |
| 24. | Test Run Without Top Quality Indents | 57 |
| 25. | Critical Load of Test Specimens Verses Non-Dimensionalized Crack Length | 60 |
| 26. | Critical Load of Test Specimens Verses Non-Dimensionalized Crack Length on Log-Log Scales . . | 61 |
| 27. | Calculated Values of G_{IIc} Based on Russell's Beam Theory | 65 |
| 28. | Calculated Values of G_{IIc} Based on Carlsson's Extension of Russell's Beam Theory | 67 |
| 29. | Experimental Laser IDG Compliance Curve | 69 |
| 30. | Laser IDG Compliance Curve with Second and Third Order Curves | 71 |
| 31. | Transition from Mode I to Mode II Fracture on a Test Specimen | 72 |
| 32. | Laser Mounting Fixture | 77 |
| 33. | Steel Box Channel Base of Laser Mounting Fixture . | 78 |
| 34. | Steel Side Brackets for the Laser Mounting Fixture | 79 |
| 35. | Aluminum Subplate of Laser Mounting Fixture . . . | 80 |
| 36. | Bottom Standoff for Laser Mounting Fixture | 81 |
| 37. | Bottom Standoff Cap for Laser Mounting Fixture . . | 82 |
| 38. | Top Standoff Side Support for Laser Mounting Fixture | 83 |
| 39. | Top Standoff Cap for Laser Mounting Fixture . . . | 84 |
| 40. | Top Standoff Joiner Piece for Laser Mounting Fixture | 85 |

| | | |
|-----|--|----|
| 41. | Plate 90C07 Specimens | 87 |
| 42. | Plate 90C08 Specimens | 88 |
| 43. | Ceramic Specimen Polishing Fixture | 92 |
| 44. | Tab Edge Polishing Fixture | 93 |
| 45. | LVDT Calibration Curve | 95 |

List of Tables

| Table | Page |
|--|------|
| 1. Adjustment Capability of Laser Mounting Fixture . | 18 |
| 2. Computed Values of Young's Modulus | 46 |
| 3. Specimen LVDT Compliance Data | 49 |
| 4. Critical Load Data | 59 |
| 5. Calculated Values of Fracture Toughness Based on Russell's Beam Theory | 64 |
| 6. Calculated Values of Fracture Toughness Based on Carlsson's Extension of Russell's Beam Theory . . | 66 |
| 7. Laser IDG Specimen Compliance Data | 68 |
| 8. Plate 90C07 Specimen Dimensions | 89 |
| 9. Plate 90C08 Specimen Dimensions | 90 |

Abstract

The need to accurately determine the Mode II (forward shear) fracture toughness of a ceramic composite was identified. A laser based interferometric technique to measure crack opening displacement (COD) was developed and applied to end notched flexure specimens of a Corning Glass Works 1723 glass matrix with silicon-carbide fibers. A fixture was designed and built to attach a laser interferometer system to an Instron machine which provided latitude for alignment of the laser system. The laser interferometer displacement gauge (IDG) monitored the COD at the location of a support while the specimens were subjected to Mode II cracking at room temperature via three point bend tests on a standard Instron compression machine. Vertical displacement was measured at the center of the test specimen using a linear variable differential transformer (LVDT). Load verses displacement curves were generated for both the LVDT displacement and the COD. The COD curve showed a marked improvement in determining the onset of crack growth. Compliance data was also calculated from the slope of the LVDT load-displacement curve and plotted as a function of non-dimensional crack length. From the enhanced measurements of the critical load, the material's fracture toughness in Mode II, G_{IIc} , was calculated for varying crack lengths. The

calculations provided estimates with a variance of only 10% from the mean thus showing the consistency of this procedure. Although this technique was only demonstrated at room temperature, it can be modified to extend into the elevated temperature regime where a more accurate method of determining fracture toughness in Mode II is needed.

I. Introduction

Problem

Ceramic materials possess many of the qualities desirable for application in modern aircraft. The high strength, high stiffness at elevated temperatures, and low density qualities are particularly attractive features for application to aircraft engines and engine components. One major drawback is the lack of material toughness; however, adding fibers to the ceramic matrix yields a composite with increased toughness that still utilizes the high environmental resistance and high temperature strength characteristics. Fracture mechanics can accurately predict crack growth behavior and provide a thorough characterization of ceramic composite materials prior to their application in aircraft.

Test specimens are small due to their limited availability mandating extremely sensitive measuring techniques to accurately determine crack growth and critical loads. The American Society for Testing and Materials (ASTM) has established standard procedures for finding the fracture toughness of metals at room temperature (1:349) but has not standardized a procedure for ceramic composites. The use of an end-notched flexure specimen to determine Mode II fracture toughness is a proven method with polymer based composite materials.

Objective

The objective of this study was to integrate a precise measuring apparatus, a laser interferometer displacement gauge (IDG), with three-point bend test hardware to enhance the quality of Mode II experimental data. The measurements obtained would be used to identify the critical load for crack growth initiation of a CGW 1723 ceramic composite at room temperature. This study would test the feasibility of using indented tabs mounted on ceramic composites to directly produce crack opening displacement (COD) measurements with a specimen subjected to Mode II fracture. The laser IDG measurements would be compared with those from an LVDT taking displacement measurements at the center of the specimen to determine if a more accurate method to determine the critical load for crack growth initiation could be obtained.

Approach

The basic approach to this project was to modify an existing test setup with the incorporation of a laser IDG to obtain an accurate determination of initiation of crack growth. A mounting fixture for the laser IDG system was designed and constructed to mount on a standard Instron machine. A new steel frame for the three point bend fixture was made and the attachment of the LVDT changed to reduce measurement error.

The ceramic composite test specimens could not be adequately marked with the microhardened indenter because of the specimen brittleness and lack of reflectivity so stainless steel and titanium tabs were cut, polished, and finally mounted to the test specimen. These tabs were then indented with a microhardened indenter within 75 microns (0.003 inches) of the polished edge. The Mode II fracture of a unidirectional CGW 1723 ceramic composite was examined with the test apparatus at room temperature with a constant load rate applied.

Load verses displacement curves were generated for both the LVDT displacement and the COD. The curves showed good correlation to each other but the COD curve showed a marked improvement in determining the onset of crack growth. Compliance data was also calculated from the slope of the LVDT load-displacement curve and plotted as a function of non-dimensional crack length. From the enhanced measurements of the critical load, the material's fracture toughness in Mode II, G_{IIc} , was calculated for varying crack lengths. The calculations provided estimates of the material's fracture toughness with a variance of less than 10% from the mean thus showing the consistency of this procedure. Although this technique was only demonstrated at room temperature, it can be modified to extend into the elevated temperature regime where a more accurate method of determining fracture toughness in Mode II is needed.

The material used was a CGW 1723 uniaxial composite, an alumino-silicate glass matrix material reinforced with silicon carbide fibers. This composite material is being developed and tested by engineers at the Wright Research and Development Center (WRDC), Wright-Patterson AFB, OH. The procedures required for the preparation of the specimen and reflective tabs are addressed in this study.

The results of this study provide an accurate method to determine the critical loading of fiber reinforced composite materials under a shear loading which can be extended to elevated temperature. The technique of using reflective tabs mounted to a non-reflective material to allow the use of laser interferometry can also be expanded to a wide range of applications.

II. Background

In the early 1920's, Griffith (2,3) did extensive work with brittle glass to derive equations that predicted crack propagation based upon the concept of critical energy. He stated that "crack propagation will occur if the energy released upon the crack growth is sufficient to provide all the energy that is required for crack growth" (5:22). Irwin (4) extended the concepts Griffith initiated in brittle materials to apply to metals with extensive work in the area of plasticity at the crack tip.

With the increased use of high strength materials during the 1940's and 1950's, the field of fracture mechanics took on greater importance. During this time that it was discovered that flaws and stress concentrations were responsible for failure and that material deficiencies in the form of pre-existing flaws could initiate cracks and fractures (5:4). Broek presents a history of the basic problems and concepts of linear elastic fracture mechanics in his text (5).

Although much of the early work in fracture mechanics was directed to isotropic, homogeneous materials, attempts have been made to extend the fundamental principles to composite materials which are anisotropic and non-homogeneous in nature. Atkins and Mai (6) give a good background discussion of the mechanics of elastic fracture in composite materials. They state that the fracture surfaces are rarely simply planar,

that they have bits of fiber sticking out of the matrix and this feature contributes to the additional toughness of composites (6:47). This phenomena has been examined on Mode I fractures but little has been explored for Mode II fractures.

Much of the work to study the toughening mechanism in fibrous ceramic composites has focused on the increased toughening effects of debonding, crack deflection, and fiber pullout. These mechanisms depend on the weak bond at the fiber matrix interface (7:253). Agarwal and Broutman propose that in Mode II loading, failure will occur by matrix shear failure, constituent debonding, or a combination of the two (8:57).

Giare (9) studied the Mode II failure of unidirectional fiber reinforced composites and concluded that linear elastic fracture mechanics principles apply for Mode II loading. He used clip gauges to measure COD as a function of load and formulated a relationship of the Mode II stress intensity factor. Kageyama (10:535) used strain gauges mounted to a cantilever to directly measure the COD of end notched flexure specimens.

Briggs and Davidge (11) investigated the properties and applications of borosilicate glass reinforced with continuous silicon fibers. Their work describes the fabrication process, mechanical properties, and proposes possible applications for this material.

Carlsson, Gillespie, and Trethewey (12:170) examined Mode II interlaminar fracture toughness for polymer based composites. They examined the characteristics of unidirectional graphite/epoxy and graphite/PEEK composites using a travelling microscope to monitor the crack tip propagation of ENF specimens.

Mall (13) took a finite element approach to examine the effect of overhang on the Mode II testing of an end-notched-flexure (ENF) specimen concluding that the overhang has little to no effect.

Vozzola (14) developed a test for fracture toughness utilizing a three point bend setup to test ENF specimens at room temperature. He used a very crude laser system in conjunction with the test fixture to calculate values for G_{IIc} . Mol (15) furthered this work by improving the test setup and looking at the effect of elevated temperatures on the uniaxial composite material. Hoobler (16) re-examined the fracture toughness at room temperature, 600 °F, 1000 °F, and extended the research into thermal cycling effects.

This study made use of the existing test setup for ENF specimens with the incorporation of a laser interferometer displacement gauge (IDG). The use of the laser IDG enhanced the data to determine the critical load and improved the accuracy in calculating Mode II fracture toughness.

III. Test Setup

A three-point bend test fixture of steel was constructed with the LVDT attachment modified from the design used by Hoobler (16) to load the specimen. The heat lamps and susceptor designed by Hoobler were intended for elevated temperature and thermal cycling testing and were not used in this study. The laser interferometer system was similar to those used extensively by the Metals and Ceramic Division of the WRDC. A platform was designed to mount the laser assembly to an Instron machine which allowed the integration of this measuring device, a linear variable differential transformer, and a load cell supporting the three-point bend fixture.

Load Cell

An Interface 1000 lb load cell was used to measure the applied load on the specimen. The signal was routed to an Endevco 4225 Power Supply and Signal Conditioner before being entered as data into a personal computer (PC). The ratio of load input to signal output measured a constant 0.622978 lb/mv in the range of testing. The load cell was bolted to a one inch steel base plate mounted to the Instron bottom load plate.

Linear Variable Differential Transformer (LVDT)

The same LVDT system used by Hoobler was used with a modification to the mounting within the three point bend support structure. The LVDT was threaded directly into the top of the steel housing rather than being supported in a clamping collar attached to the side of the housing. A Daytronics Model DS200A LVDT was used in conjunction with a Daytronics Model 3130 LVDT Signal Conditioner and Model 3200 Digital Indicator to measure the displacement of the specimen at the point of applied load. The ratio of displacement input to signal output was a constant $6.26 \text{ E-}06 \text{ in/mv}$ which yielded a 10 V_{DC} signal change for a 0.0626 inch deflection. The LVDT was mounted inside a steel support frame which rested directly upon the load cell.

Three Point Bend Fixture

The three-point bend fixture used by Hoobler (Figure 1) was modified using steel in place of aluminum for the LVDT housing. Using simple beam theory, the structural bending of the housing top due to a distributive load is inversely proportional to its moment of inertia. In this case, the center displacement was reduced by a factor of eight (2^3) by doubling the height of the piece from $\frac{1}{2}$ inch to one inch. Threading the LVDT directly into the top plate of the structure also reducing the effect of any structural bending. The three-point bend load base, bottom rollers, and half-moon

top roller assembly were made out of Inconel 718 to provide thermal resistance to 1500°C for elevated temperature testing. The modified fixture is shown in Figure 2.

Instron TTD Tension/Compression Tester

An Instron TTD Tension/Compression Tester (Model TTP, Serial Number 2036) was used to apply the actual load to the specimens. The Instron had been modified with an automatic speed controller and a one inch diameter rod of alumina attached to the standard stainless steel ram to provide heat protection. No other modifications were made to the loading mechanism of the Instron Tester for the tests run in this study.

Laser Interferometer Displacement Gauge (IDG)

A laser interferometer displacement gauge system was mounted to an Instron machine and used to measure crack opening displacements. The laser IDG was similar to the ones used by the WRDC and its operation is extensively defined in the Mate Laser Interferometer Technical Reference Manual (17). Figure 3 shows the major component layup of the photo detector section of the laser IDG system. A software program, LASEXT, written and maintained by Mr George Hartman (18) of the WRDC, provided displacement measurements for the microhardened indentations placed in the reflective tabs mounted on the test specimen. The IDG operation is based on photo detectors

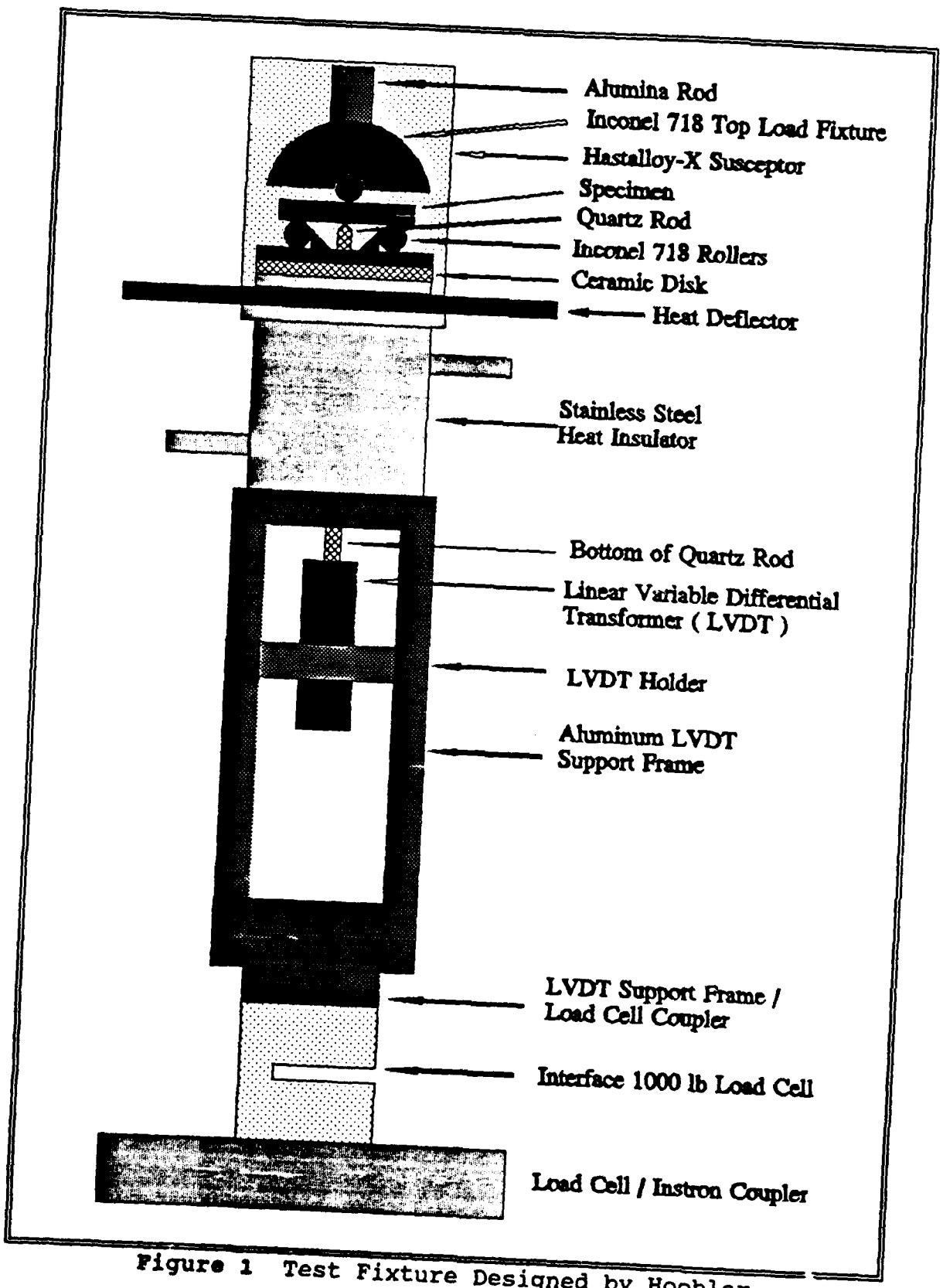


Figure 1 Test Fixture Designed by Hoobler

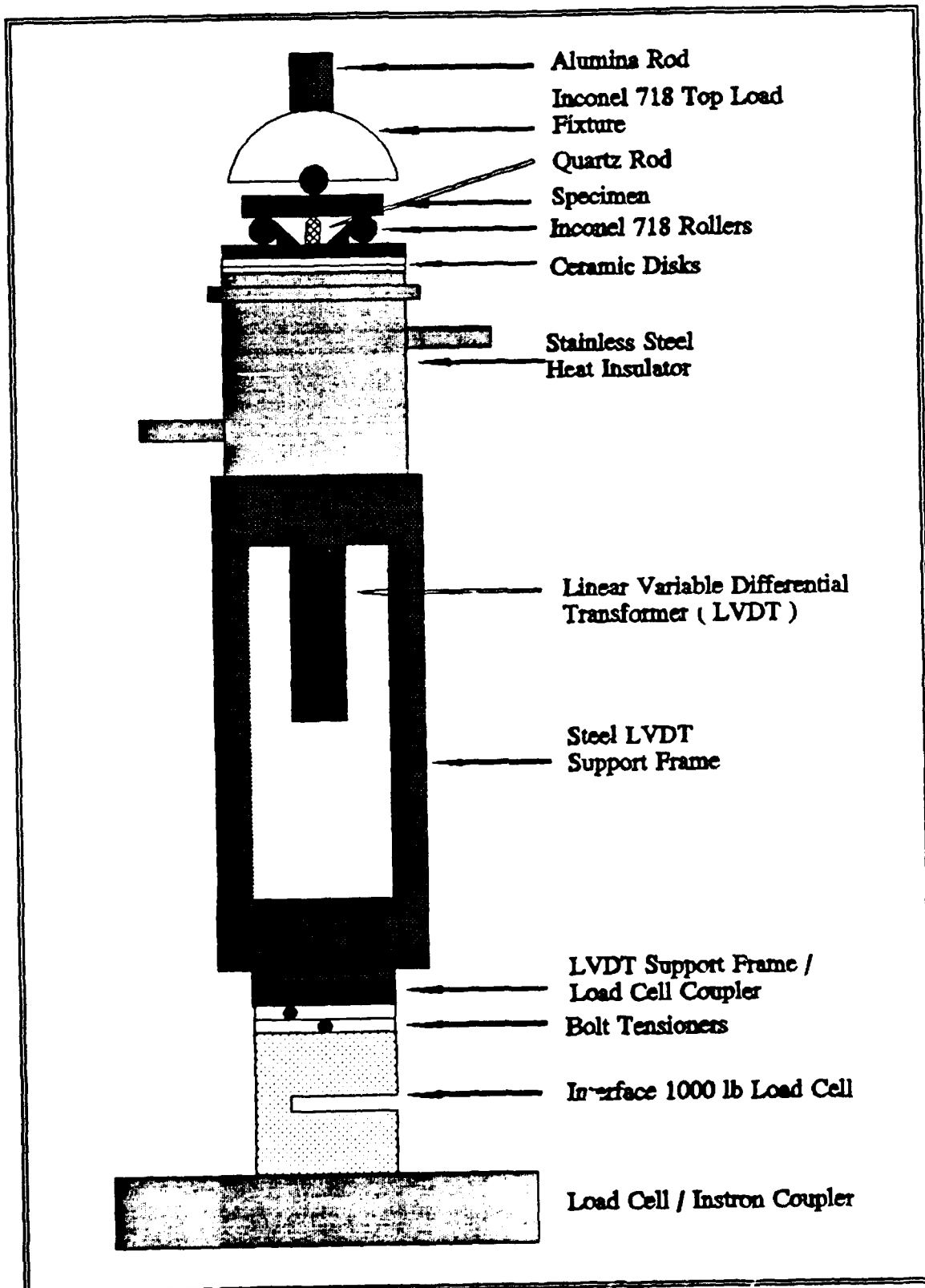


Figure 2 Modified Three-Point Bend Fixture

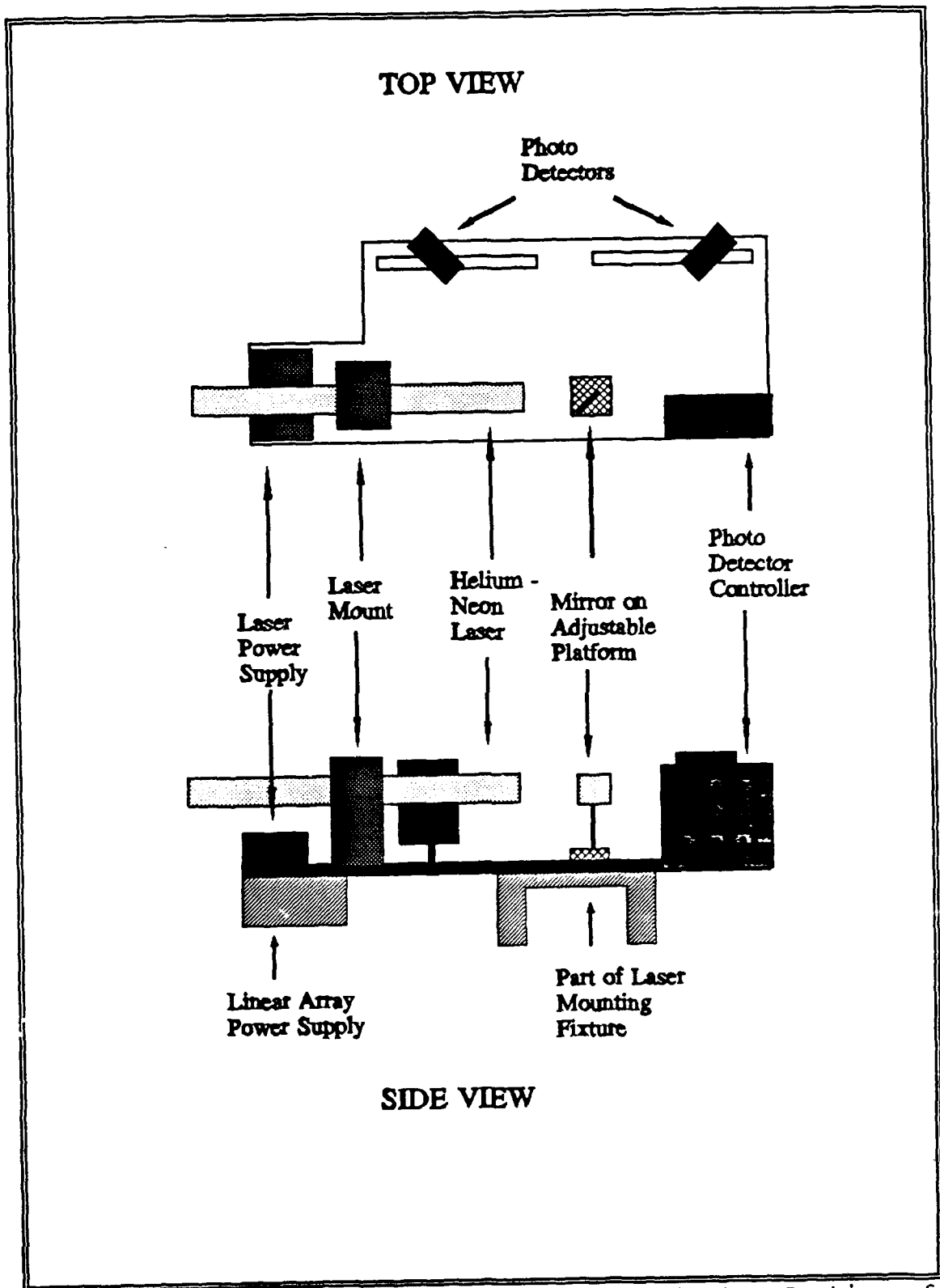


Figure 3 Component Layout of the Photo Detector Section of the Laser Interferometer Displacement Gauge System

picking up the interference of reflections from an illuminated target and converting these signals to linear displacement (17:1). A laser source produced a beam of light which was positioned onto the specimen and reflected off the indented tabs. The 50 micron indents were placed close together (within 150 microns center to center) which caused the reflected light to overlap and form a fringe pattern. Figure 4 graphically displays this interaction.

As the load was applied, the horizontal displacement of the indents from one another was monitored by two photo detectors attached to the laser platform. Using a photo detector on each side of the incident beam allowed the fringe patterns to be averaged and effectively eliminated any lateral rigid body displacement (17:2). The positioning of the indents directly above one of the bottom rollers eliminated virtually all vertical rigid body displacement.

Laser Mounting Fixture

A mounting fixture was designed to attach the laser IDG to the Instron TTD Tension/Compression Tester. A frame comprised of two inch square steel channel with a steel bracket welded to it was attached to the vertical tracks of the Instron machine. This method of attachment provided a rough vertical adjustment of the entire laser platform which aided the positioning of the beam on the specimen. An anodized aluminum subplate was mounted to this steel frame

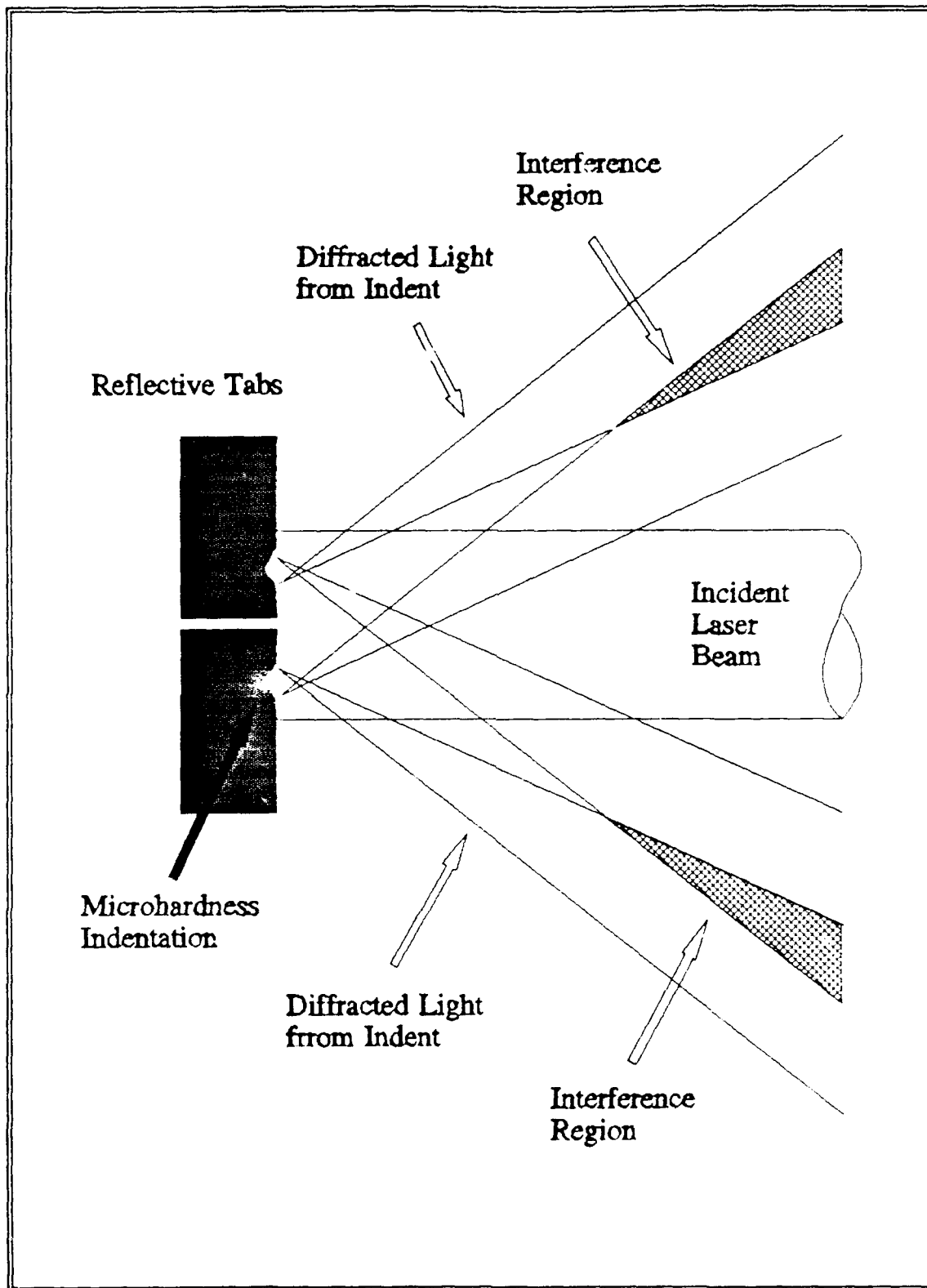


Figure 4 Laser Fringe Generation (Adapted from Reference 7, Figure 2, page 23)

using bolts in three-inch channels. This type of mounting allowed the distance of the photo sensors to the target specimen to be varied. Lateral variation of the laser system was achieved by mounting the laser platform to the aluminum subplate using an anodized aluminum standoff and saddle assembly onto a solid two inch stainless steel bar. The saddle and bar connection also allowed angle variances of the laser platform. Figure 5 graphically displays the mounting fixture. Detailed drawings of the fixture are contained in Appendix A.

The mounting fixture allowed freedom of movement in the three major axes and rotation of the laser system about the lateral axis. Total allowable movement of the beam from the center of the three point bend fixture is shown in Table 1.

System Integration

In order for an accurate comparison of the LVDT load-displacement curve and the laser IDG load-displacement curve, it was necessary to have the outputs from the LVDT, the laser IDG, and the load cell recorded simultaneously. These outputs were channeled into an analog to digital (A/D) board and recorded on a personal computer. Figure 6 graphically depicts the interaction of these components. The software program to adjust the voltage inputs to a data file was modified by Mr. Jay Anderson (19).

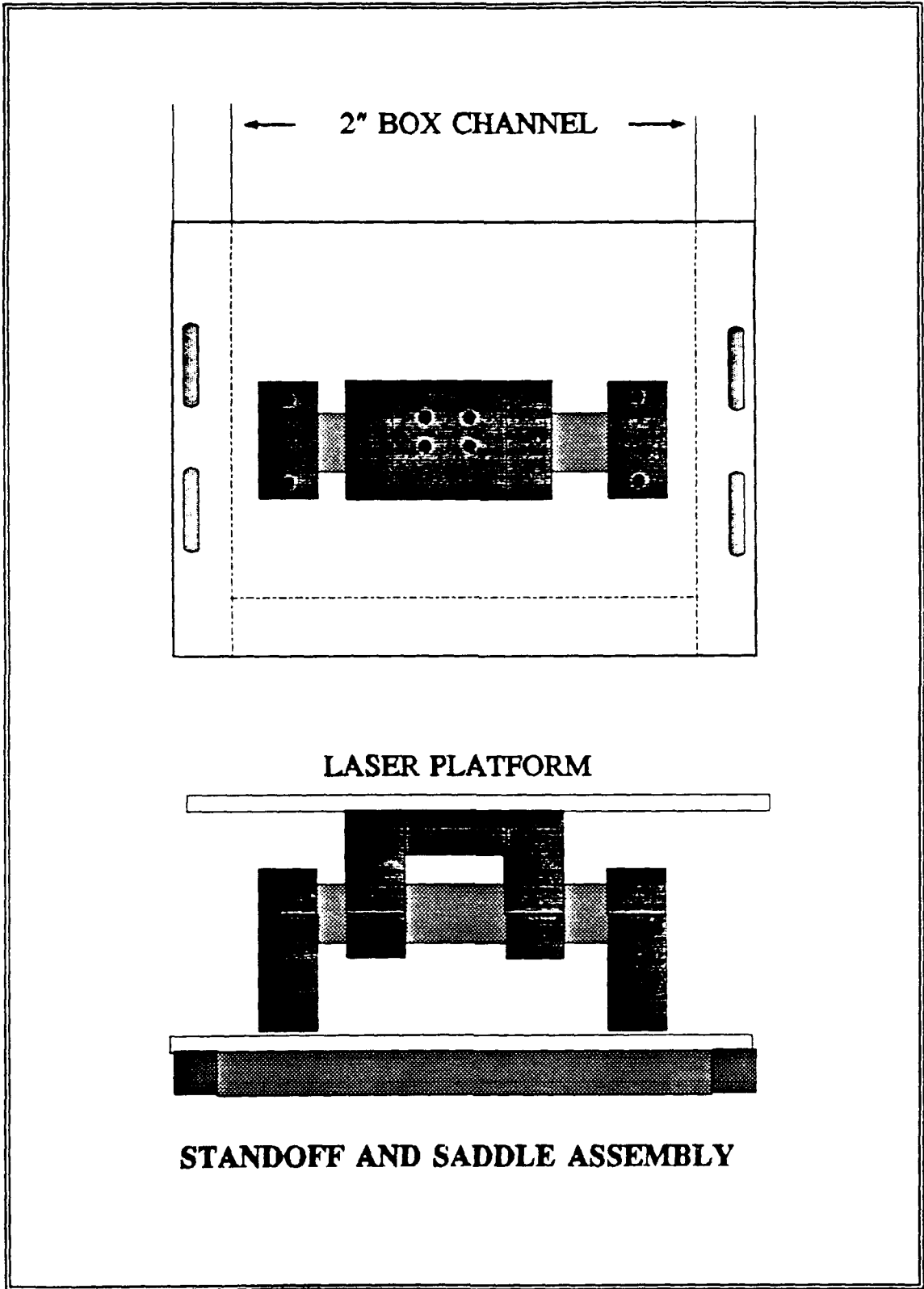


Figure 5 Laser Mounting Fixture

Table 1 Adjustment Capability of Laser Mounting Fixture

| | | |
|--|------|---------|
| <u>Vertical Direction</u> | | |
| Downward from the top of LVDT rod: | 1.0 | inches |
| Upward from the top of the LVDT rod: | 12.0 | inches |
| <u>Lateral Direction</u> | | |
| Left of center of the LVDT: | 2.5 | inches |
| Right of center of the LVDT: | 1.5 | inches |
| <u>Depth Direction</u> | | |
| Minimum distance from the plane of the photo detectors to tip of LVDT | 7.0 | inches |
| Maximum distance from the plane of the photo detectors to tip of LVDT | 9.5 | inches |
| <u>Rotation about Lateral Direction</u> | | |
| Angle below level | -45 | degrees |
| Angle above level | +45 | degrees |

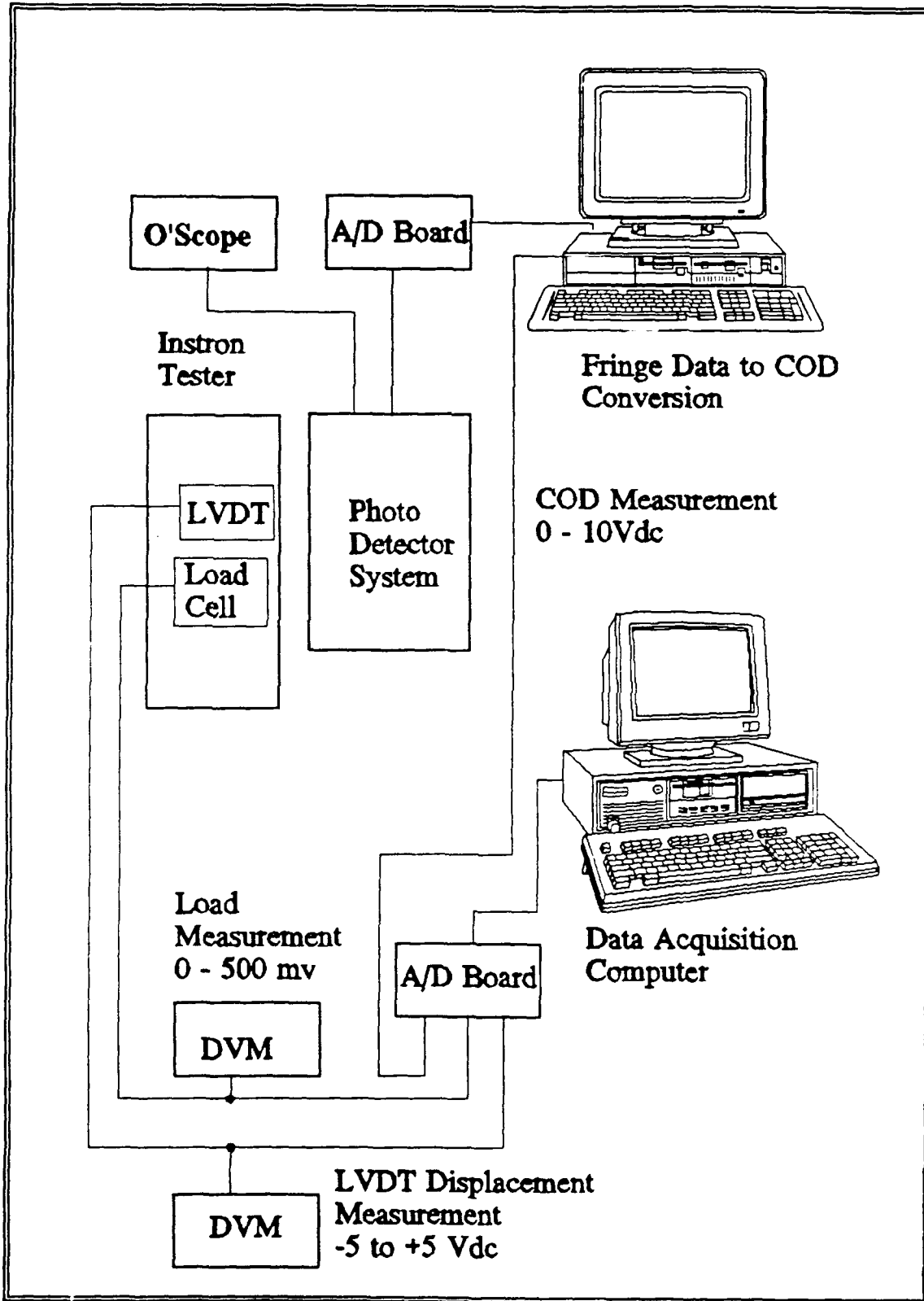


Figure 6 Test System Component Interaction

IV. Experimental Procedure

This section addresses the procedures that were taken to test the end notched flexure specimens. The section begins with the fabrication of the plate from which the specimens were cut and addresses the machining and precracking of the final specimens. A detailed discussion is given on the preparation of reflective tabs which were needed for the laser interferometry and the application of the tabs to the test specimens as well as the indentation process. The alignment of the test fixture is also included as are the procedures followed for the application of the load. Finally, a brief discussion is given on the post-mortem examination which was used to confirm the length and Mode II crack propagation.

Specimen Preparation

The specimens used in this study were from a composite of Corning Glass Works 1723 matrix material with a Nicalon¹ silicon carbide yarn. The yarn consisted of fibers averaging 12.5 micron in diameter from Lot # 124. The slurry was comprised of:

100 grams CGW 1723 glass frit in a finely ground powder
93 milliliters of R Hoplex Grade L-12 liquid binder and
232 grams distilled water.

¹ Nicalon is a registered product of the Nippon Carbon Company of Japan

The yarn was pulled through a furnace at 700° C to burn off the sizing then through the slurry. The slurry impregnated yarn was wound on an eight-faced mandrel and lamp dried. The mandrel was mechanically turned and moved laterally to produce sheets of parallel fibers. A light roller was outfitted on top of the impregnated yarn to smooth the yarn so fibers did not overlap and to ensure a uniform surface. The slurry impregnated fibers were allowed to dry on the mandrel for three days. Eight sheets were then cut from the mandrel measuring approximately 8 inches long by 4 inches wide. These sheets were further cut into squares about 4 inches wide. Each sheet was then visually examined to make sure the quality was sufficient for hot pressing. The predetermined specimen thickness of 0.1 inch dictated ten sheets were required to be hot-pressed per plate. The final layup of the unidirectional composite specimen was $[0]_{10}^{\circ}$.

After the plates were hot-pressed, they were visually examined for defects. Two specimens were cut from each plate and four point flexure tests were run on each specimen. Mr. Larry Zawada (20) compared this test data to data from other plates manufactured at WRDC for quality assurance purposes. Each plate was then cut into a number of specimens approximately 0.3" wide and 2.0" long using a low speed diamond wafering blade. Each specimen was machined on a 20 micron grinding wheel at 300 - 400 R.P.M.s using a holding fixture to provide a variation in width of less than 0.0025".

The grinding fixture provided a broad base to eliminate any excessive angling of the specimen edge and is shown in detail in Appendix C. The thickness of every specimen was already within the 0.0025" tolerance so no polishing was done to the wide face of any specimen. The length of each specimen was approximately 2.0" but the three point bend fixture had rollers spaced at a fixed distance of 1.5". Mall (13) had shown that the overhang does not significantly influence the initiation of crack growth so no polishing was done to the end surfaces. Final specimen dimensions are given in Appendix B. Figure 7 shows the microstructure of the composite material magnified 100 times.

Precracking of Specimen

A 0.1" long notch was cut in the center of the wide edge of each specimen along the fiber direction using a diamond blade on a low speed saw which produced a slit 0.015" wide. The length of the final pre-crack for each specimen was determined as per need of each test, but all were done in the same manner. Each specimen was first clamped at the position of maximum allowable pre-crack into a jig designed by Hoobler (Figure 8). A modified jewelers screwdriver was slowly driven into the machined notch as a wedge by turning an extending micrometer. A traveling microscope was used to monitor the crack length as the screwdriver was advanced. The goal of this method was not to grow an exact pre-crack length but

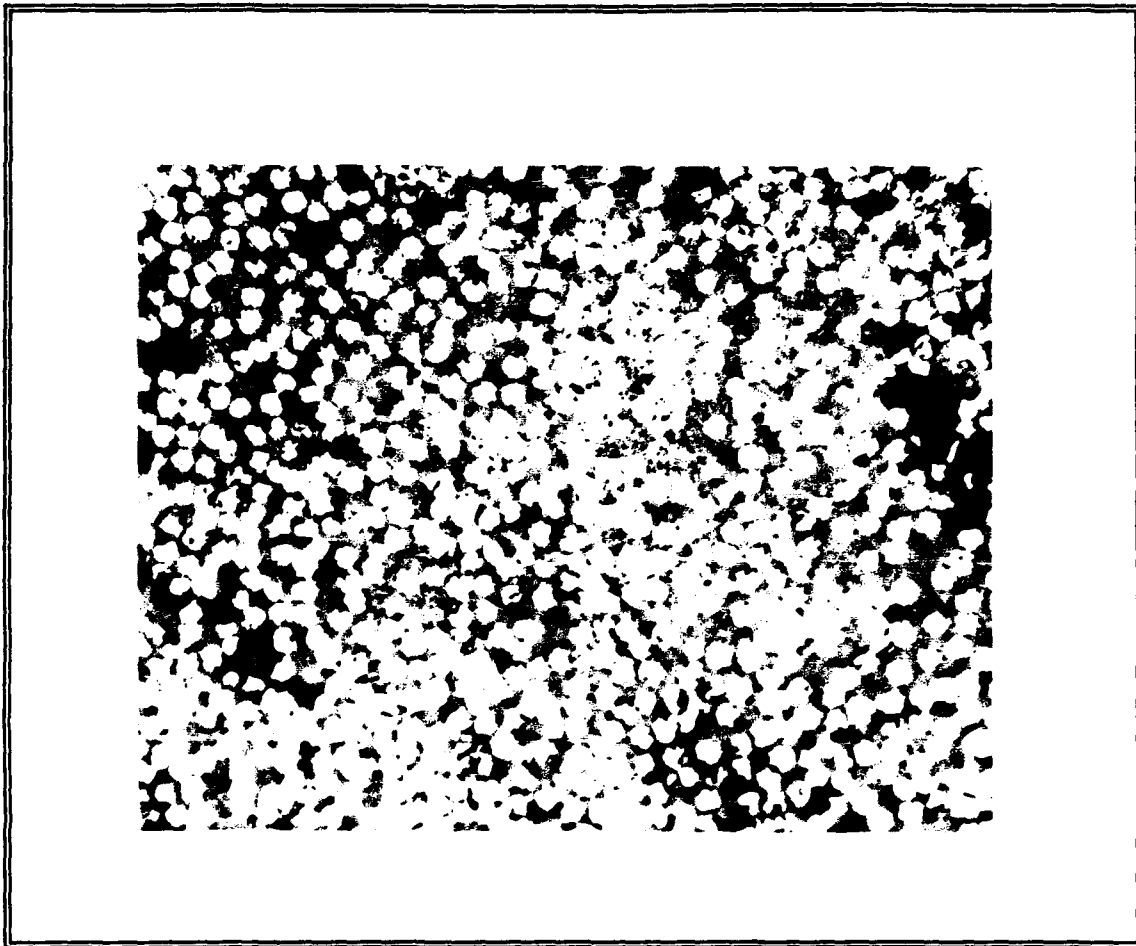


Figure 7 Microstructure of Composite Specimen Magnified 100X

simply to provide a crack in a usable range. The pre-crack length used in experimentation and for calculations was based on the length which extended beyond the roller toward the center load rather than the length from the end of the specimen. A pencil mark was made on the surface at the observed crack tip and the wedge backed out. After the reflective tabs were mounted to a specimen, the distance from the pencil mark at the crack tip to the middle of the tabs was measured using the travelling microscope and recorded as the

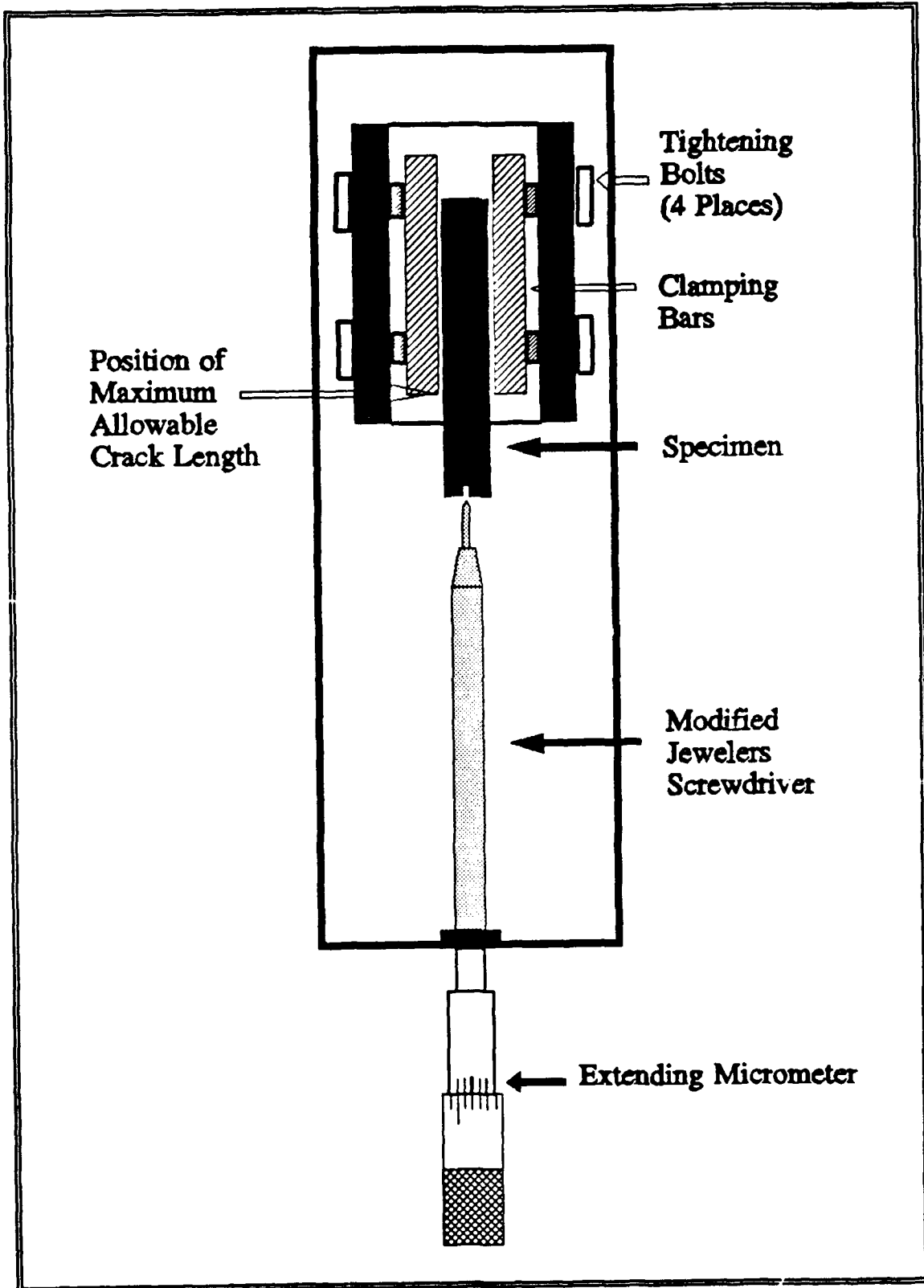


Figure 8 Pre-cracking Jig

probable pre-crack length. During testing, the space between the tabs was positioned directly above the center of a roller. Figure 9 shows the end-notched flexure specimen with applicable dimensions illustrated.

Reflective Tabs Preparation

Ceramic materials lack the necessary reflectivity to produce quality interference fringes with a laser if simply indented themselves. This problem was overcome by using indented tabs of a material with a high reflectivity physically attached to the specimen. For tests conducted at room temperature, stainless steel and titanium tabs were sufficient but non-oxidizing materials such as platinum should be used at elevated temperatures. Two tabs were attached to each specimen and the preparation procedures were identical for each tab.

Each tab was cut from a 0.020" sheet of material by wire electron discharge machining (EDM) to dimensions of 0.1" x 0.2". The EDM process was selected because of the need to reduce curvature at the edge which results when material is sheared to size. The tab length was determined by the need for the tab to be long enough to be indented above the crack and still be affixed to the test specimen. Smaller sized tabs were too difficult to work with during the polishing phase.

An accepted procedure of polishing each tab individually to reduce the chance of generating false light fringes

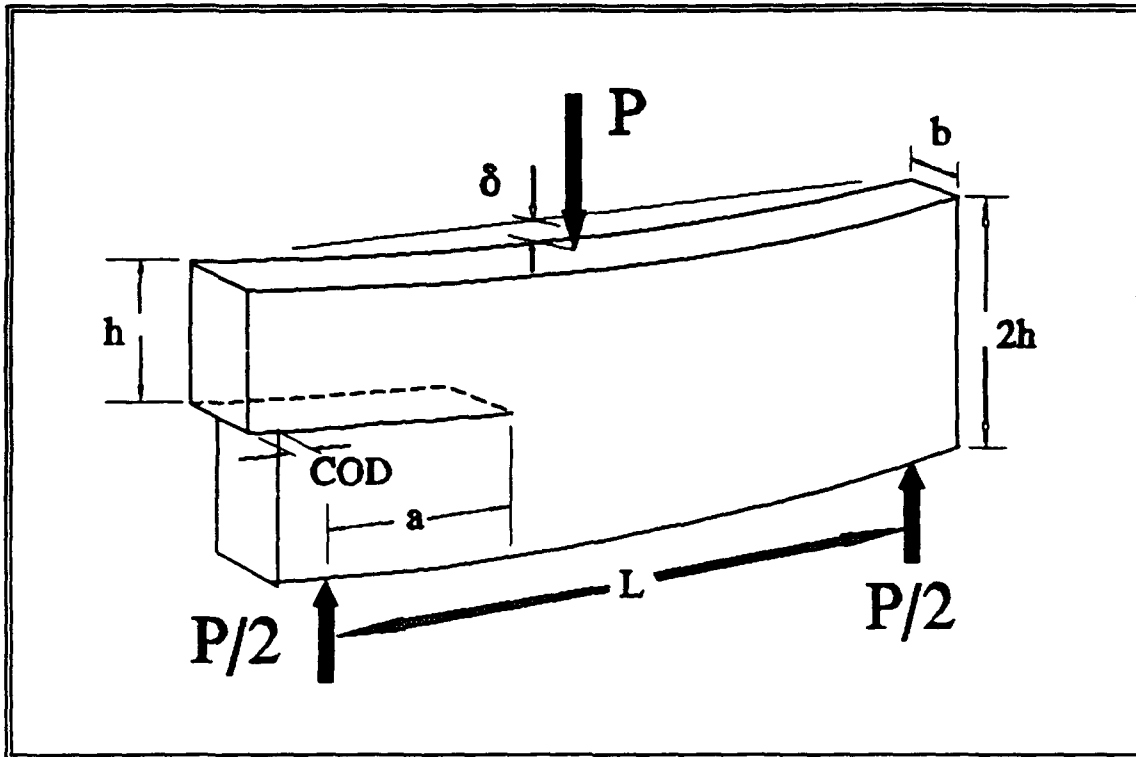


Figure 9 Specimen Dimensions

developed by Dr. Reji John (21) of WRDC was tried and modified with some success. The original procedure removed scratches in the tabs using a felt pad on an eight inch polishing wheel with water and a 0.5 micron polishing solution. The standard technique was to have the polishing pad wetted and a small amount of solution applied. The tab was held on the felt with one's finger while the wheel spin rate was increased to approximately 400 R.P.M. for a few minutes. Care was taken to apply enough pressure on the tab to keep it from losing contact with the finger and spinning off. Too much pressure caused the polishing solution to be pushed out from under the tab resulting in the specimen riding on only felt. If enough

pressure was not applied, the tab would spin off the wheel surface and was retrieved with a pair of tweezers. The tab's surface was periodically checked under a microscope to determine when the tab had been sufficiently polished. Figure 10 shows a tab surface that was not yet finished at a 200 power magnification. Note the voids and scratches that are present. Figure 11 shows the same tab after adequate polishing had been done. Total surface polishing time was roughly 15 minutes per tab using this method.

Due to the large number of tabs needed, the polishing process was modified with some success. An aluminum holding block (1" x 1½" x ½") was made planar by sanding on a 600 grit silicon carbide roller. Roughly 45 tabs were then attached with an cyanoacrylate adhesive to this block. The tabs were first laid out in rows of 15 with edges touching. A piece of adhesive tape was then used to pick up each row. A liquid adhesive was placed on the block and the three rows transferred over. A small weight was then placed across the tape. This technique allowed the tabs to be quickly placed on the block with an even distribution of adhesive under each tab. Figure 12 shows the tabs laid out on the aluminum block. After the adhesive cured, the adhesive tape was removed and the tabs were smoothed on a 600 grit roller. The blocked tabs were then polished on a flat surface covered with a nine micron diamond paste followed by polishing with a three micron diamond paste. The tabs were steam cleaned periodically

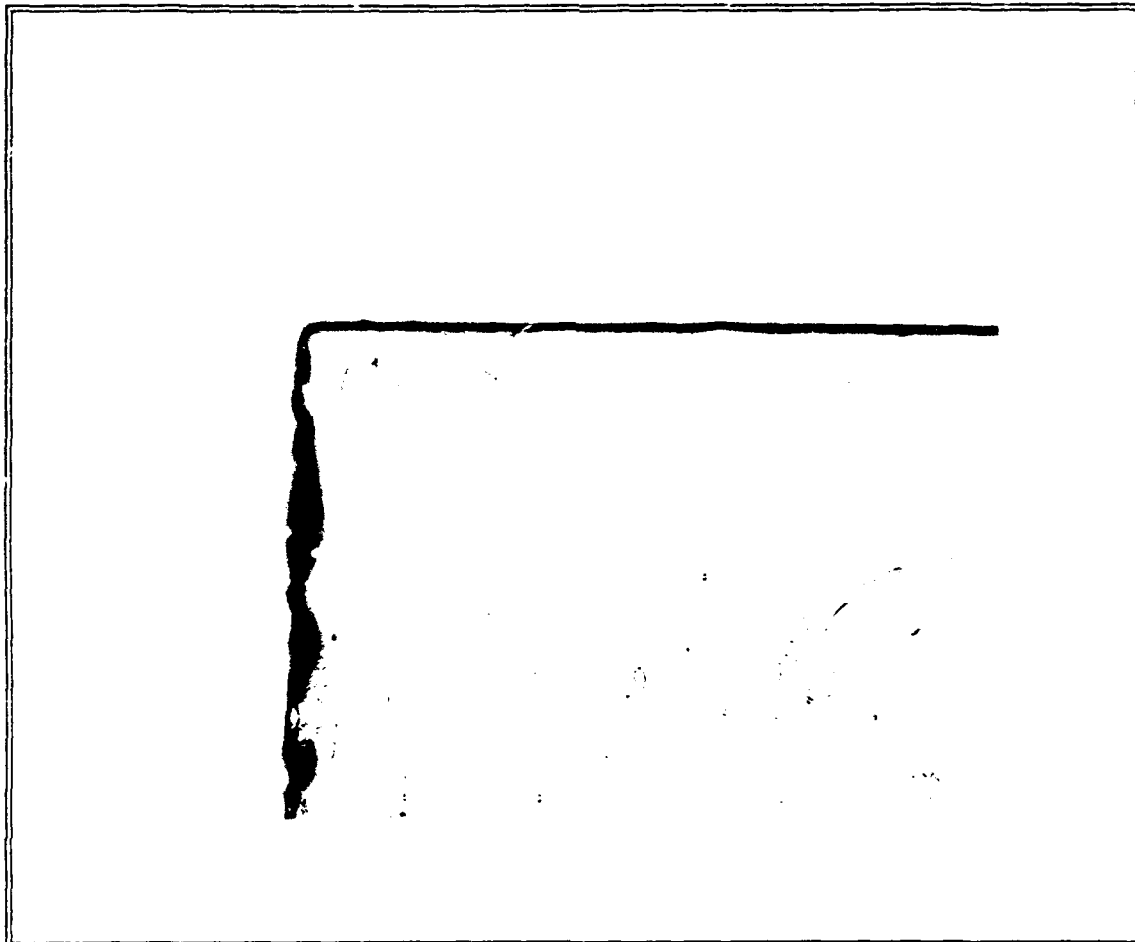


Figure 10 Tab Not Sufficiently Polished for Microindentation
Magnified 200 X

during this intermediate polishing and examined under a microscope to check progress. When most the tabs had scratches no larger than three microns remaining, the blocked tabs were polished on an eight inch polishing wheel using a Chemomet² surface and Mastermet³ solution. The Mastermet solution had a particle size of 0.05 microns and a ph of 9.5.

² Chemomet is a registered product of Buehler LTD

³ Mastermet is a registered product of Buehler LTD

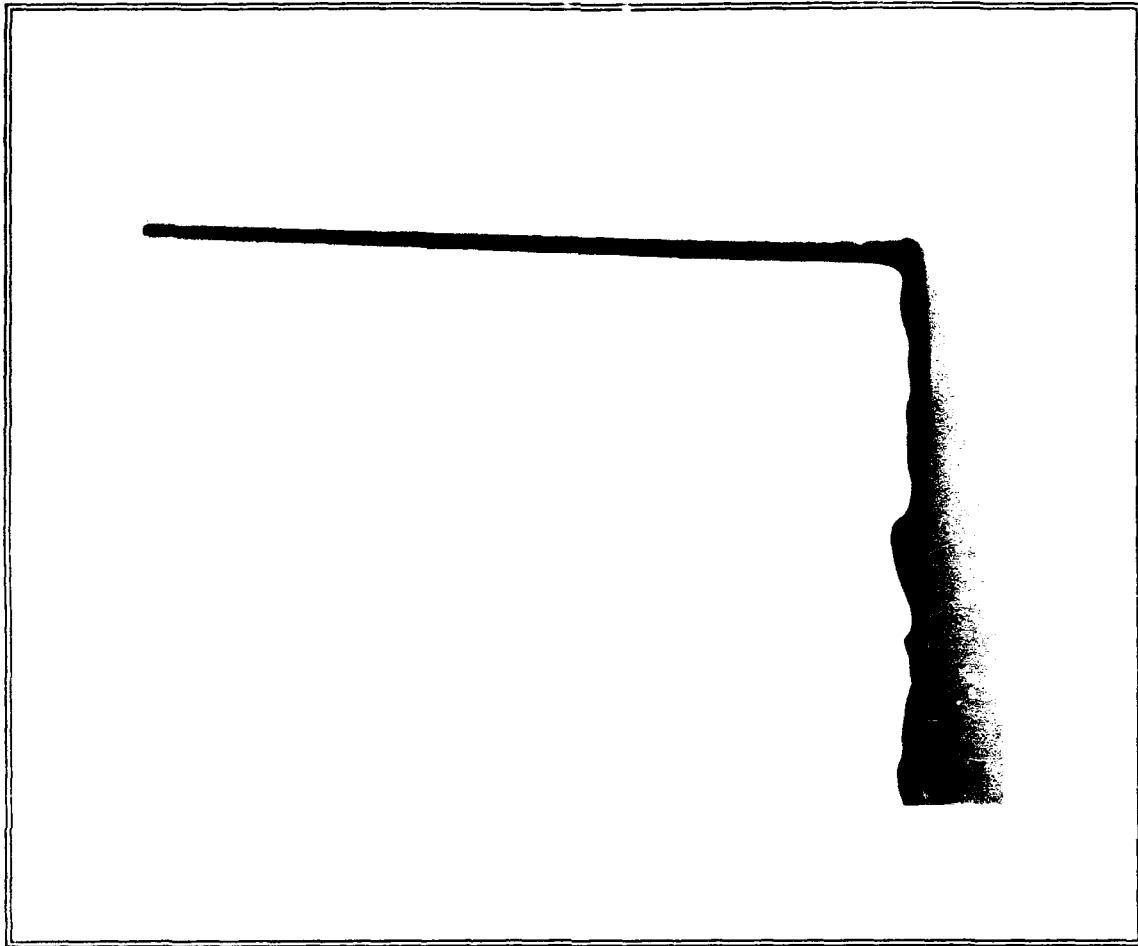


Figure 11 Tab Sufficiently Polished for Microindentation
Magnified 200 X

The tabs were chemically polished for about ten minutes on the polishing wheel then steam cleaned. After the tabs looked free of scratches greater than one micron, the block was placed in a glass petri dish filled with acetone and allowed to soak overnight. The acetone dissolved the adhesive and the tabs fell from the aluminum block without being scratched.

Once the surface of a tab had been polished, one of the long edges was made as perpendicular to the surface as possible. This was necessary to eliminate any false fringes

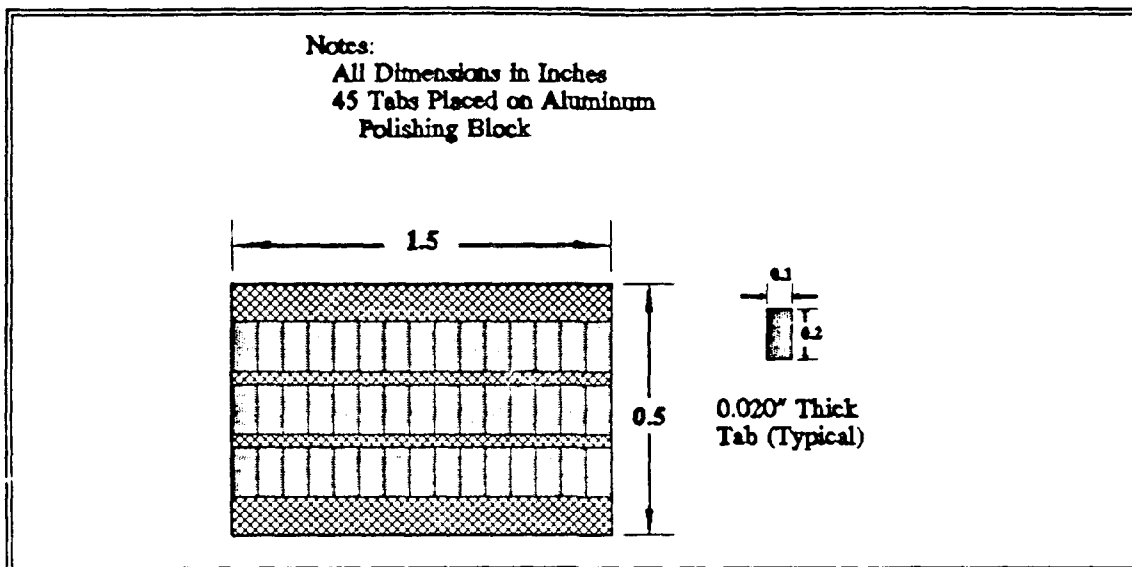


Figure 12 Tabs Placed on Aluminum Block in Preparation for Polishing

from being reflected to the photo detectors by imperfections on the edge. Ten tabs were stacked in each of four slots on the bottom plate of a fixture designed by the author and fabricated by the AFIT shop. The fixture allowed a very small portion of each tab to extend beyond the edge of the block. Appendix C contains the detailed drawings of this polishing fixture. The edges of the fixture with the tabs protruding were first run over 600 grit silicon carbide paper to give a fairly normal edge to all the tabs. These surfaces were then polished in the same way the tab surfaces had been done. Both surfaces of the fixture with tabs were polished with nine micron diamond paste, three micron diamond paste, and then Mastermet solution. After examination under a microscope showed no scratches greater than one micron, the assembly was taken apart and the tabs soaked in acetone. This provided 40

tabs with a surface acceptable for indentation and a normalized edge. The tabs were then ultrasonically cleaned in acetone and finally rinsed in methanol.

Tab Application to the Specimen

The area of the specimen where the tab was applied was first abraded with 600 grit emery paper to assure a good bonding area. The specimen was cleaned with acetone and a cotton swab to remove oily contaminants. The specimen was then wetted down with distilled water and wiped dry to minimize the chance of debonding caused by the material wicking moisture from the adhesive during the curing stage. A special teflon mounting fixture shown in Figure 13 was designed to simplify the mounting procedure. Teflon was chosen because of its resistance to adhesives and non-reactance to acetone. The mounting fixture was fabricated at the AFIT shop using a milling machine without changing the bit to produce both grooves. This fabrication technique yielded two cutouts that were parallel in depth to each other which caused the tabs to be co-planar with the specimen when attached. The lower groove was cut 0.002" deeper than the 0.020" tab thickness to provide room for the adhesive to expand.

The reflective tabs were placed with the reflective surface face down in the lower groove of the fixture with the normalized edges adjacent. A small amount of cyanoacrylic

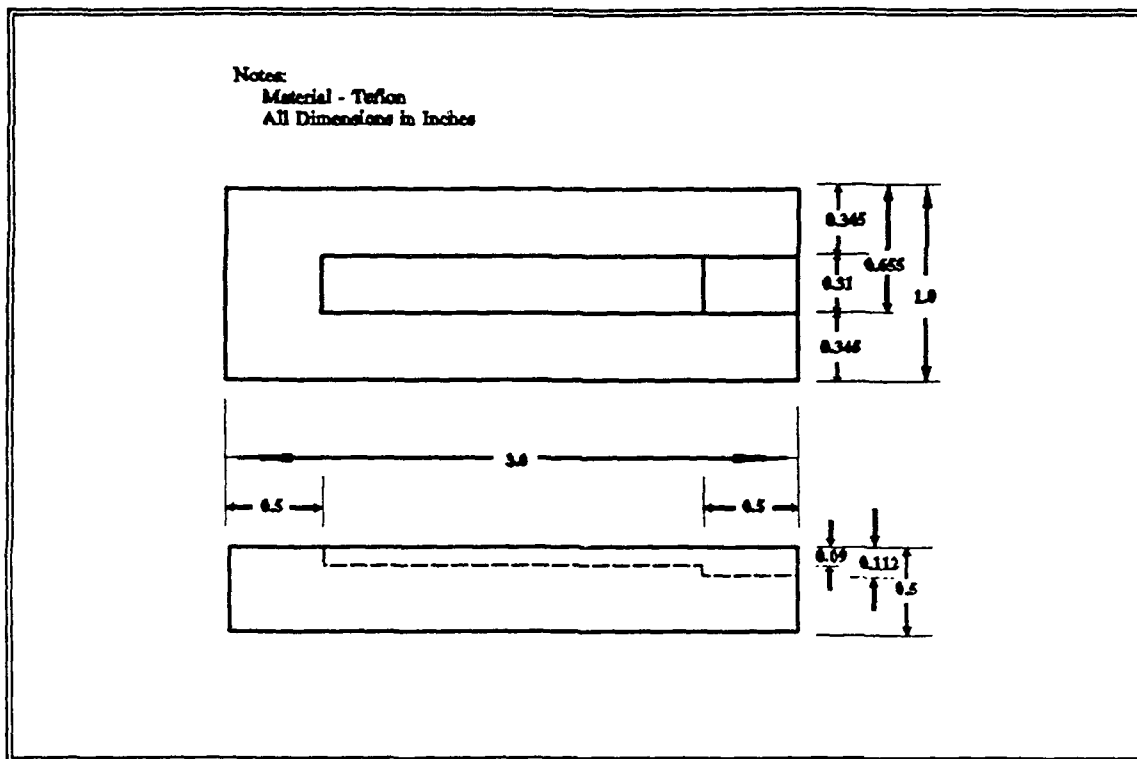


Figure 13 Teflon Tab Mounting Fixture

adhesive was placed on the tabs in the designated areas and the specimen was gently placed in the upper groove over the tabs. Figure 14 shows the placement of adhesive on the tabs prior to the specimen being placed on top. Light pressure was applied for a few seconds until the adhesive set. The specimen was then examined to ensure no adhesive had flowed from under one tab to contact the other. If this happened, the specimen was soaked in acetone to remove the tabs and another attempt made after the specimen was cleaned.

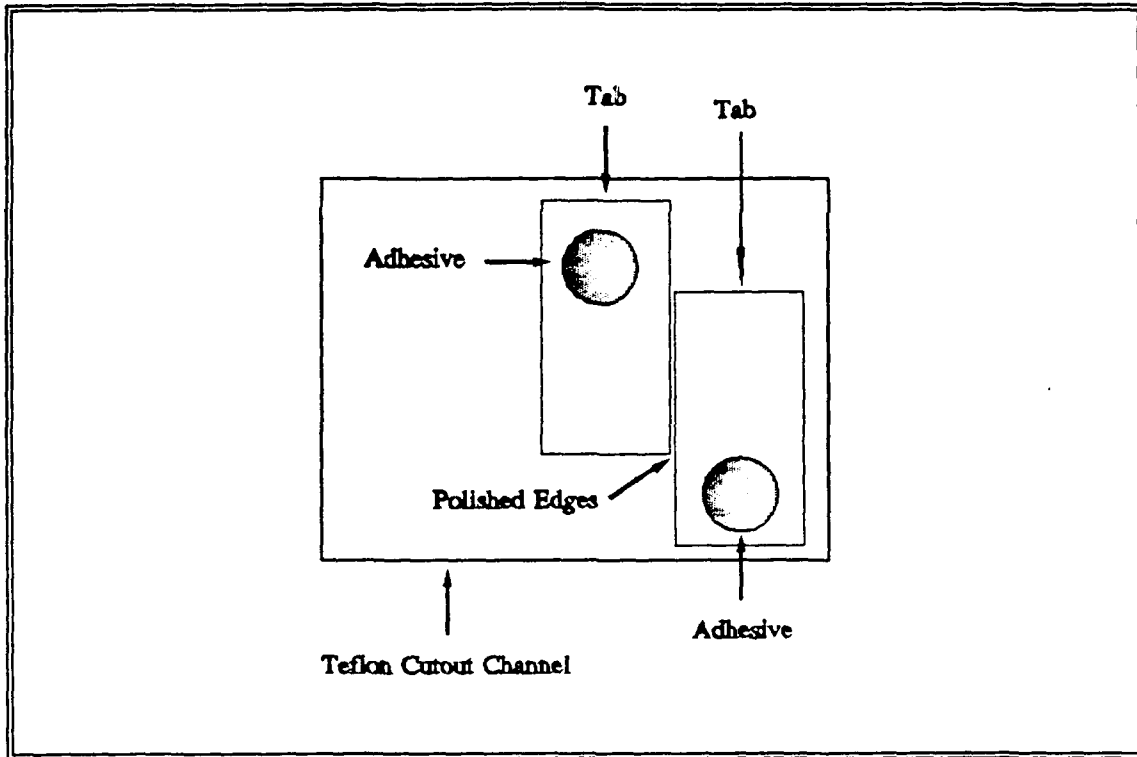


Figure 14 Placement of Adhesive on Tabs

Indentation of Reflective Tabs

After the tabs had been affixed to the test specimen and the adhesive cured, the specimens were steam cleaned to clear the tabs of any contaminants. The tabs were indented with a Wilson microhardness tester using a pyramid shaped diamond microhardness indenter and a 700 gram load. The 50 micron indents were positioned with their centers within 75 microns (0.003 inches) of the normalized edge and directly across from one another.

After the indents had been impressed into the tabs, they were examined to ensure well defined surface indentations had been made and that the indents were not angled. The position

of each indent was also checked to verify proximity to the other. In the event the indents were not properly oriented with respect to one another or angled, a new set of indents was placed in the tabs more than 0.02 inches away from the previous set. Figure 15 shows the proper placement and orientation of the indents. It was found that the titanium tabs caused deposits to be left on the diamond tip of the microhardness indenter. This resulted in poor quality indents requiring the cleaning of the diamond head with Kroll's reagent after each set of indents made.

Specimen Alignment

The orientation of the specimen was critical for the photo detectors to be in line with the generated fringe patterns and to ensure an accurate measurement of crack length. The first task was to align the three point bend fixture on the Instron testing machine so the laser beam would be directly perpendicular to the roller base. This was accomplished by using the bolt tensioners to tighten the fixture at the proper position (Figure 2). The support rollers were placed on the fixture and the laser directed along the top of one roller. When part of the beam was barely visible along the length of the centerline on the top of one roller, the bolt tighteners were turned to lock the fixture in place. This provided a fixed distance of 1.5 inches between the rollers perpendicular to the laser beam.

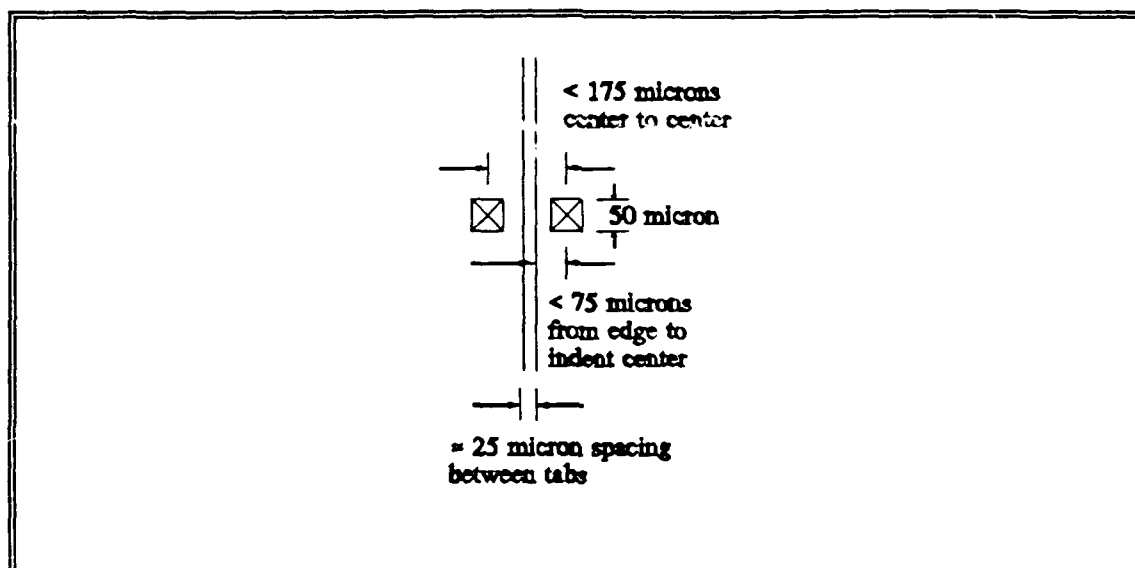


Figure 15 Proper Placement and Orientation of a Set of Indents

A specimen was then placed on the three point bend fixture perpendicular to the laser beam with the reflective tabs directly above one of the rollers. The load head was then brought down to secure the specimen in place. The laser platform was raised to position the center of the beam at the same height as the center of the reflective tabs of the specimen and the mounting fixture support bolts tightened in place. Lateral movement of the entire laser platform was then done to direct the beam onto the junction of the reflective tabs with the mounting platform already secured into place. The end result was a beam directed onto the reflective tabs mounted on the specimen which in turn reflected directly back onto the laser system's reflective mirror and back to the aperture of the laser.

After this initial alignment of the test system, each specimen was also aligned prior to testing. The small size of the test specimens required a consistent placement in the load fixture to achieve an accurate correlation between tests. Each specimen was placed in the three point bend fixture and a beam directed at the indents positioned directly above a roller. A check was done to ensure the laser beam reflected back to the reflective mirror. If the reflected beam did not come close to being reflected back to the laser aperture, the specimen was adjusted. The load head was slowly brought down and a small preload (approximately five pounds) placed on the specimen to hold it in place. The edges contacting the rollers had been polished normal to the front surface so tilting of the test specimen was not a problem.

An index card was then used to locate the generated fringe pattern. The card was pulled back and used to position the photo detectors on each side of the tabs. The laser IDG had been designed to allow the fringes to be displayed on the computer monitor using another program developed by Mr. Hartman at WRDC called FRNGDSPL. This feature was used to ensure a good fringe pattern was being sensed by the photo detectors. The filtering and gain adjustments for the detectors were used to produce a clear sine wave pattern of 2 volts peak-to-peak on the oscilloscope.

Load Application

All equipment used during the testing phase was turned on and allowed to warm up for 30 minutes prior to running any tests. After the initial warm up period, the load cell was zeroed using the adjust located on the signal conditioner. The half moon top roller fixture and test specimen were placed on the three point bend fixture base and the specimen aligned as described in the previous section. This procedure had the laser directed onto the reflective tabs and a preload of approximately 5 pounds on the specimen. The laser IDG system was run under the program LASEXT using a full scale range of 0.002 inches. The initial relative position of the indents was set to zero which allowed all displacements from the initial position to be entered directly into the data accumulation file. If the measured displacement varied prior to any load application, the fringes were considered suspect and the photo detectors moved to try to improve the quality of fringes detected. After this, the laser IDG was re-initialized by exiting out of LASEXT and then re-entering the program.

The data collection program was started by loading the basic program, LIDG1, on the data collection computer. This program, tailored by Mr Jay Anderson (19) of AFIT/ENY, automatically zeroed the position of the LVDT, converted the voltage input from the load cell to a load in pounds, and

recorded the COD displacement value directly. The sample rate was set at one sample per second.

Once everything was initialized, the specimen was loaded at a constant crosshead speed of 0.005 in/min. The specimen was loaded to an upper limit of 150 pounds due to the limitations of the analog to digital board. If this range had been increased, the accuracy of test data from the load cell would decrease from a 2 percent error to an error of 10 percent. Test specimens with crack lengths less than 0.35 inches were tested to this limit but specimens with larger cracks were run to 150 percent of their estimated critical loads. Data was collected for both the loading and unloading phases of testing.

After the first test of a specimen at a crack length, the specimen was visibly examined to see if crack growth could be detected under a lighted ten power magnifying glass. If the crack tip was obvious, a small pencil mark was placed on the specimen at that point. The specimen was then placed in the precracking jig and the crack grown as described earlier in the section on precracking to generate a Mode I crack extending at least 0.1 inches past the observed stop of Mode II crack growth. This new crack tip was marked with a pencil and the length to the middle of the indents measured and recorded as a new crack length. This Mode I crack extension of 0.1 inches was assumed sufficient to negate any fiber interlocking and entanglement that occurred during the Mode II

crack growth and assured that all testing began with similar conditions. The specimen was then aligned and tested with the new crack length. This sequence was repeated until the crack length exceeded 0.7 inches.

Post Test Analysis

After a specimen had been tested to its useful limits, it was separated into two halves by subjecting it to Mode I failure in the precracking jig. The fracture surfaces were then examined under varying powers of magnification to determine correlation of the pencil marks made during precracking to changes in fiber fractures. The difference between the Mode I and Mode II fracture surfaces was occasionally a drastic transition in fiber damage but more often the transition occurred over a range of 0.02 inches and was not as distinct. If the pencil marks differed by more than 0.02 inches, the data for the crack length was excluded from analysis.

Results and Discussions

The objective of this study was to determine if the use of a laser interferometer displacement gauge (IDG) would enhance the calculation of Mode II fracture toughness, G_{IIc} , of a ceramic composite. One parameter needed for the calculation of G_{IIc} was Young's modulus. Young's Modulus, E_{11} is the ratio of a simple tension stress applied to a material to the resulting strain parallel to the tension. After E_{11} was determined, specimens with different crack lengths were tested and the compliance calculated. Once found, these experimental compliance values were compared to theoretical values. The test data was next examined to determine the critical load, P_{cr} , for the onset of crack growth. This load value was based upon the laser IDG displacement-load curves rather than the previously established method using the LVDT displacement-load curves. From this information, the experimental values of G_{IIc} were calculated and plotted. The compliance of the COD was also calculated and plotted verses the non-dimensionalized crack length.

Young's Modulus

Russell (1) developed an analytical relationship for compliance based on linear beam theory for end-notched flexure specimens that is given in Equation 1. For this equation, C is the compliance; a , the crack length; L , the span between

rollers; E_{11} , the value of Young's Modulus; b , the thickness of the specimen; and h , the height to the mid-plane of the specimen.

$$C = \frac{1 + 1.5 \left(\frac{2a}{L} \right)^3}{4E_{11}b \left(\frac{2h}{L} \right)^3} \quad (1)$$

By solving this equation for E_{11} , it was possible to determine the experimental value of Young's Modulus for the composite specimens. The values for b and h were measured using the procedures given in Appendix B, L was fixed at 1.5 inches, and C was experimentally calculated.

Two specimens were cut and machined to the dimensions of the standard test specimens (0.1" x 0.3" x 2.0"). These specimens were dedicated solely for the determination of a value for Young's Modulus. These specimens were tested at different orientations to provide an average value of compliance with the roller support spacing, L , fixed at 1.5 inches. Each specimen was subjected to a total of six loadings and the midpoint displacement plotted verses load. Figures 16 and 17 show the test results for the two specimens. The test fixture was also tested using a piece of Nicalon as the test specimen to determine the compliance of the test rig. The sample size was 1.0" in height, 0.75" wide, and 2.0" long. This sample was run two times and provided the data shown in Figure 18.

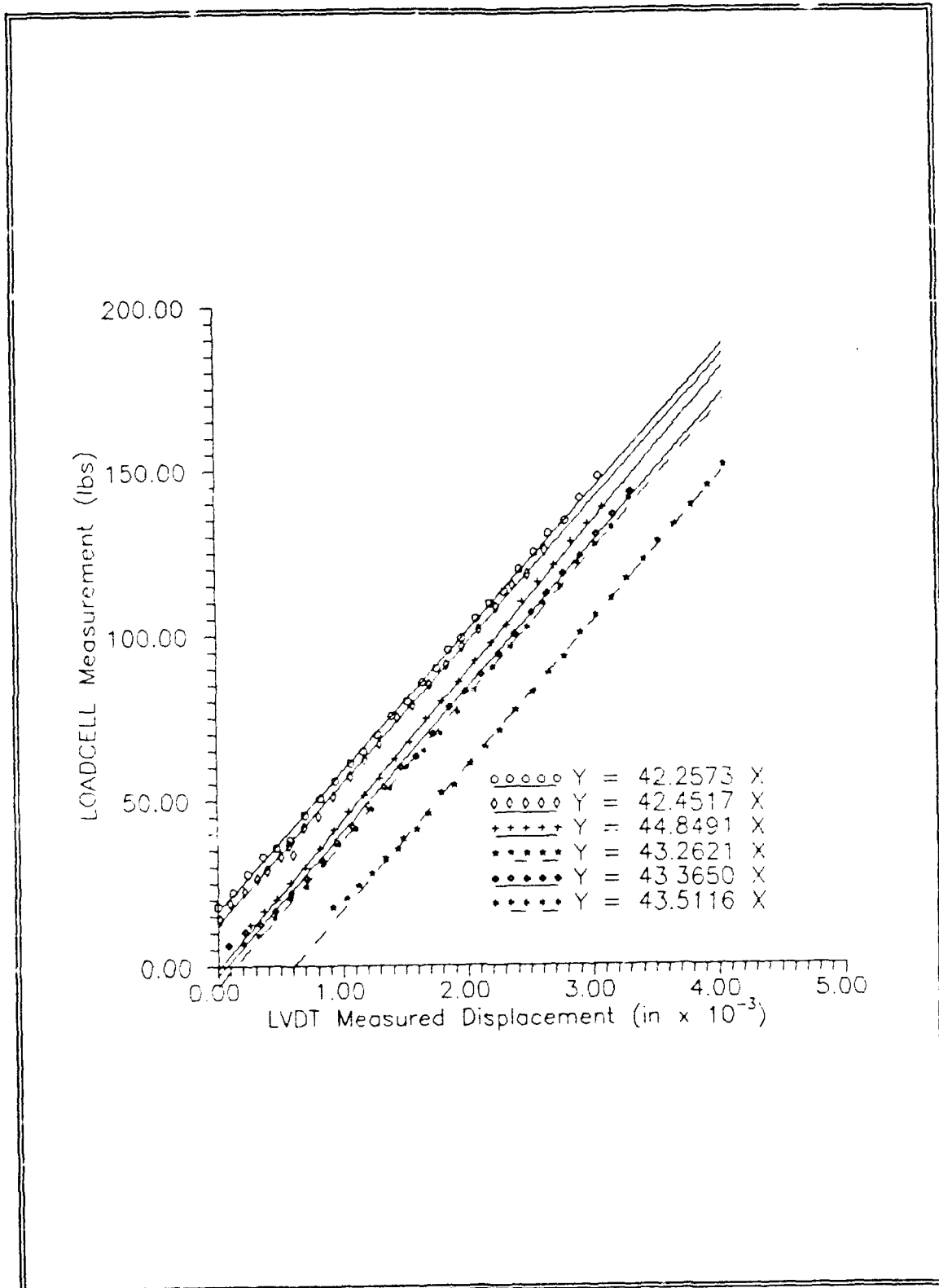


Figure 16 Load-Displacement Curves of Specimen 713 with No Crack Present

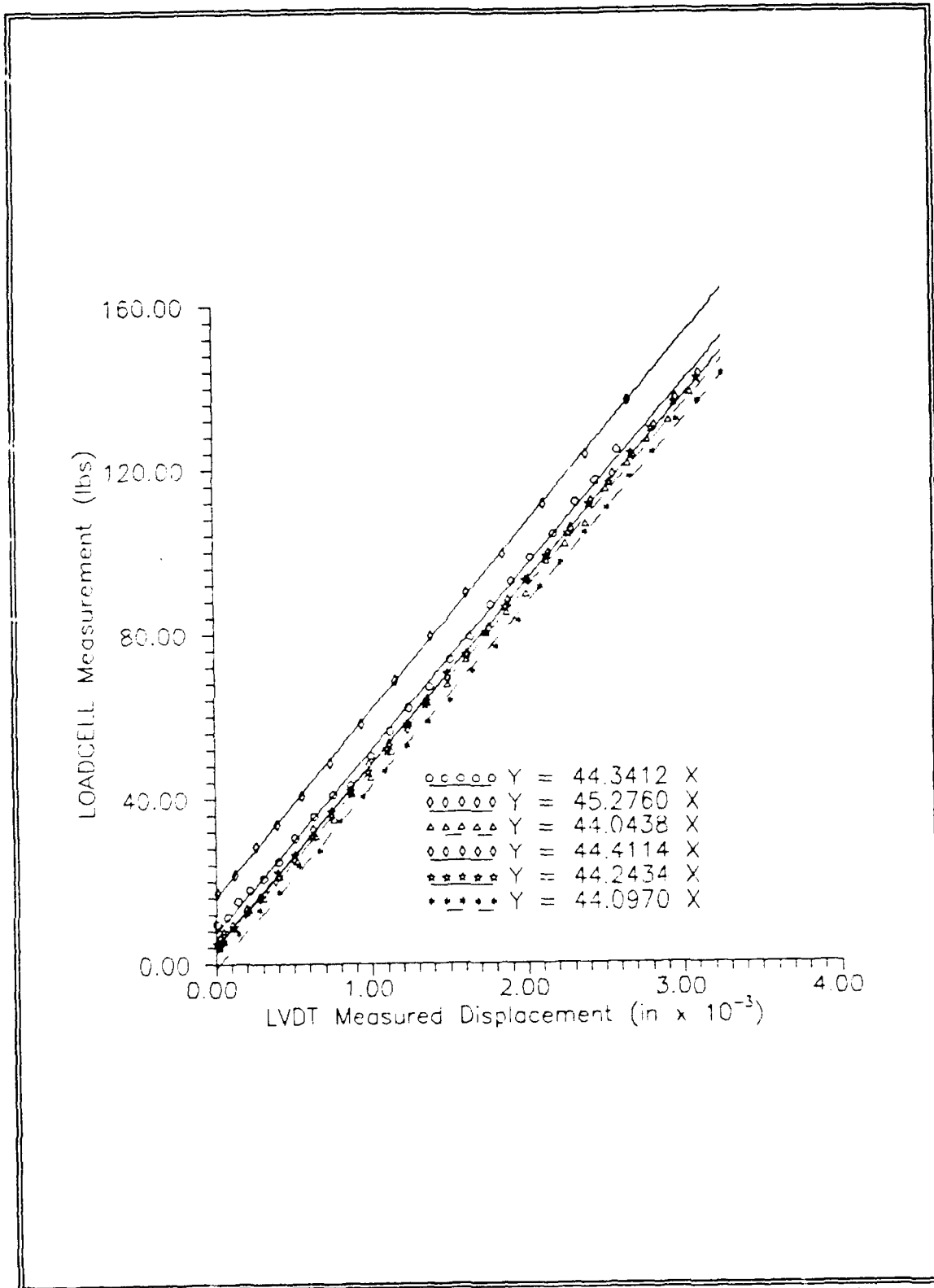
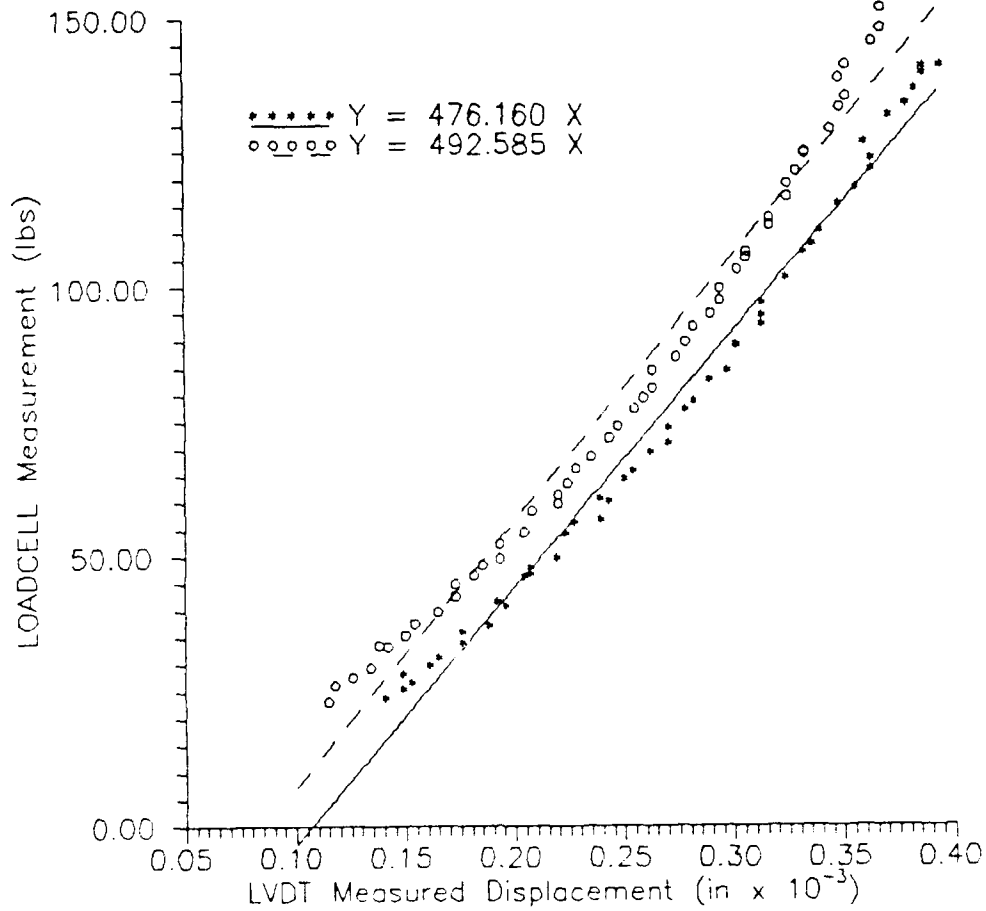


Figure 17 Load-Displacement Curves for Specimen 714 with No Crack Present



LVDT MEASUREMENT vs. LOAD MEASUREMENTS
FOR THE TEST SETUP USING NICALON SAMPLE

Figure 18 Load-Displacement Curves of Nicalon Test Sample Used to Determine Machine Test Setup Compliance

The next step in determining a value of Young's Modulus was to find the compliance from the test data obtained. The compliance was calculated using Equation 2 where δ is the deflection of the midpoint and P, the applied load.

$$C = \frac{\delta}{P} \quad (2)$$

This value is the inverse of the slope of the load-deflection curve and does not compensate for the bending of the test fixture. Although the curve of the test setup compliance is not exactly linear, a linear approximation based upon an average linear best fit line produces an error of only 1% in comparison to the compliance of test specimens. This approximation was deemed an acceptable error without compromising the objectives of this study. To compensate for the deflection of the test setup, the experimentally determined compliance value was decreased by the amount of compliance of the test setup. This is shown in Equation 3.

$$C_{\text{experimental}} = C_{\text{observed}} - C_{\text{testsetup}} \quad (3)$$

The computed values of compliance were then used in Equation 1 to determine the experimental values for Young's Modulus, E_{11} . The results of these calculations are shown in Table 2.

The values for E_{11} were then averaged which produced a value of 1.5953×10^7 lbs/in². This value of E_{11} is within 10% of the expected value based on previous studies of this type

Table 2 Computed Values of Young's Modulus

| Specimen Number | Slope $\times 10^3$ lbs/in | Young's Modulus $\times 10^7$ lb/in |
|-----------------|-------------------------------|--|
| 90C0713-1 | 42.2573 | 1.525 |
| 713-2 | 42.4517 | 1.533 |
| 713-3 | 44.8491 | 1.630 |
| 713-4 | 43.2621 | 1.565 |
| 713-5 | 43.3650 | 1.569 |
| 713-6 | 43.5116 | 1.575 |
| 90C0714-1 | 44.3412 | 1.623 |
| 714-2 | 45.2760 | 1.662 |
| 714-3 | 44.0438 | 1.611 |
| 714-4 | 44.4114 | 1.626 |
| 714-5 | 44.2434 | 1.619 |
| 714-6 | 44.0970 | 1.613 |

composite material indicating that the modifications made to the test setup did not have a detrimental effect.

LVDT Compliance Calculations

With the average value of E_{11} established, Russell's Equation (Equation 1) could be used to determine the compliance of specimen's containing cracks at the midplane. Although all the specimens were approximately the same size, the variances in height and width were accounted for by normalizing the compliance using an equation developed by Mol (15).

$$C_{Normalized} = C_{Experimental} \left(\frac{b}{0.1} \right) \left(\frac{2h}{0.3} \right)^3 \quad (4)$$

After being normalized, the experimentally determined values of compliance were then plotted for non-dimensional crack lengths to compare with Russell's theoretical relationship. The crack length was non-dimensionalized by dividing the measured crack length by the half span between the rollers (0.75"). Figure 19 graphically displays the comparison of Russell's theoretical values and the normalized compliance values. Table 3 shows the specimen LVDT compliance data obtained in this study.

In comparison to Russell's theoretical values, the data correlates well for the non-dimensional crack lengths below 0.65 but appears lower for larger crack lengths. The scatter of data below Russell's curve for non-dimensional crack lengths beyond 0.6 is consistent with the trends experienced by Vozzola (14:35), Mol (15:43), and Hoobler (16:47) for room temperature tests and indicates a discrepancy between the

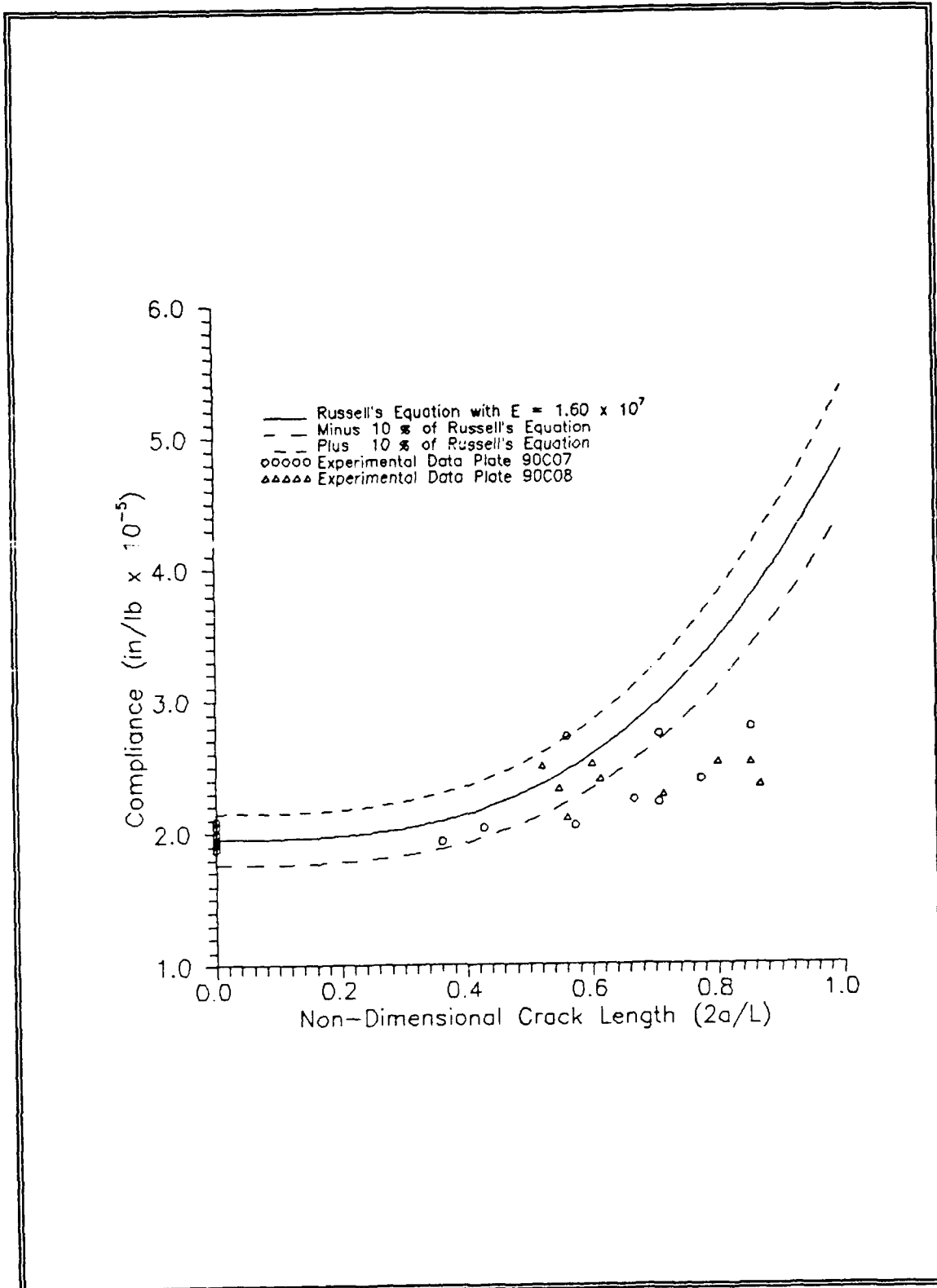


Figure 19 Comparison of Russell's Beam Theory and Experimental Compliance Values

Table 3 Specimen LVDT Compliance Data

| Specimen Number | Non-Dimensional Crack Length | Normalized Compliance ($\times 10^{-5}$ in/lbs) |
|-----------------|------------------------------|---|
| 90C0703-1 | 0.507 | 2.668 |
| 703-2 | 0.707 | 2.739 |
| 705-1 | 0.427 | 2.033 |
| 705-2 | 0.667 | 2.239 |
| 707-1 | 0.360 | 1.937 |
| 707-2 | 0.707 | 2.219 |
| 708-1 | 0.573 | 2.049 |
| 708-2 | 0.773 | 2.400 |
| 710-1 | 0.560 | 2.719 |
| 710-2 | 0.853 | 2.792 |
| 90C0803-1 | 0.520 | 2.497 |
| 803-2 | 0.600 | 2.515 |
| 803-3 | 0.787 | 2.522 |
| 804-1 | 0.547 | 2.327 |
| 804-2 | 0.613 | 2.398 |
| 805-1 | 0.713 | 2.283 |
| 805-2 | 0.852 | 2.521 |
| 806-1 | 0.560 | 2.109 |
| 806-2 | 0.867 | 2.354 |

theoretical and experimental compliance. This lack of correlation may be due in part to an increased interaction of the two fracture surfaces and the deviation from pure Mode II fracture.

To explore the effect of shear deformation, a second approach to calculate the fracture toughness of the material was examined. An extension to Russell's basic beam theory equation was developed by Carlsson (22) which included a term for the shear deformation. According to Carlsson, the compliance of the end notched flexure specimen is given as:

$$C = \frac{\delta}{P} = \frac{(2L^3+3a^3)}{(8E_{11}bh^3)} \left[1 + \frac{2(1.2L + 0.9a)h^2E_{11}}{(2L^3+3a^3)G_{13}} \right] \quad (5)$$

where a is the crack length; b , the base thickness; h , the beam half height; L , half the fixed length between rollers; E_{11} , the flexure modulus; and G_{13} , the interlaminar shear modulus. A previously experimentally determined value of 5.801×10^6 lb/in (40 GPa) was used for G_{13} for the interlaminar shear modulus of CGW 1723 with SiC fibers. Equation 5 was first used to re-evaluate the value for E_{11} using the compliance values for the specimens run without any precracks. This produced an adjusted value of 1.842×10^7 lb/in for E_{11} , 15% higher than the value obtained without the shear deformation term. The ratio of G_{13} to E_{11} was 1:3.175 which is in the acceptable range for this type of composite material suggesting the given value for G_{13} was a valid

estimate. The theoretical curve for Carlsson's extended equation is shown in Figure 20 along with the actual test data and Russell's beam theory model. The curve generated from Carlsson's extension is very close to the theoretical curve from Russell's beam theory illustrating the additional shear term has very little influence on the compliance of the composite used in this study.

Critical Load

The load required for a crack to grow, P_{cr} , was the final parameter needed to calculate the fracture toughness of the material based upon an equation developed by Russell (2).

$$G_{IIC} = \left(\frac{P_{cr}^2}{2b} \right) \left(\frac{\partial C}{\partial a} \right) \quad (6)$$

When simple linear beam theory is applied, the relationship developed by Russell for theoretical compliance, Equation 1, becomes

$$G_{IIC} = \frac{9P_{cr}^2 a^2}{16b^2 E_{11} h^3} \quad (7)$$

where G_{IIC} is the fracture toughness; P_{cr} , the critical load; a , the crack length; b , the thickness of the specimen; and h , the height to the midplane of the specimen.

In previous studies, the value for P_{cr} was determined by examining the load-displacement curve generated at the center of the specimen for the point of non-linearity. Determining

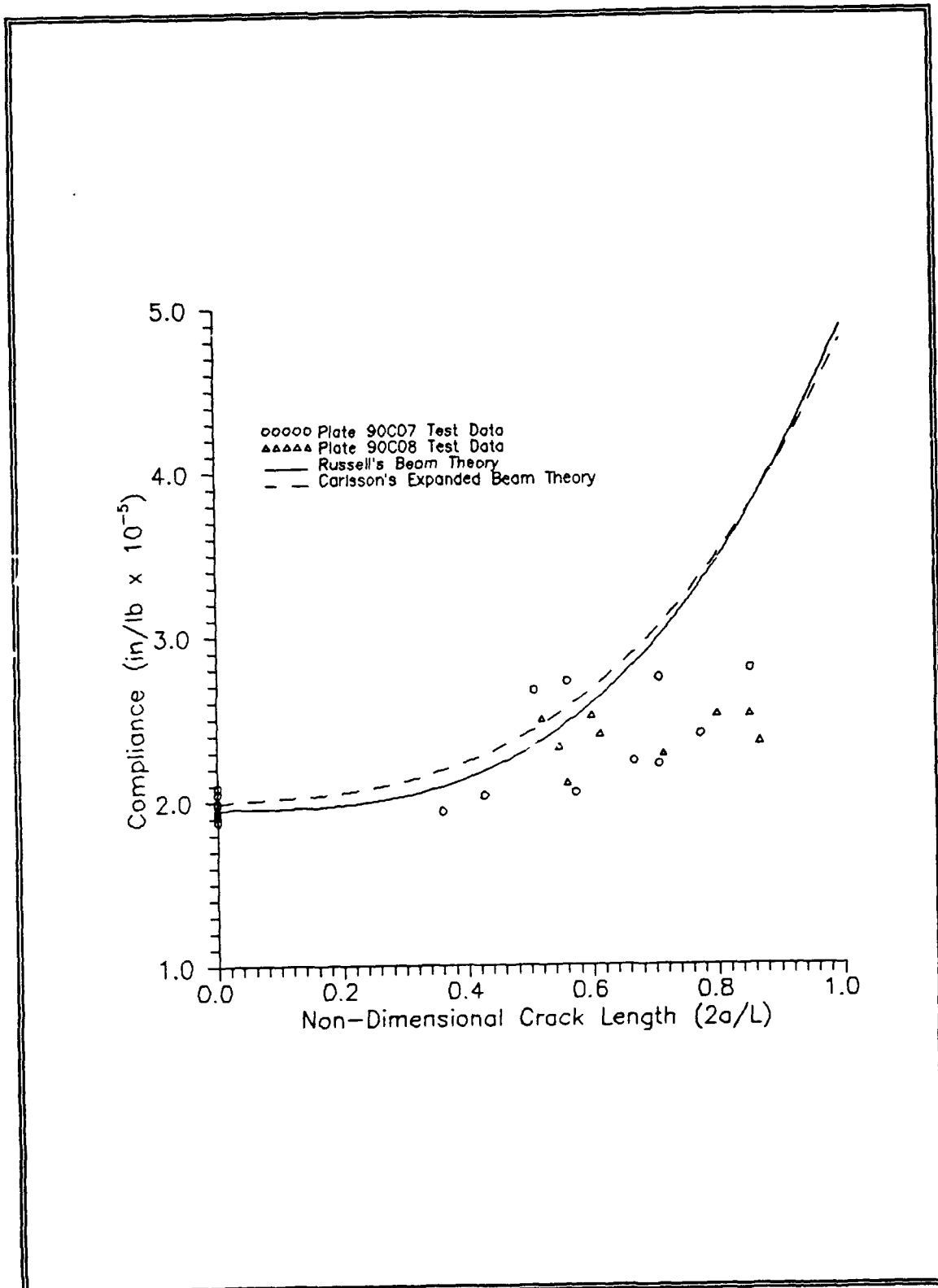


Figure 20 Comparison of Russell's Beam Theory Model and Carlsson's Extension with Actual Test Data

the point where the curve deviated from a straight line was often ambiguous and covered a sizable load range causing a substantial margin of error. An example of this is shown in Figure 20. Incorporation of the laser IDG to create a load-COD curve attempted to fine tune the determination of the critical load beyond what was available from the center mounted LVDT. Figures 21 and 22 show the data obtained from typical test runs. Although there is not a distinct point on either the LVDT or LIDG curve where the non-linearity is apparent, the range of deviation from a straight line is much smaller on the LIDG curve than on the LVDT curve. The critical load was extracted from the LIDG curve with high accuracy by using the 5% less secant line proposed in ASTM E399 Standard.

The quality of reflective indents had a direct influence over the quality of LIDG data obtained. When the indents were not of the highest quality, the laser IDG would not produce a consistent curve. Figure 23 displays a test run where the LIDG was not able to track on the fringes generated by reflection off the indents throughout the entire loading phase. In this illustration, the laser IDG lost track at a load of about 45 pounds but was able to latch onto a different set of fringes and still monitor the COD. For cases such as these, the curve was still examined for a point of non-linearity at a higher load but the data were considered suspect.

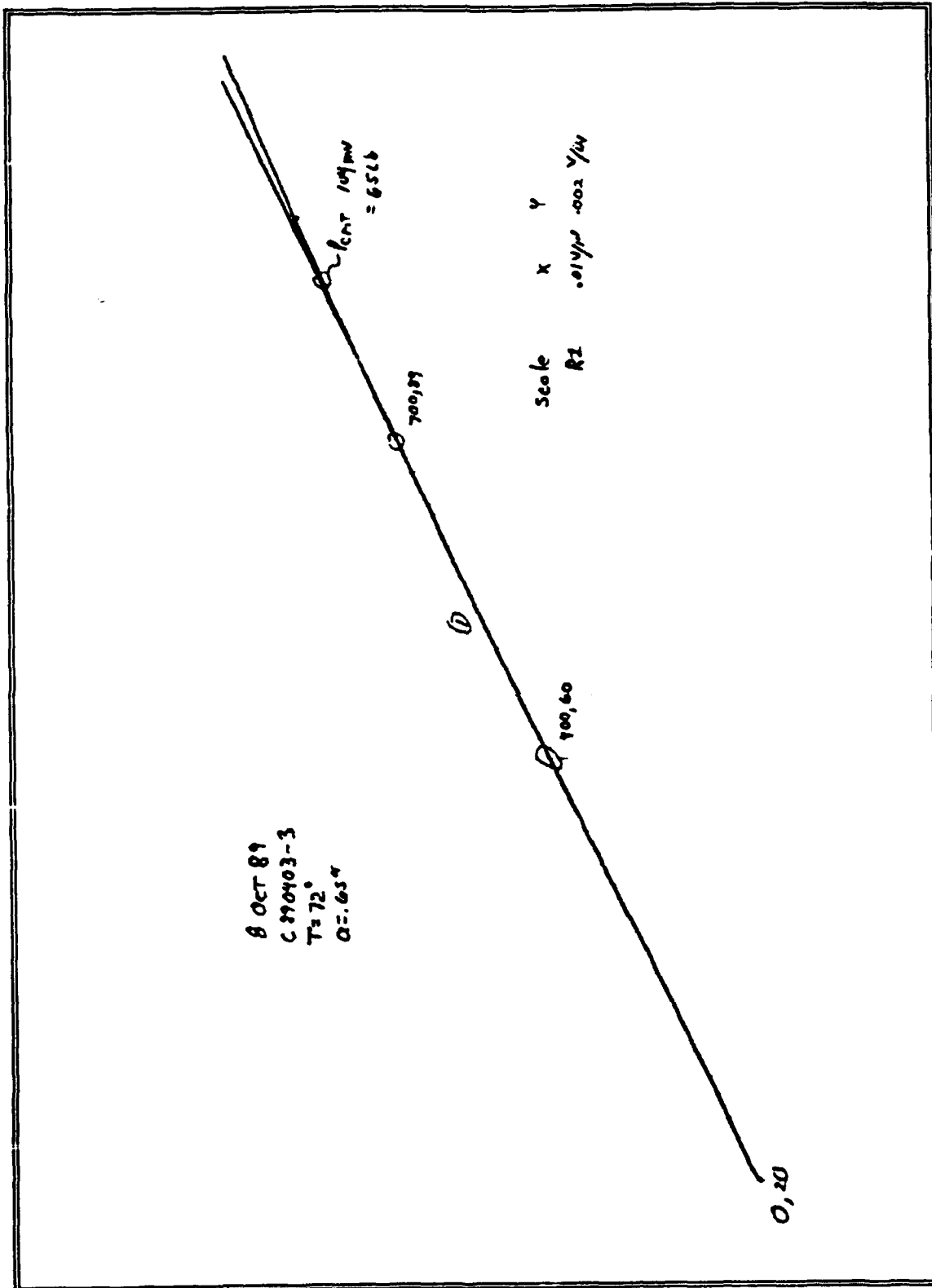
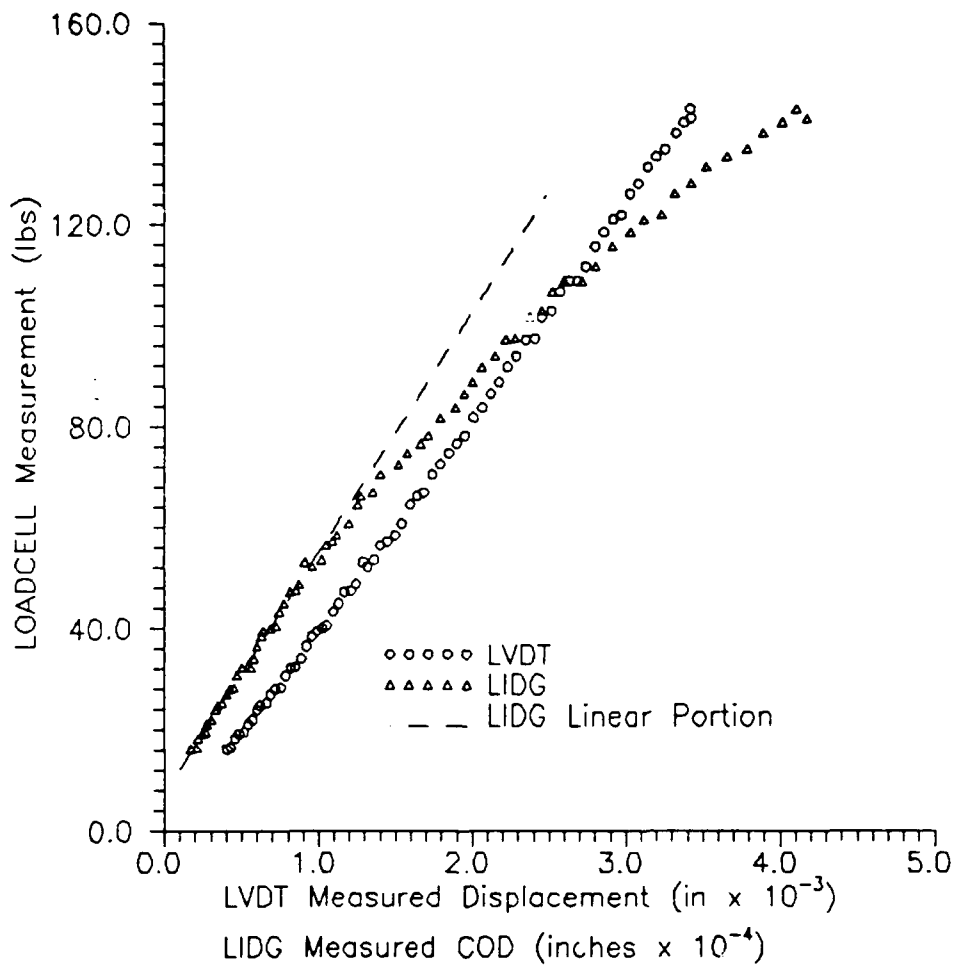


Figure 21 Determination of Critical Load Using Only LVDT Curve on an X-Y Recorder



Typical Test Run Data

Figure 22 Typical Data from a Test Run

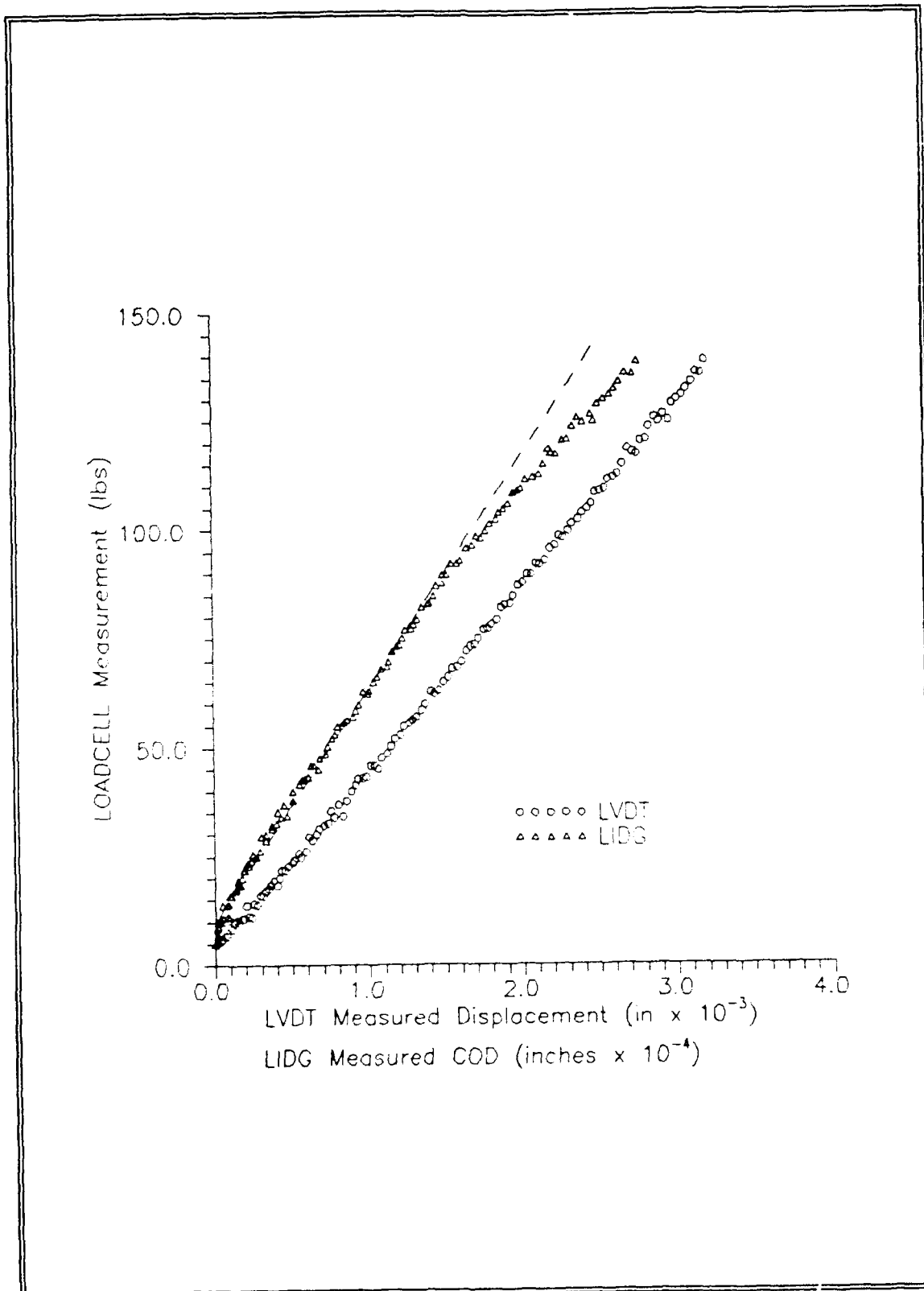


Figure 23 Second Example of Typical Test Run Data

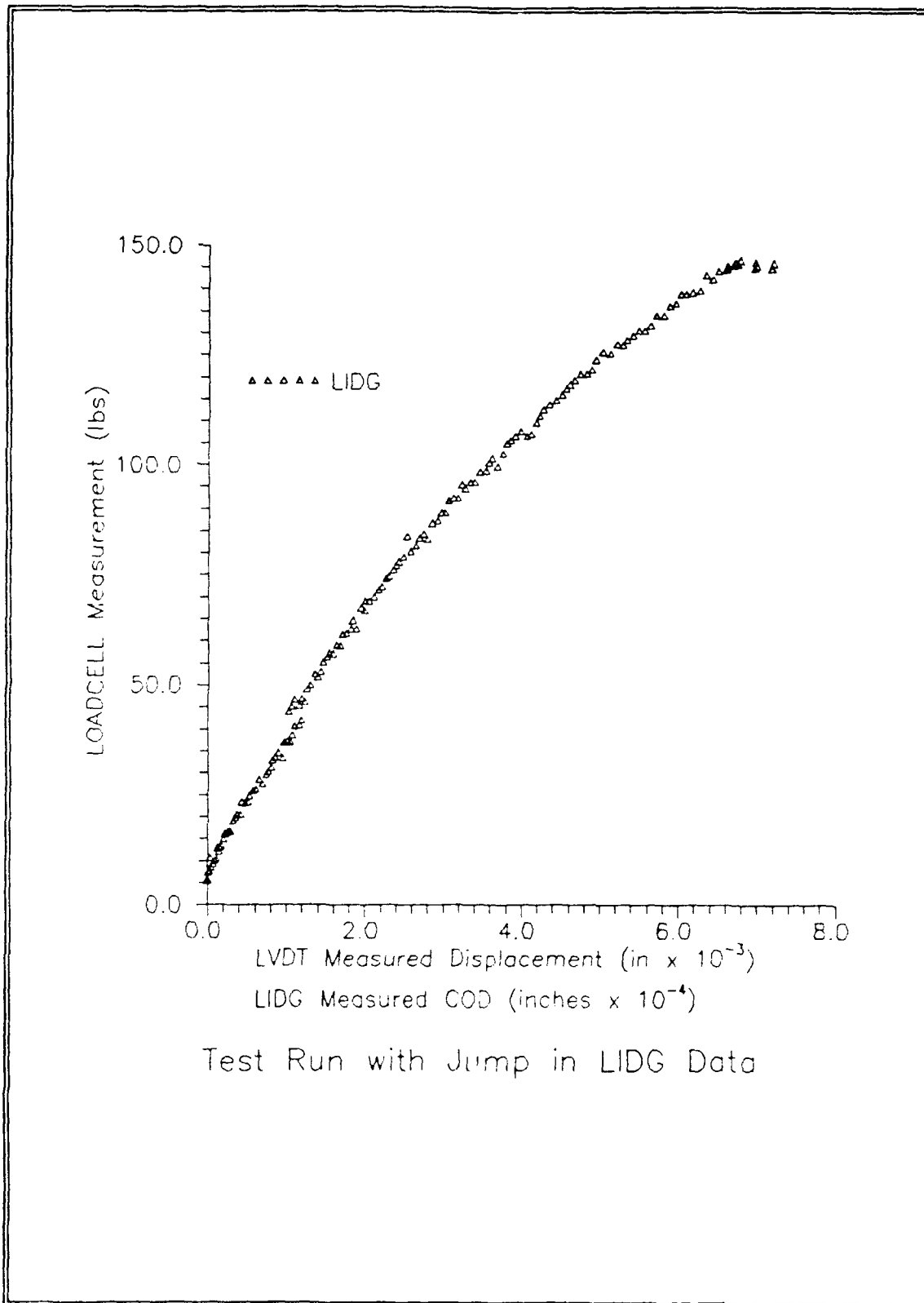


Figure 24 Test Run Without Top Quality Indents

The critical load test results are summarized in Table 4. The critical load is also plotted as a function of non-dimensional crack length in Figure 25. The second-order polynomial curve fit was expected and yielded a straight line with slope of -1 as seen in Figure 26 when plotted on log-log scales. This corresponds directly to the theoretical relationship for a constant value of fracture toughness.

Fracture Toughness

The primary goal of this study was to examine if the incorporation of a laser IDG would enhance the determination of fracture toughness. All the variables needed to determine G_{IIC} from Russell's theoretical relationship, Equation 6, were determined for each specimen as described earlier in this chapter. Employing Equation 7, repeated here, the value of G_{IIC} was calculated for each specimen.

$$G_{IIC} = \frac{9P_{cr}^2 a^2}{16b^2 E_{11} h^3} \quad (7)$$

The results of these calculations are presented in Table 5 and graphically displayed in Figure 27. The average value of 1.691 lb/in is within 1% of the average value of 1.698 lb/in obtained by Mol at room temperature using a similar test setup (15:65). Although the plate fabrication process rarely yields plates of such similarity, the comparable average values of fracture toughness at room temperature helps to verify the

Table 4 Critical Load Data

| Specimen Number | Non-dimensional Crack Length | Critical Load (lbs) |
|--------------------|---------------------------------|------------------------|
| 90C0703-1 | 0.507 | 105 |
| 703-2 | 0.707 | 76 |
| 705-1 | 0.427 | 118 |
| 705-2 | 0.667 | 75 |
| 707-1 | 0.360 | 135 |
| 707-2 | 0.707 | 70 |
| 708-1 | 0.573 | 92 |
| 708-2 | 0.773 | 68 |
| 710-1 | 0.560 | 90 |
| 710-2 | 0.853 | 58 |
| 90C0803-1 | 0.520 | 90 |
| 803-2 | 0.600 | 82 |
| 803-3 | 0.787 | 60 |
| 804-1 | 0.547 | 95 |
| 804-2 | 0.613 | 85 |
| 806-1 | 0.560 | 95 |
| 806-2 | 0.867 | 62 |

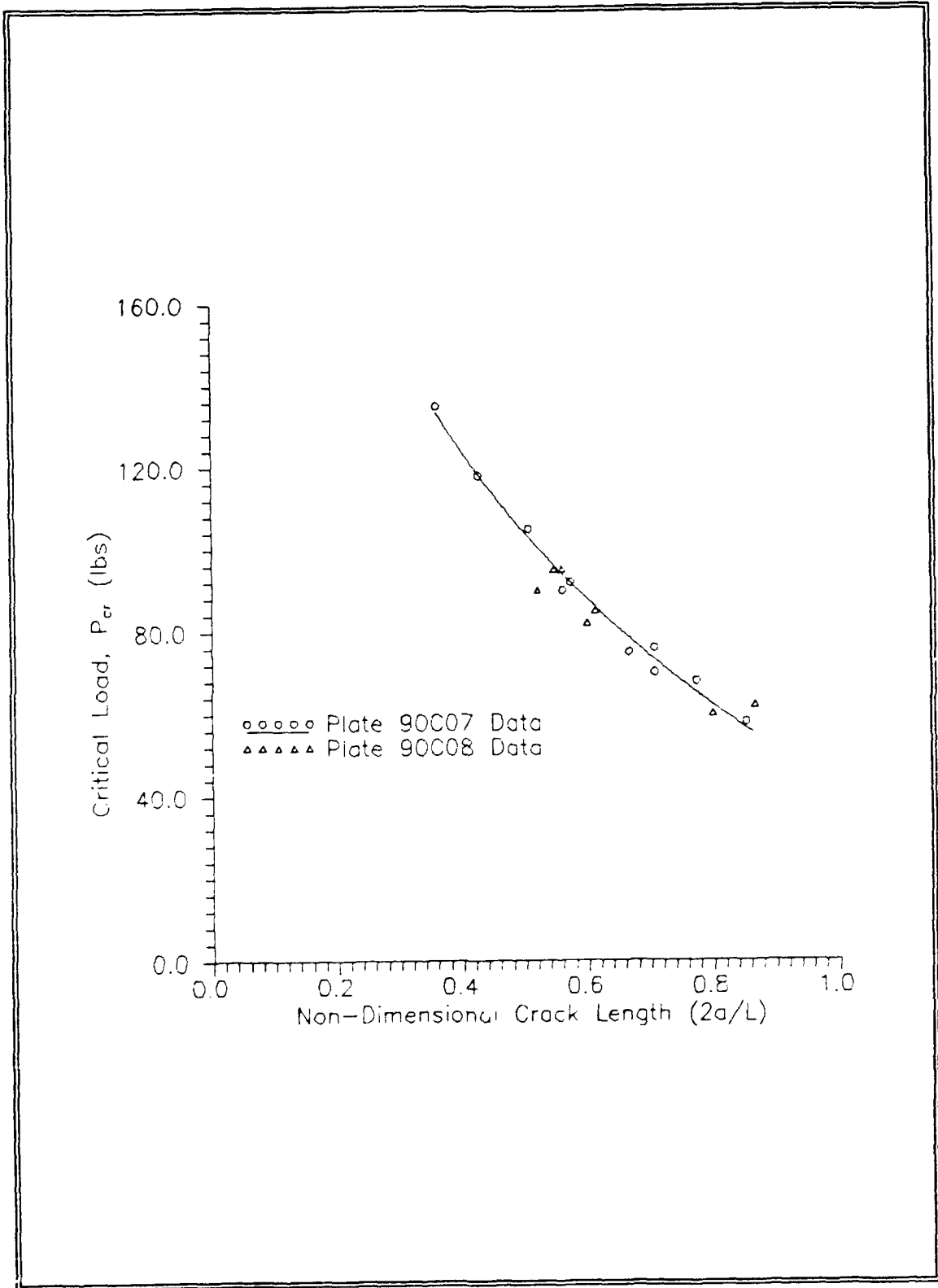


Figure 25 Critical Load of Test Specimens Verses Non-Dimensional Crack Length

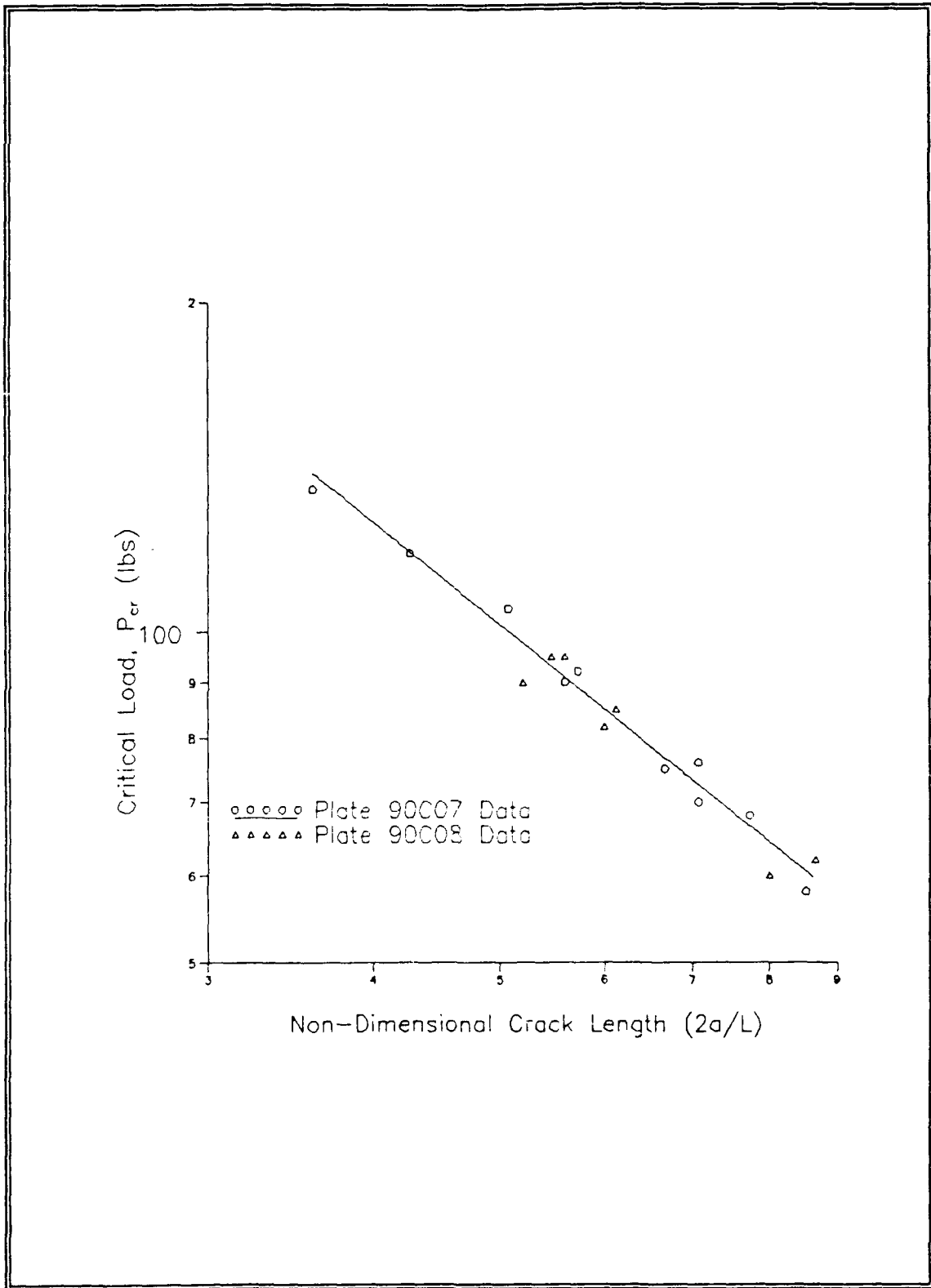


Figure 26 Critical Load of Test Specimens Verses Non-Dimensionalized Crack Length on Log-Log Scales

Table 5 Calculated Values of Fracture Toughness Based on Russell's Beam Theory

| Specimen Number | Non-dimensional Crack Length | Fracture Toughness (G_{IIc}) (lbs/in) |
|-----------------|------------------------------|---|
| 90C0703-1 | 0.507 | 1.592 |
| 705-1 | 0.427 | 1.701 |
| 707-1 | 0.360 | 1.625 |
| 708-1 | 0.573 | 1.725 |
| 710-1 | 0.560 | 1.783 |
| 90C0803-1 | 0.520 | 1.653 |
| 803-2 | 0.600 | 1.827 |
| 804-1 | 0.547 | 1.675 |
| 804-2 | 0.613 | 1.688 |
| 806-1 | 0.560 | 1.677 |

results of the laser IDG in determining the critical load.

A second approach to calculate the fracture toughness of the material was also examined. This method used the extension developed by Carlsson (22) which included a term for the shear deformation discussed earlier in this chapter. Carlsson's equation is repeated here for convenience. The

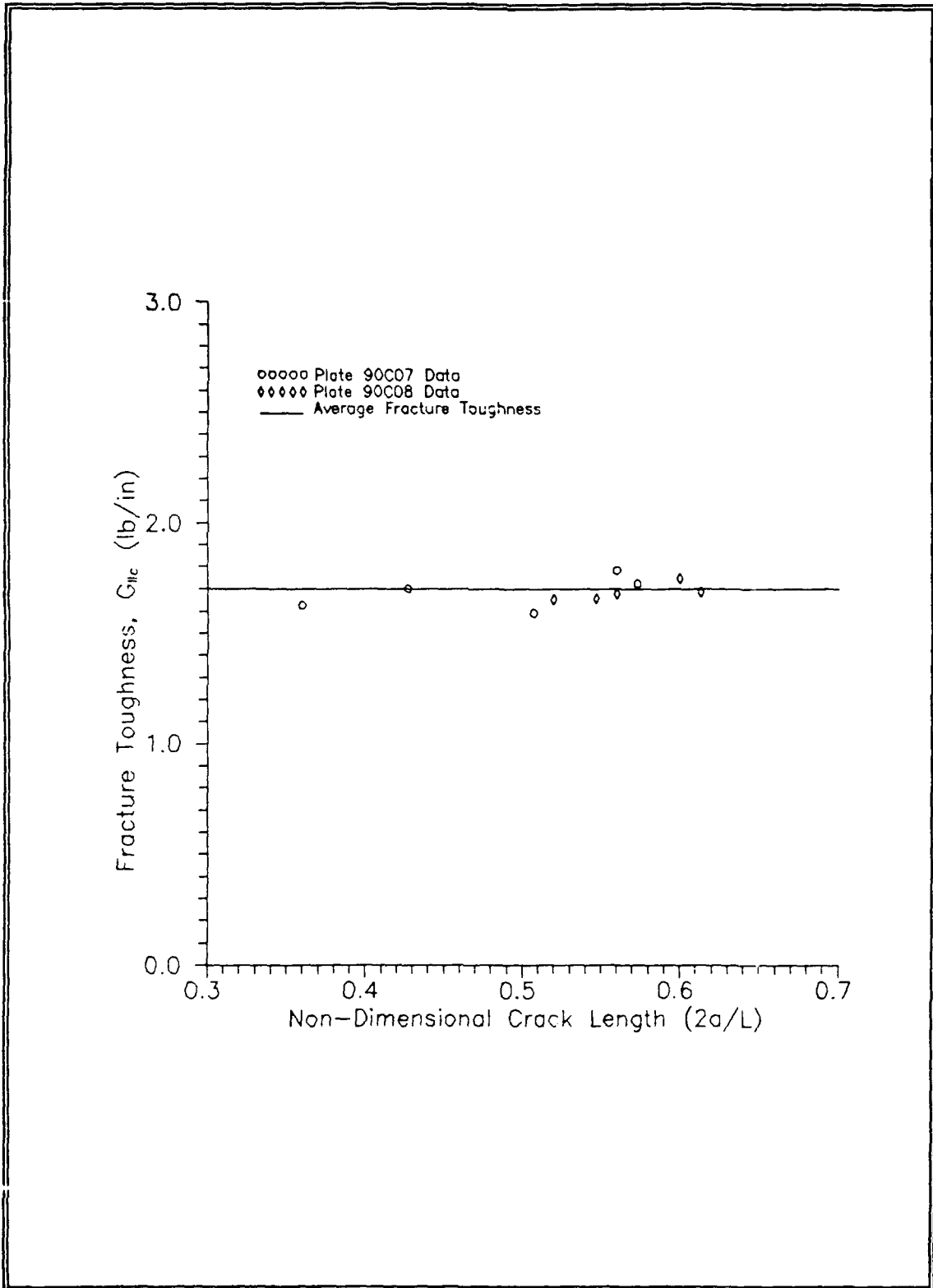


Figure 27 Calculated Values of G_{IIc} Based on Russell's Beam Theory

compliance of the end notched flexure specimen is given as:

$$C = \frac{\delta}{P} = \frac{(2L^3+3a^3)}{(8E_{11}bh^3)} \left[1 + \frac{2(1.2L + 0.9a)h^2E_{11}}{(2L^3+3a^3)G_{13}} \right] \quad (6)$$

where a is the crack length; b , the base thickness; h , the beam half height; L , half the fixed length between rollers; E_{11} , the flexure modulus; and G_{13} , the interlaminar shear modulus. As mentioned earlier, a value of 5.801×10^6 lb/in (40 GPa) was used for G_{13} in all calculations for the interlaminar shear modulus of CGW 1723 with SiC fibers. A modified value of 1.842 lb/in was used for E_{11} based on the calculations with the crack length set at 0.0 in this equation.

From Equation 5, it follows mathematically that,

$$\frac{\partial C}{\partial a} = \frac{9a^2}{8E_{11}bh^3} \left[1 + 0.2 \left(\frac{E_{11}}{G_{13}} \right) \left(\frac{h}{a} \right)^2 \right] \quad (8)$$

When applied to Russell's expression for beam compliance,

$$G_{IIC} = \left(\frac{P_{cr}^2}{2b} \right) \left(\frac{\partial C}{\partial a} \right) \quad (5)$$

the following equation is produced.

$$G_{IIC} = \frac{9P_{cr}^2a^2}{16b^2E_{11}h^3} \left[1 + 0.2 \left(\frac{E_{11}}{G_{13}} \right) \left(\frac{h}{a} \right)^2 \right] \quad (9)$$

This equation utilizes the material properties as well as the specimen geometry to produce the Mode II fracture toughness.

The calculated values for the test specimens are presented in Table 6 and shown graphically in Figure 28. The use of Carlsson's extension to Russell's beam theory expression yielded an average fracture toughness value of 1.648 in/lbs for the composite material tested which is within 10% of the value obtained neglecting the shear deformation.

LIDG Compliance Calculations

The LIDG data was used primarily to help determine the onset of crack growth initiation but also provided a curve which could be used to correlate to the existing crack length. The compliance for the LIDG was calculated directly from the observed compliance. The LVDT compliance needed to compensate for the test setup deflection however the laser IDG measured displacement of the tabs relative to one another. Assuming the LIDG experimental compliance was also a function of specimen geometry, the LIDG compliance was normalized to account for the small variances in specimen dimensions in the same way as the LVDT had been using Equation 4, repeated here.

$$C_{Normalized} = C_{Experimental} \left(\frac{b}{0.1} \right) \left(\frac{2h}{0.3} \right)^3 \quad (4)$$

The normalized compliance values obtained from the laser IDG are presented in Table 7 and shown plotted verses non-dimensional crack length in Figure 29. The curve shows the same basic trend as found by Giare (9:15) and indicates that a relationship can be developed to link existing crack length

Table 6 Calculated Values of Fracture Toughness Based on Carlsson's Extension of Russell's Beam Theory

| Specimen Number | Non-dimensional Crack Length | Fracture Toughness (G_{IIc}) (lbs/in) |
|-----------------|------------------------------|---|
| 90C0703-1 | 0.507 | 1.548 |
| 705-1 | 0.427 | 1.702 |
| 707-1 | 0.360 | 1.723 |
| 708-1 | 0.573 | 1.649 |
| 710-1 | 0.560 | 1.710 |
| 90C0803-1 | 0.520 | 1.598 |
| 803-2 | 0.600 | 1.731 |
| 804-1 | 0.547 | 1.610 |
| 804-2 | 0.613 | 1.597 |
| 806-1 | 0.560 | 1.607 |

0

to COD compliance values. A second order equation was generated to match the compliance data which yielded Equation 9.

$$Y = 14.145 X^2 - 9.416 X + 2.48 \quad (9)$$

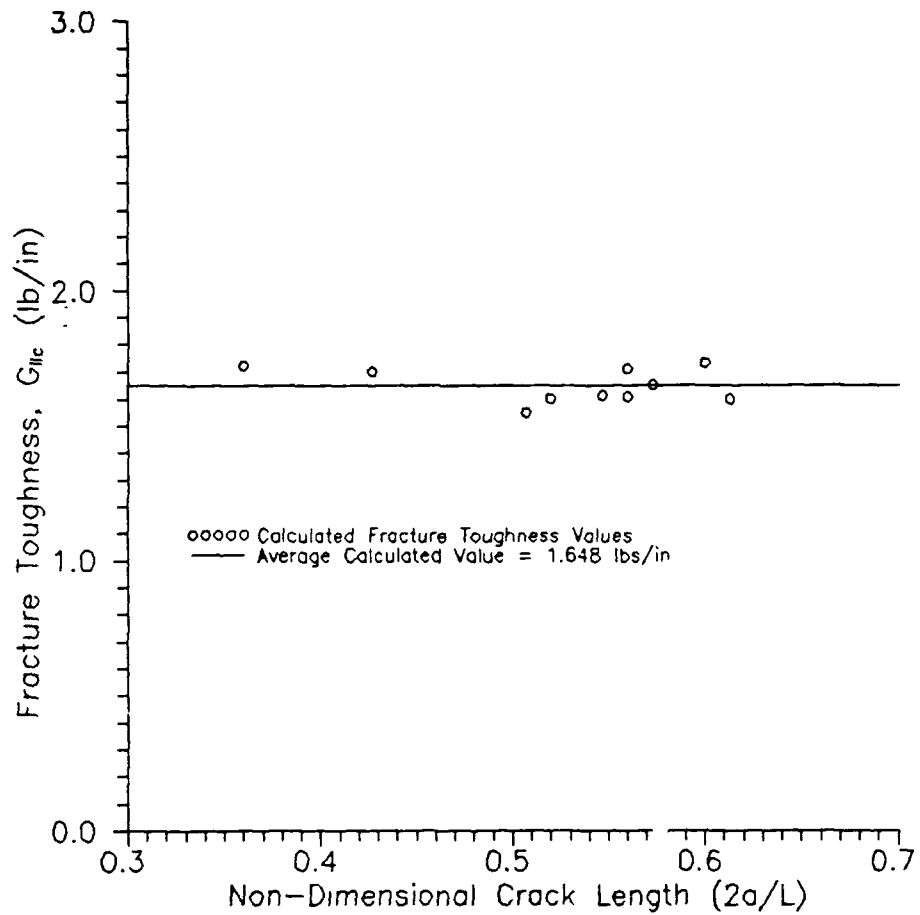


Figure 28 Calculated Values of G_{IIc} Based on Carlsson's Extension of Russell's Beam Theory

Table 7 Laser IDG Specimen Compliance Data

| Specimen Number | Non-Dimensional Crack Length | Normalized Compliance (x 10 ⁻⁵ in/lbs) |
|-----------------|------------------------------|--|
| 703-2 | 0.707 | 3.991 |
| 705-1 | 0.427 | 1.431 |
| 705-2 | 0.667 | 1.994 |
| 707-1 | 0.360 | 1.276 |
| 707-2 | 0.707 | 3.051 |
| 708-1 | 0.573 | 1.083 |
| 708-2 | 0.773 | 3.121 |
| 710-1 | 0.560 | 2.257 |
| 710-2 | 0.853 | 4.437 |
| 90C0803-1 | 0.520 | 1.669 |
| 803-2 | 0.600 | 1.383 |
| 803-3 | 0.787 | 3.895 |
| 804-1 | 0.547 | 1.480 |
| 804-2 | 0.613 | 2.042 |
| 806-1 | 0.560 | 1.843 |
| 806-2 | 0.867 | 5.228 |

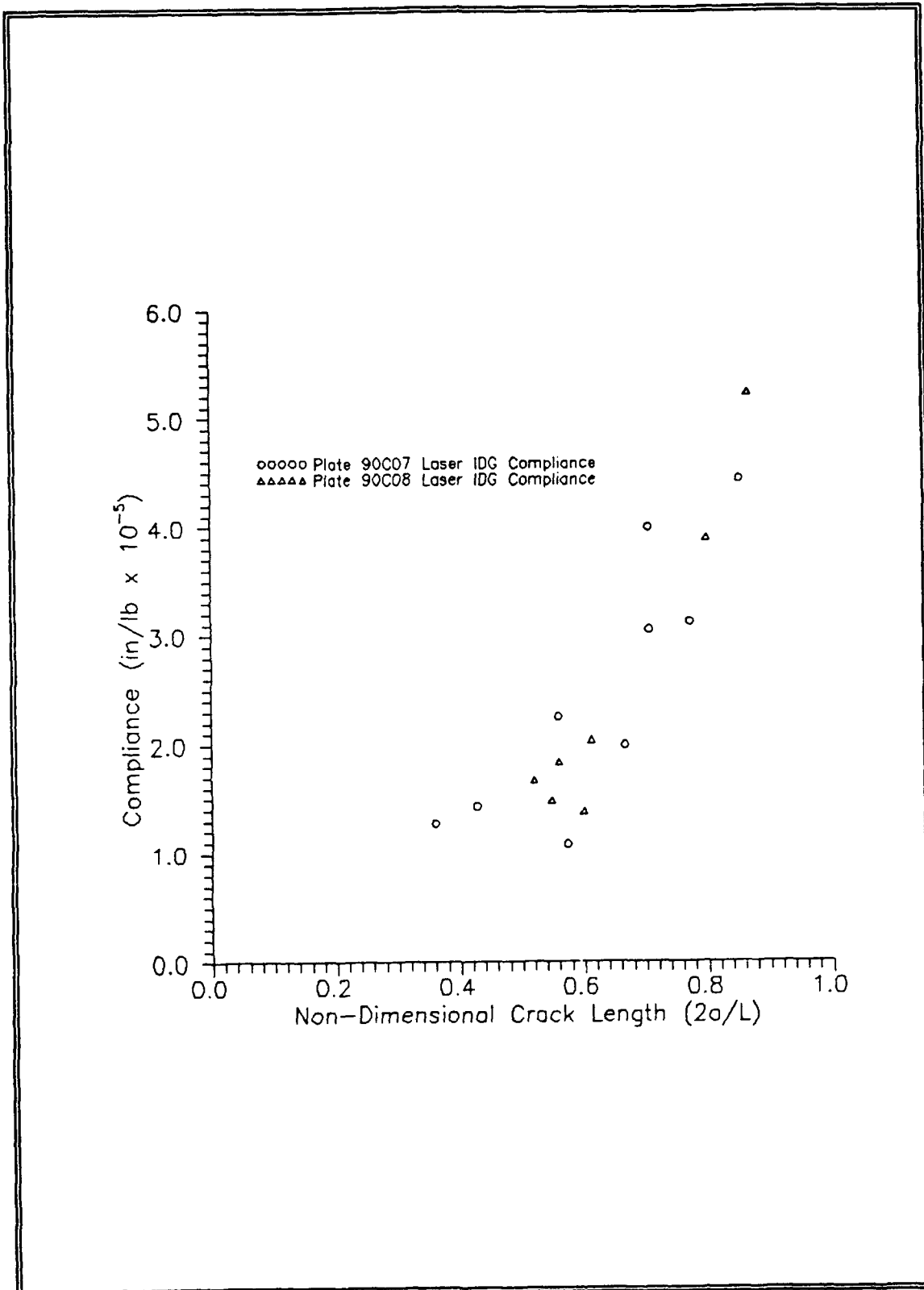


Figure 29 Laser IDG Compliance Curve

A third order curve fit was also computer generated for the LIDG compliance crack length relationship and is given in Equation 10.

$$Y = -7.4 X^3 + 27.76 X^2 - 17.43 X + 3.98 \quad (10)$$

These curve are shown plotted against the actual test data in Figure 30.

Post-Mortem Examination

After a specimen had been tested to its useful limits, it was separated into two halves by subjecting it to Mode I failure in the precracking jig. The fracture surfaces were then examined under varying powers of magnification to verify correlation between the pencil marks made during the testing to the differences in fracture surfaces. Often the transition from Mode I to Mode II occurred over a range of 0.02 inches. An example of this transition is shown in Figure 31. In the few cases where the location of the pencil mark differed from the fiber transition on the test specimen, the test data for the suspect crack length was considered suspect and the data from that test point not used.

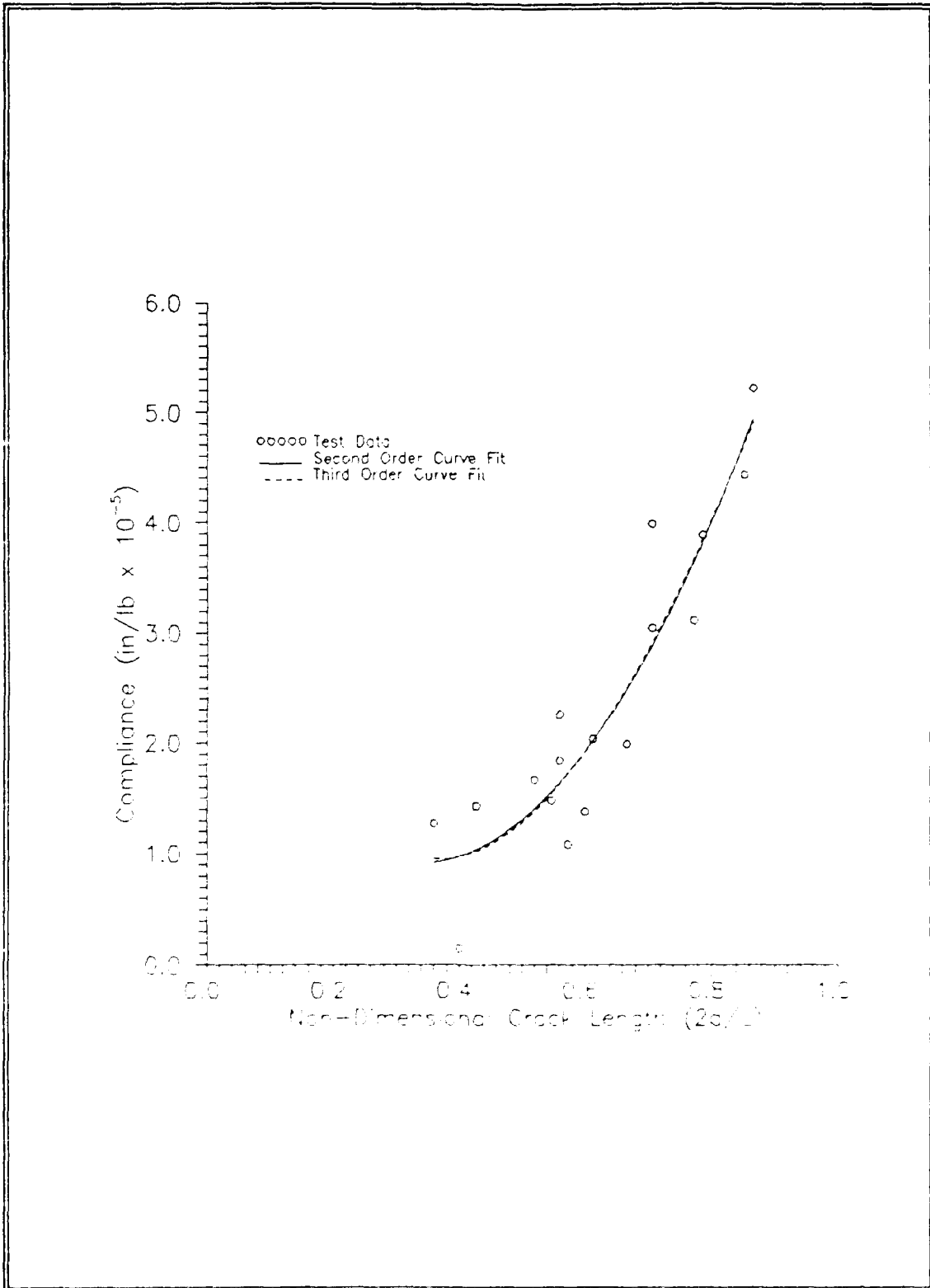


Figure 30 Laser IDG Compliance Curve with Second and Third Order Curves

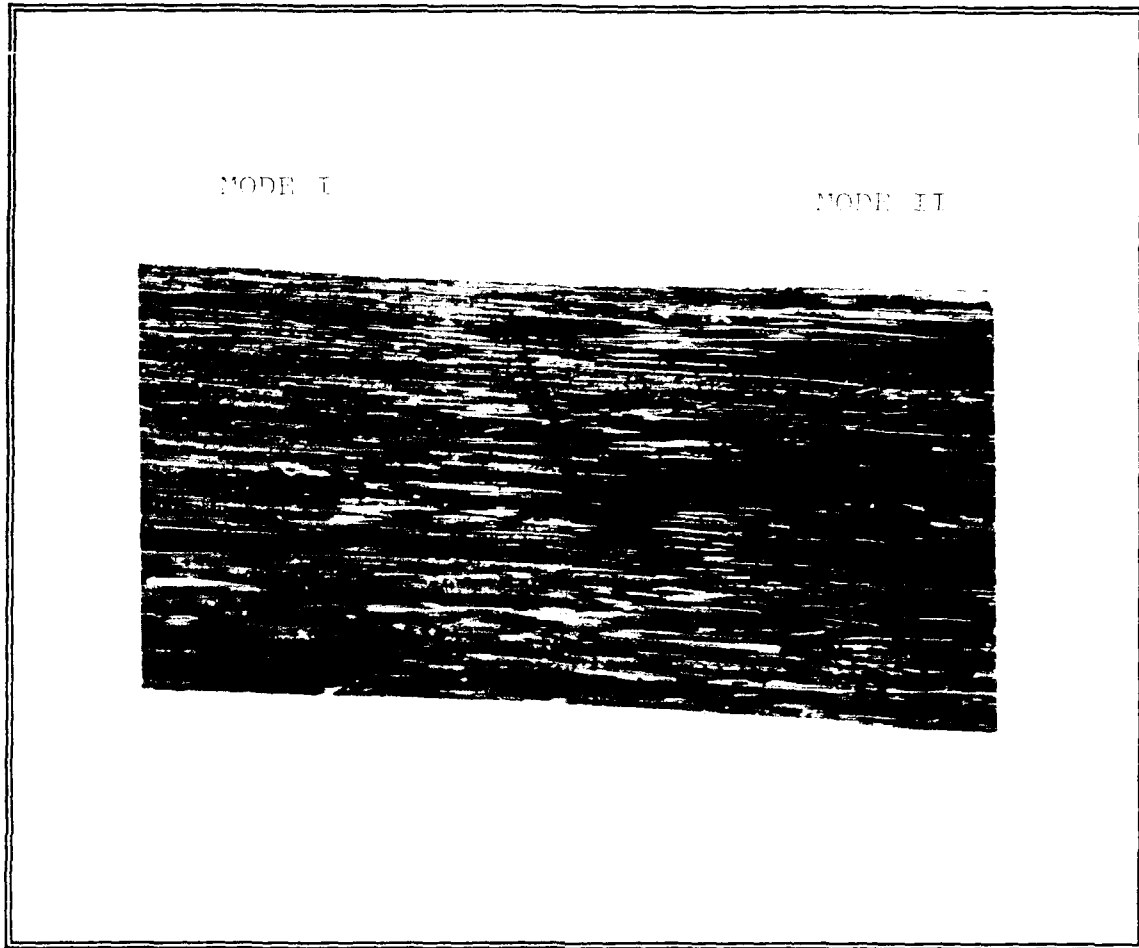


Figure 31 Transition from Mode I to Mode II Fracture on a Test Specimen Magnified 20 X

VI. Conclusions and Recommendations

The primary goal of this study was to determine if laser interferometry would be a viable procedure to incorporate into the Mode II testing of composite materials on a three point bend fixture to extract more accurate test data. This study pursued the use of the established three-point-bend test fixture with an end-notched flexure specimen rather than exploring other test fixtures and specimen geometries. This attempt to monitor the COD of a CGW 1723 ceramic composite used indented reflective tabs mounted on the test specimen provided substantially better test data to identify the onset of crack growth than was previously obtained. Several conclusions and recommendations for future testing have come forth as a result of this study.

Conclusions

The following conclusions can be made as a result of the findings of this study:

- 1) The incorporation of a laser IDG with test specimens undergoing a three point bend load is a viable option to produce a more precise determination of the onset of crack growth. The ability to identify the point of critical load using the laser IDG provided a mechanism to estimate the fracture toughness of a composite material with a greater degree of accuracy than was previously accomplished relying

solely on the measurement of the deflection of the load point using an LVDT.

2) The techniques described in this thesis to prepare a large number of reflective tabs substantially reduced the total preparation time and should be employed for testing requiring more than 10 tabs. Polishing the tabs to eliminate surface scratches, voids, and edge abnormalities to less than one (1) micron was more than sufficient to reduce false fringes from being generated.

3) The use of stainless steel for the tab material instead of titanium should be encouraged because titanium adheres to the diamond indenter and produced unclean indents after each set of indents had been made. Marginal indents were more likely to be unable to be tracked during loading and caused ambiguous COD-load curves.

Recommendations

Several recommendations for further study can be made based upon the experiences encountered during this study.

1) The test fixture should be modified to provide a more exact placement of the specimen on the rollers. The traveling microscope used in conjunction with the pre-cracking jig establishes the distance from the space between the reflective tabs to the precrack tip very well. However, positioning the specimen on the test fixture rollers such that the space

between the tabs is directly above the center of a roller is not exact and induces an error in the testing precrack length.

2) A computer software program should be written which allows the data acquisition to be accomplished on the same computer that runs the laser IDG conversion. This would permit a more consolidated operation and free up an expensive asset.

3) The effect of the deviation of the precrack from the midplane of the specimen should be examined. Although the initial precrack was placed as close to the midplane of the specimen as possible, some variance was observed. This variance was even more pronounced for the second and subsequent tests run on each specimen after the Mode II crack had propagated and a Mode I crack grown to produce similar starting conditions.

4) Elevated temperature experimentation should be done using a refined laser system which can eliminate the light noise from the heat lamps. The type adhesive used to mount the reflective tabs will have to be changed which may require the use of a spacer (0.002 inch shim stock) under the tabs during the microindentation. Also, the tab material may need to be changed if the stainless steel exhibits oxidation to a degree which degrades the observed fringe patterns.

Appendix A: Laser Mounting Fixture

Figures 32 through 40 show the detailed drawing of the fixture designed to mount the laser interferometer system to the Instron Compression/Tension Tester. This fixture was designed by the author and made at the AFIT Fabrication Shop.

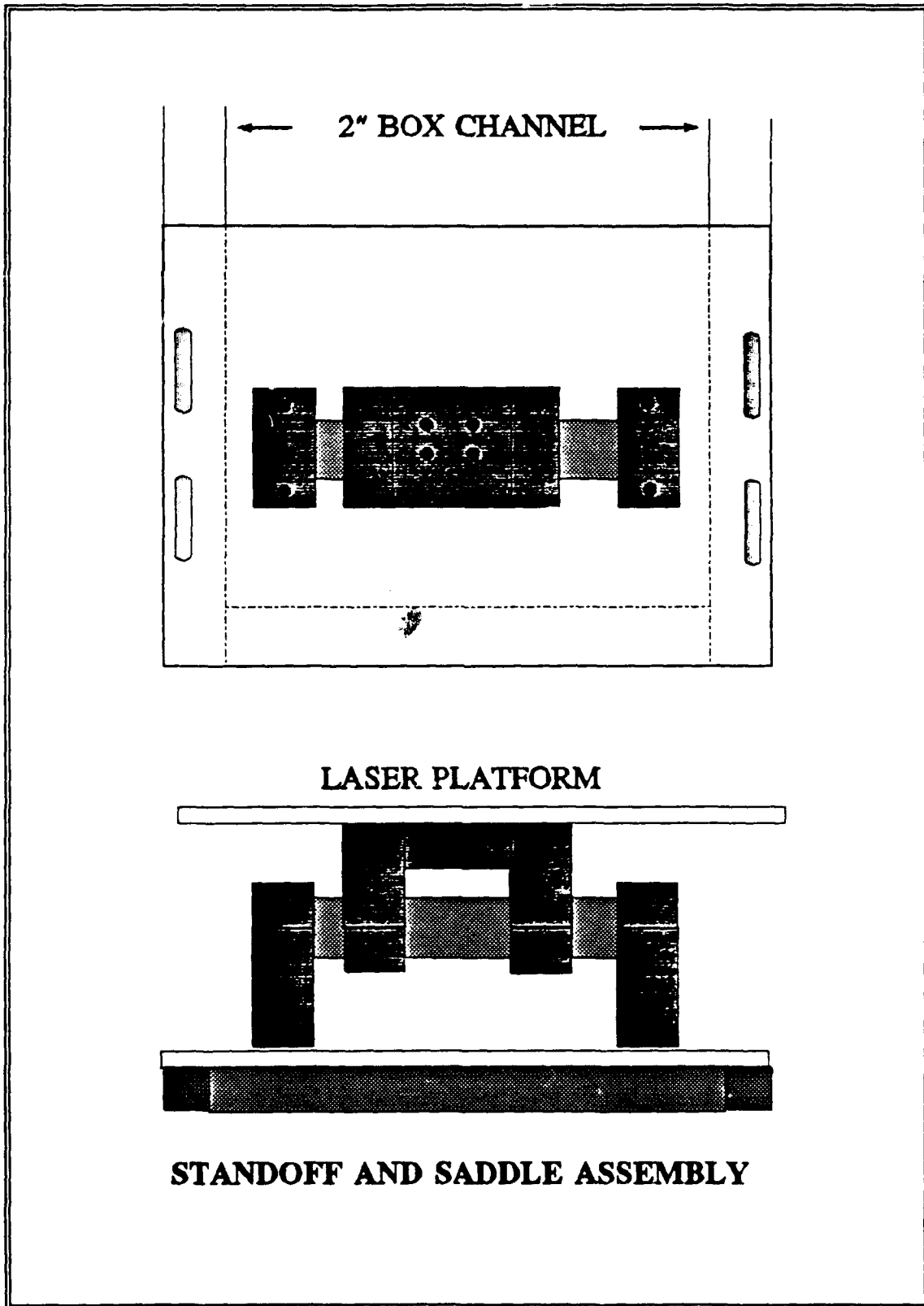


Figure 32 Laser Mounting Fixture

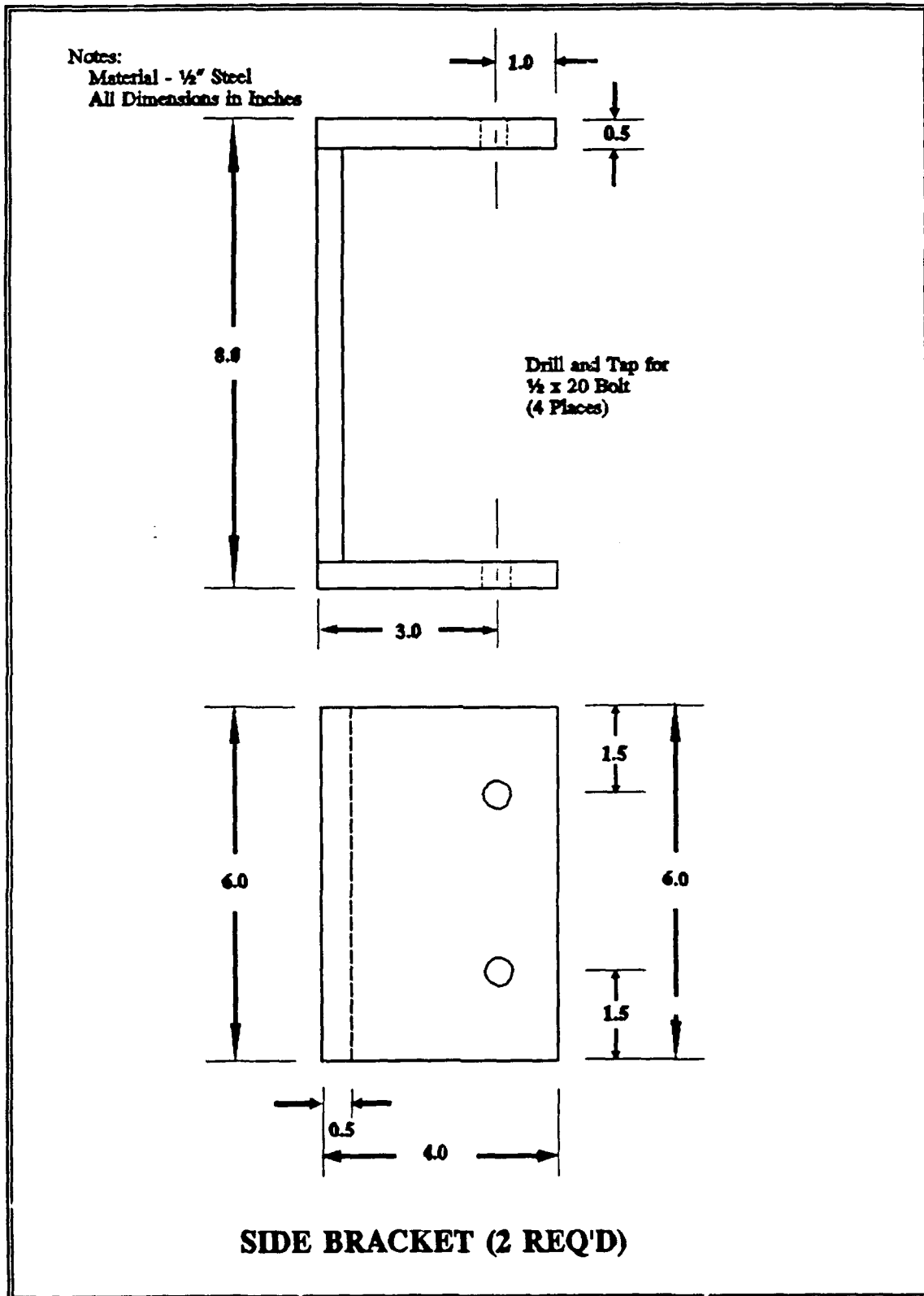
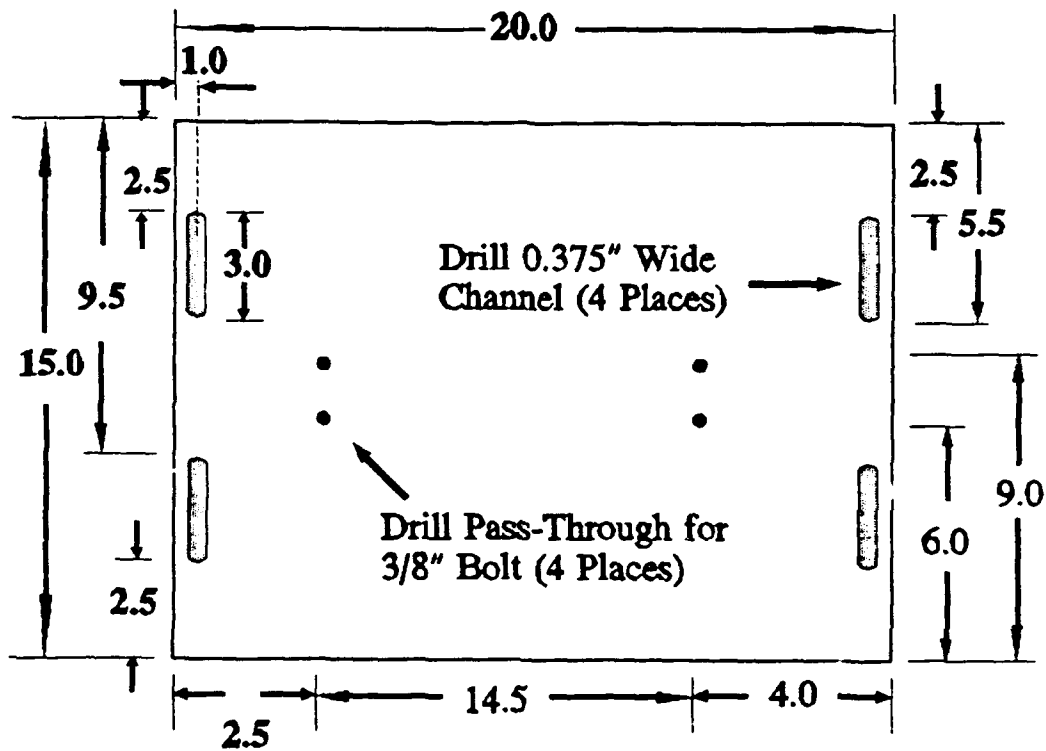


Figure 34 Steel Side Brackets for the Laser Mounting Fixture

Notes:
 Material - 1/2" Aluminum
 All Dimensions in Inches



SUBPLATE

Figure 35 Aluminum Subplate of Laser Mounting Fixture

Notes:
Material - Aluminum
All Dimensions in Inches
Black Anodized

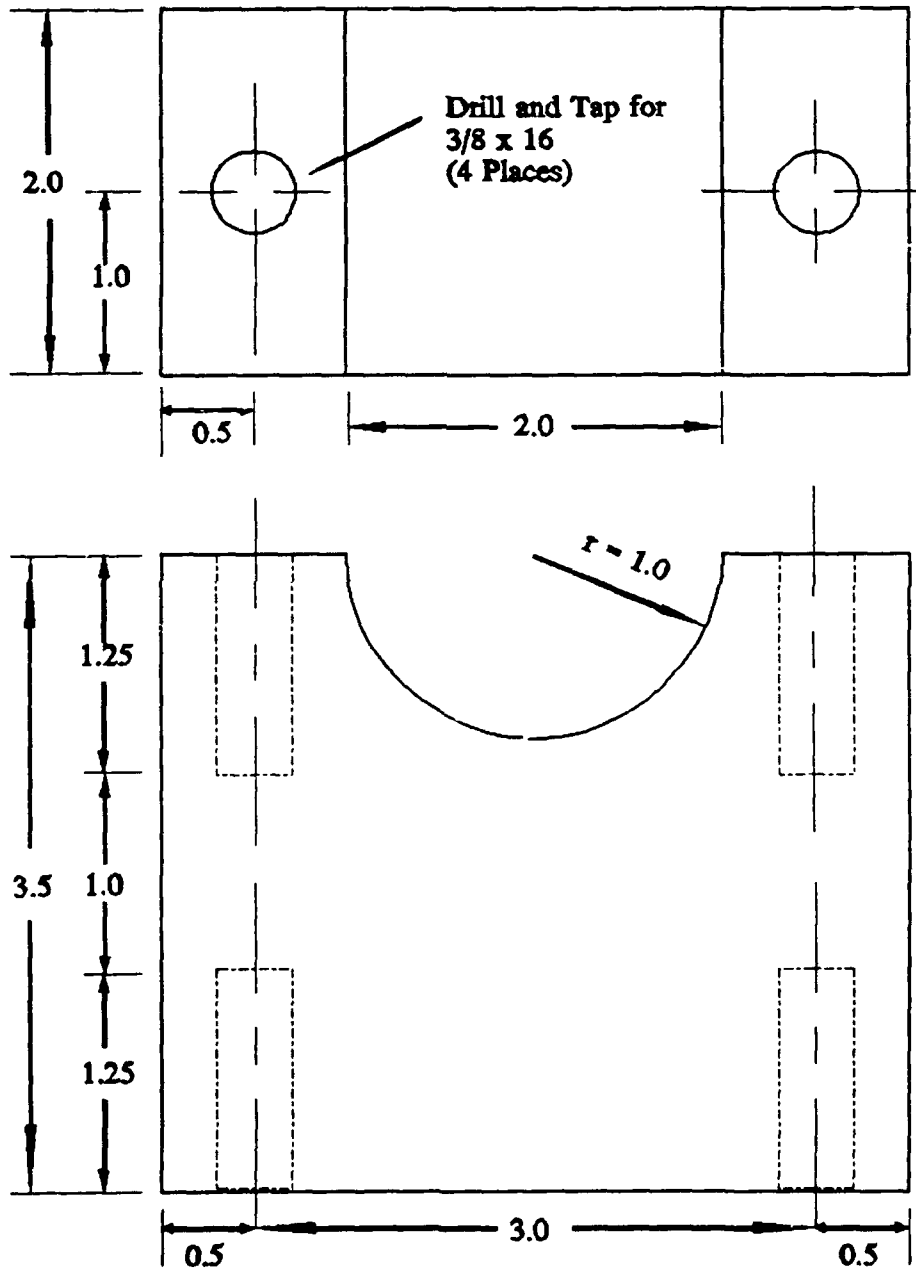
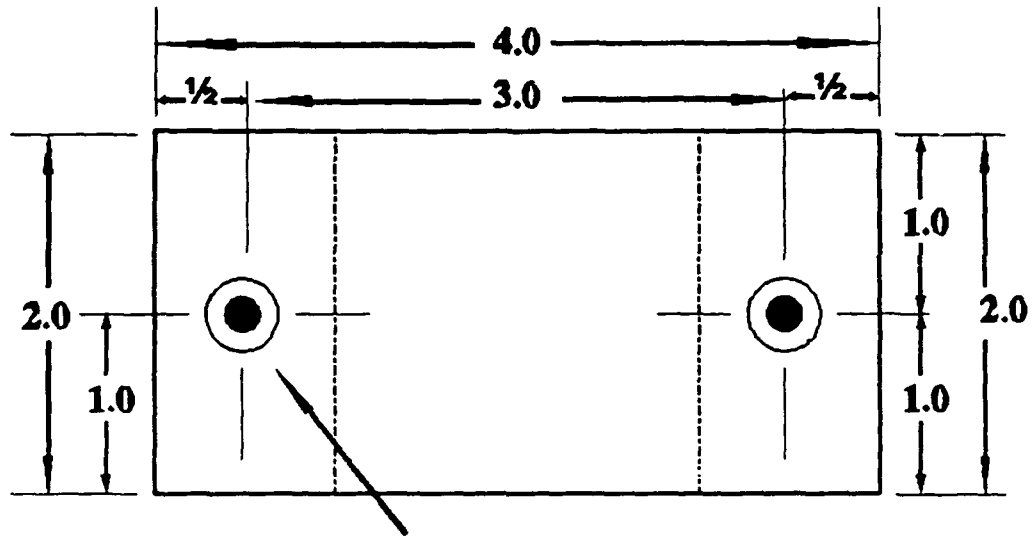
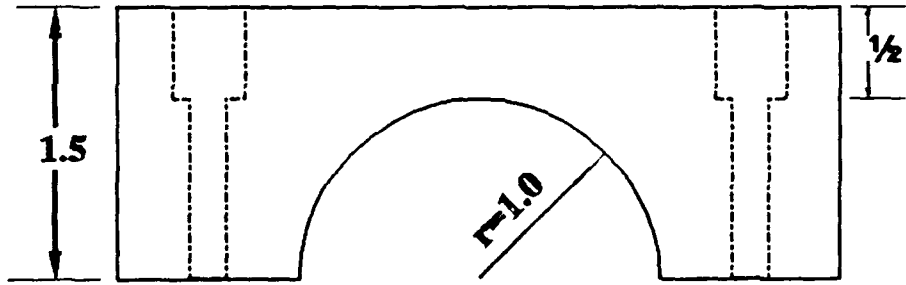


Figure 36 Bottom Standoff for Laser Mounting Fixture

NOTES:
Material - Aluminum
All Dimensions in Inches
Black Anodized



Drill Pass-Through
with Countersink for
3/8" Allen Bolt
(2 Places)



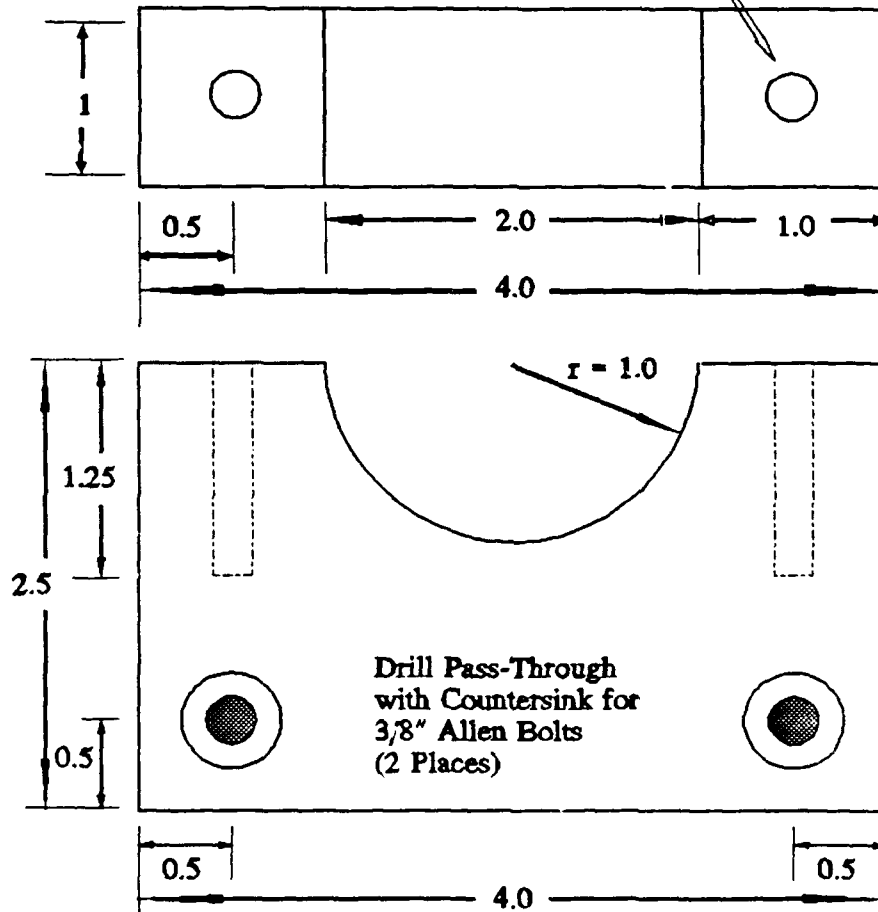
STAND-OFF CAP (2 required)

Figure 37 Bottom Standoff Cap for Laser Mounting Fixture

NOTES:

Material - Aluminum
All Dimensions in Inches
Black Anodized

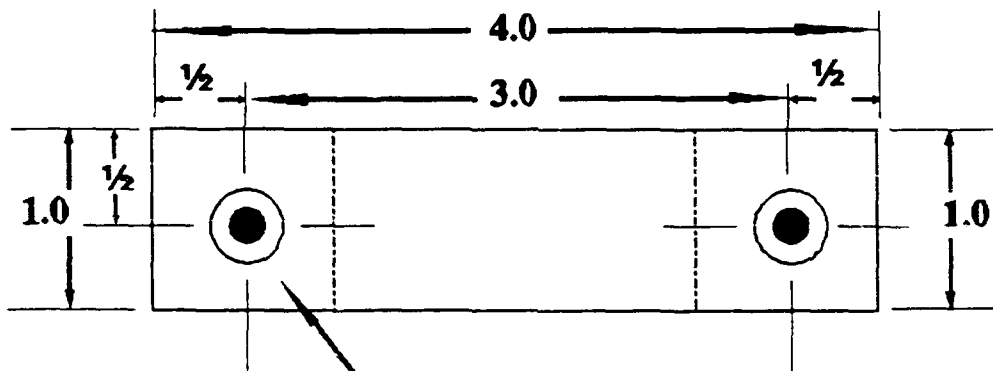
Drill and Tap
for 3/8 x 20
(2 Places)



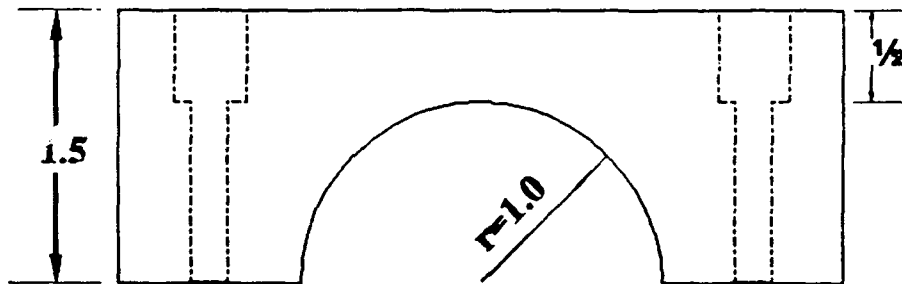
TOP STANDOFF SIDE SUPPORT (2 REQ'D)

Figure 38 Top Standoff Side Support for Laser Mounting
Fixture

NOTES:
Material - Aluminum
All Dimensions in Inches
Black Anodized



Drill Pass-Through
with Countersink for
3/8" Allen Bolt
(2 Places)



STAND-OFF CAP (2 required)

Figure 39 Top Standoff Cap for Laser Mounting Fixture

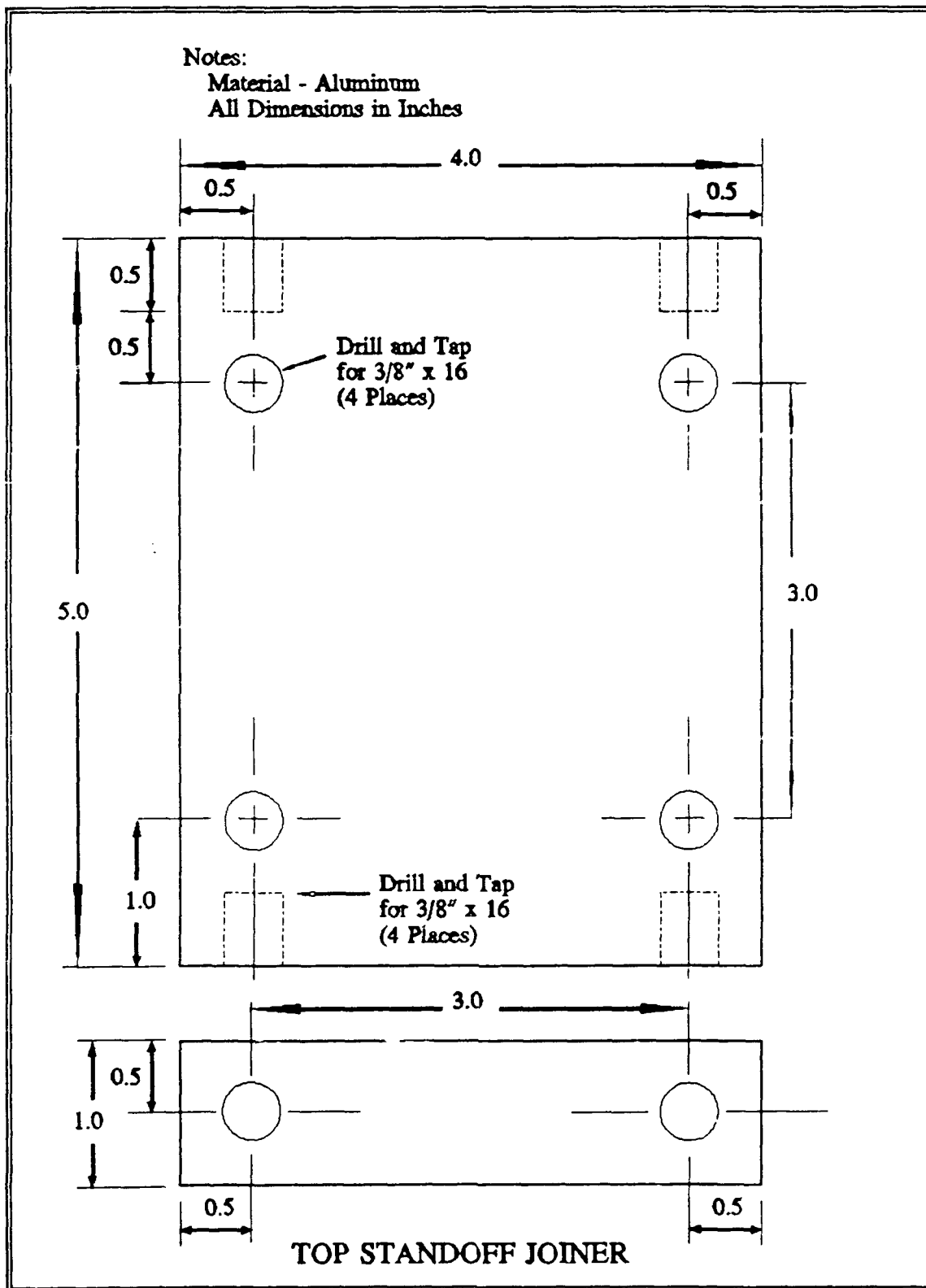


Figure 40 Top Standoff Joiner Piece for Laser Mounting Fixture

Appendix B: Specimen Dimensions

All the specimens used in this project came from two plates manufactured at the WRDC. The plates were designated as Plate 90C07 and Plate 90C08. As a specimen was cut from a plate, it was given a number to distinctly identify it. The numbering system simply added a suffix to the plate number representing the number of the piece cut from the plate. For example, specimen 90C0701 was the designated number for the first specimen cut from plate 90C07 and specimen 90C0809 represented the ninth piece cut from plate 90C08. Figures outlining where the specimens were cut from the plate were kept and are shown in Figures 41 and 42.

Each test specimen was measured at both ends and in the middle using a standard micrometer after all machining had been done to provide an average value for the thickness. Similar measurements were taken to find the average overall height, $2h$, of the specimen. If any two measurements differed by greater than 0.003 inches, the specimen was machined to bring it into tolerance. Although all specimens were about 1.8 inches in length, the lengths were not recorded because the test setup had the effective lengths fixed at 1.5 inches for all tests. Exact dimensions are given for the test specimens in Tables 8 and 9.

Fiber Direction

| SCRAP | |
|-------|-----|
| 719 | 720 |
| 717 | 718 |
| 715 | 716 |
| 713 | 714 |
| 711 | 712 |
| 709 | 710 |
| 707 | 708 |
| 705 | 706 |
| 702 | |
| 701 | |
| 703 | 704 |
| SCRAP | |

Figure 41 Plate 90C07 Specimens

Fiber Direction

| SCRAP | |
|-------|-----|
| 819 | 820 |
| 817 | 818 |
| 815 | 816 |
| 813 | 814 |
| 811 | 812 |
| 809 | 810 |
| 807 | 808 |
| 805 | 806 |
| 802 | |
| 801 | |
| 803 | 804 |
| SCRAP | |

Figure 42 Plate 90C08 Specimens

Table 8 Plate 90C07 Specimen Dimensions

| Specimen Number | Average Thickness (b) (inches) | Average Height (2h) (inches) |
|--------------------|--------------------------------------|------------------------------------|
| 703 | 0.1093 | 0.2867 |
| 704 | 0.1044 | 0.2955 |
| 705 | 0.0994 | 0.2879 |
| 706 | 0.0947 | 0.2962 |
| 707 | 0.0920 | 0.3006 |
| 708 | 0.0974 | 0.2996 |
| 709 | 0.0957 | 0.2982 |
| 710 | 0.0916 | 0.2995 |
| 711 | 0.0958 | 0.3015 |
| 712 | 0.0932 | 0.3007 |
| 713 | 0.0959 | 0.3004 |
| 714 | 0.0930 | 0.3026 |
| 715 | 0.0932 | 0.3024 |
| 716 | 0.0968 | 0.2988 |
| 717 | 0.0928 | 0.3005 |
| 718 | 0.0931 | 0.2995 |
| 719 | 0.0981 | 0.3012 |
| 720 | 0.0930 | 0.3002 |

Table 9 Plate 90C08 Specimen Dimensions

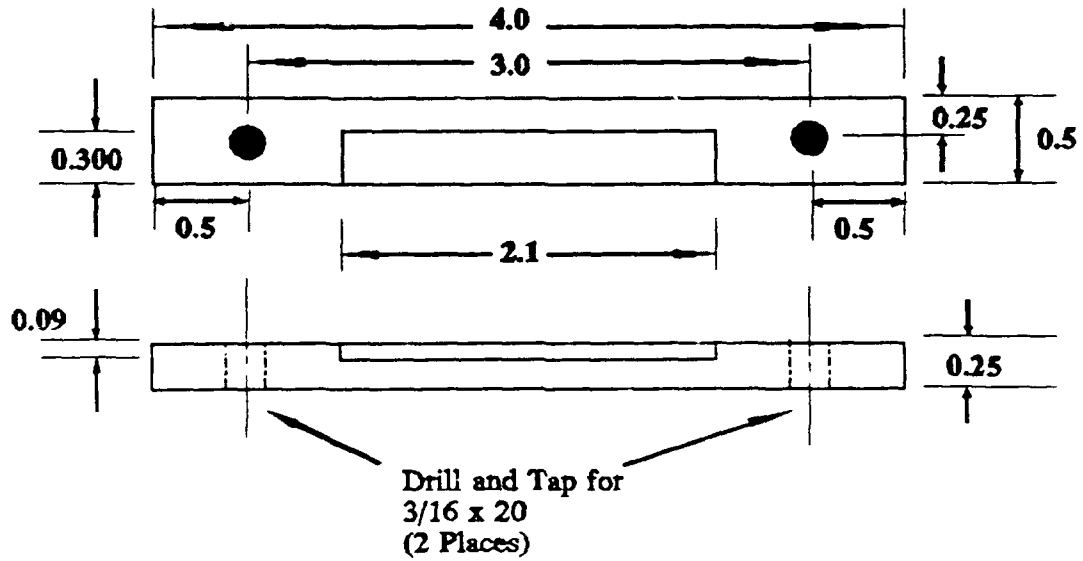
| Specimen Number | Average Thickness (b) (inches) | Average Height (2h) (inches) |
|--------------------|--------------------------------------|------------------------------------|
| 803 | 0.0912 | 0.2932 |
| 804 | 0.0988 | 0.2966 |
| 805 | 0.0974 | 0.2902 |
| 806 | 0.1001 | 0.2987 |
| 807 | 0.0982 | 0.2989 |
| 808 | 0.1010 | 0.2996 |
| 809 | 0.1016 | 0.2824 |
| 810 | 0.0988 | 0.2903 |
| 811 | 0.1002 | 0.3006 |
| 812 | 0.0989 | 0.3017 |
| 813 | 0.0976 | 0.3011 |
| 814 | 0.0997 | 0.3006 |
| 815 | 0.962 | 0.3005 |
| 816 | 0.0978 | 0.2998 |
| 817 | 0.0971 | 0.3015 |
| 818 | 0.0939 | 0.2970 |
| 819 | 0.0910 | 0.2847 |
| 820 | 0.0968 | 0.2994 |

Appendix C: Polishing Fixtures

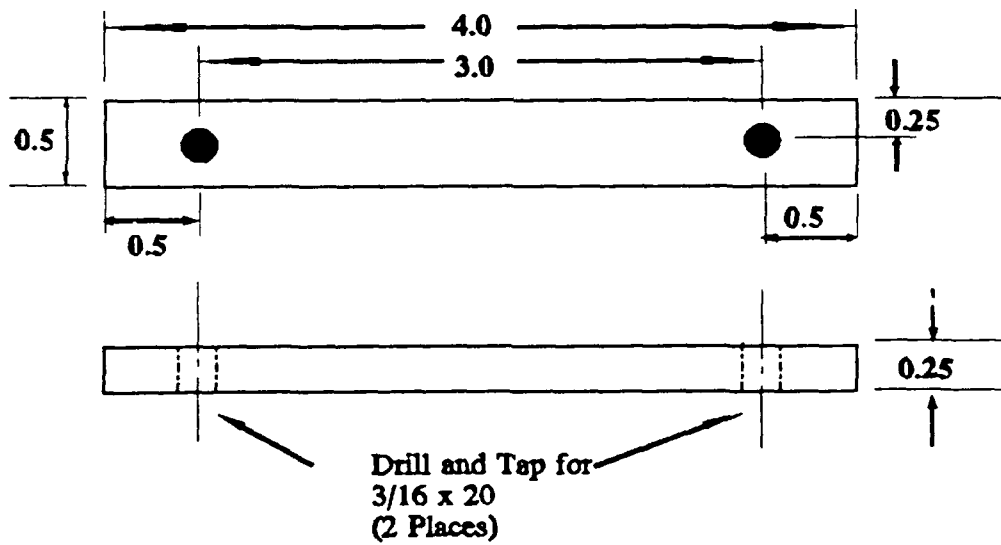
A fixture was designed and fabricated for polishing the ceramic specimens to have a uniform height, $2h$, of approximately 0.30 inches. Figure 43 shows the specifications of this fixture.

Another fixture was needed for the polishing of reflective tabs to ensure the edge normal to the reflective surface was free of large scratches and protrusions caused during the fabrication or handling of the tabs. The specifications of this holder are shown in Figure 44.

Notes:
 Material - Aluminum
 All Dimensions in Inches



Back Plate



Front Plate

Figure 43 Ceramic Specimen Polishing Fixture

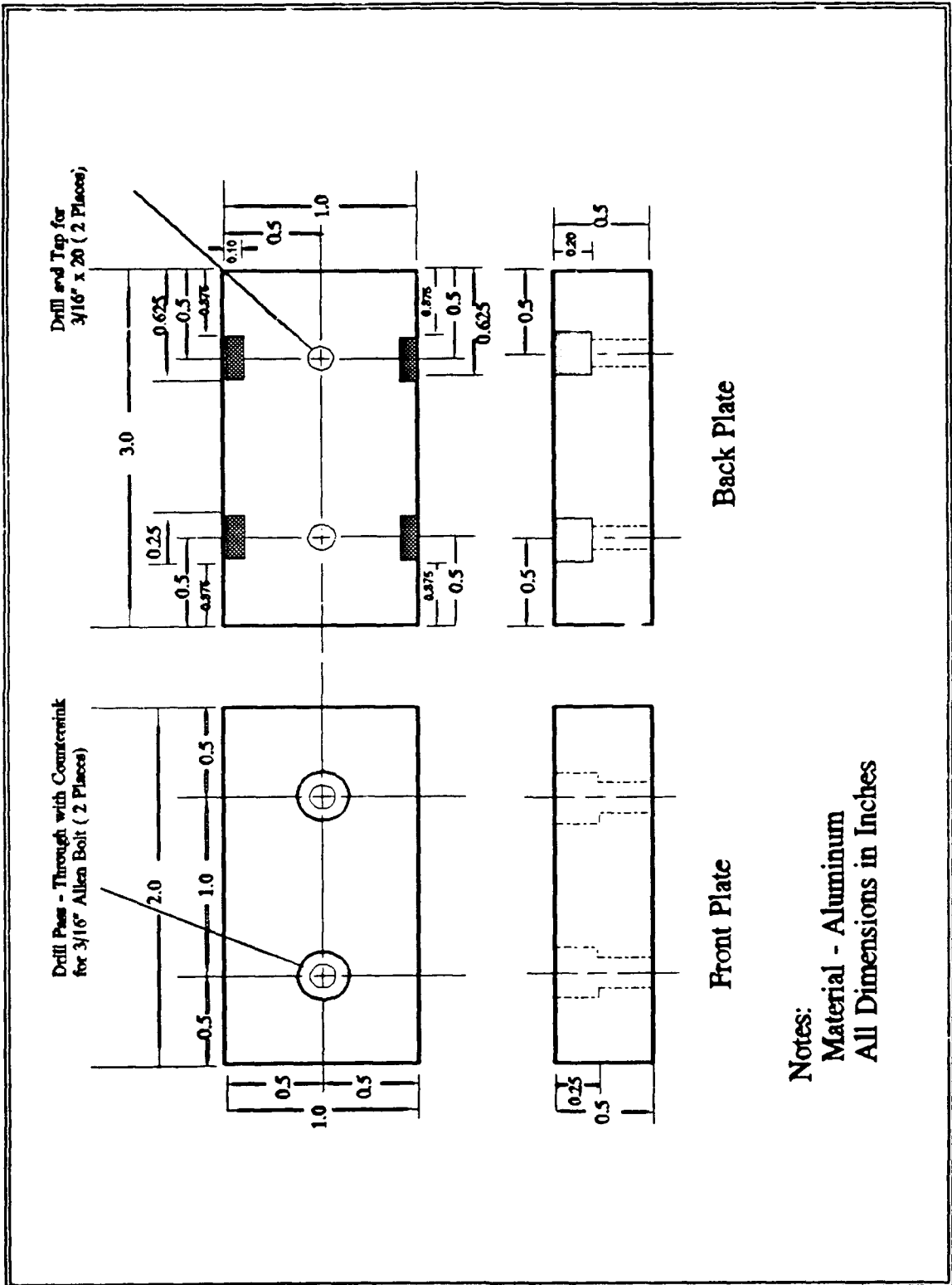
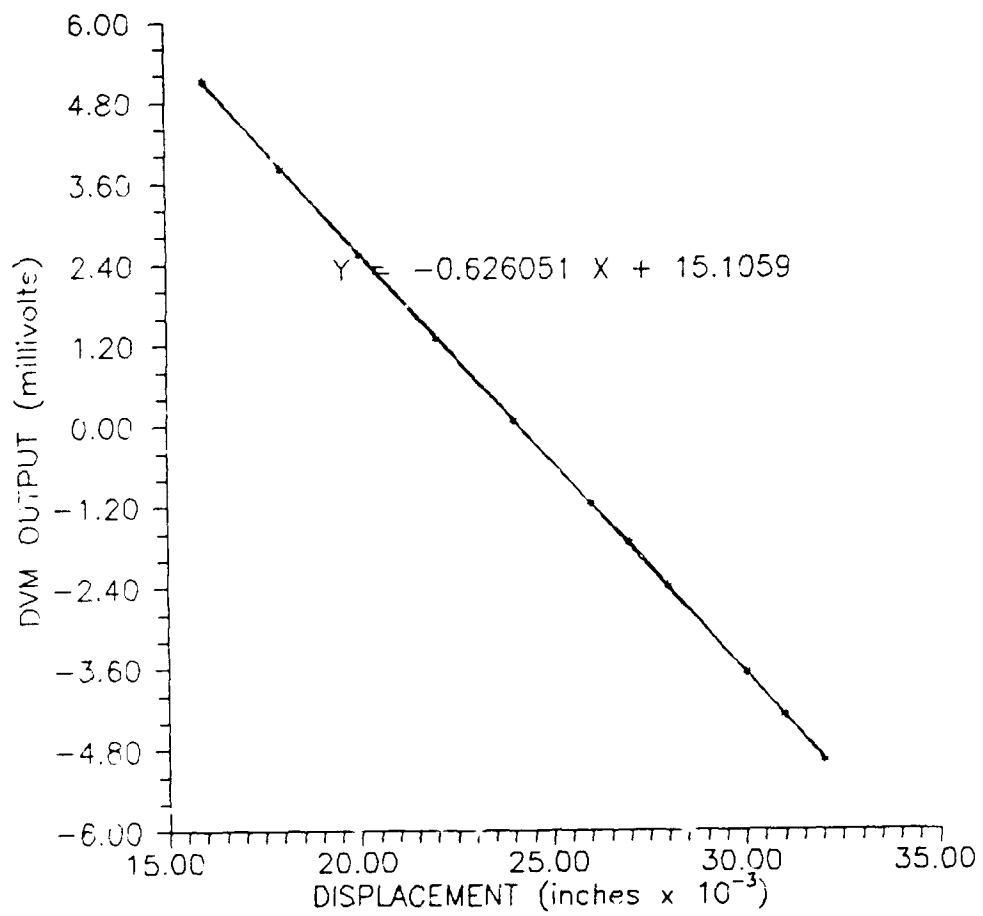


Figure 44 Tab Edge Polishing Fixture

Appendix D: LVDT Calibration

The LVDT used throughout this study was similar to the one used extensively by Hoobler on a similar test frame. The calibration was required to ensure the deflection - voltage relationship before testing was conducted. This calibration was critical because compliance data was produced directly from the displacement measured by this device. The LVDT was positioned in a clamping fixture and the center rod depressed into the housing by a travelling micrometer. Data points were taken at equal intervals and plotted to produce the displacement - voltage relationship shown in Figure 45. The slope of the curve fit was used to convert the output voltage to the midpoint deflection needed for compliance.



LVDT CALIBRATION DATA CURVE

Figure 45 LVDT Calibration Curve

Bibliography

1. ASTM Standard Practice 876, "Standard Test Methods for Flexure Properties of Unreinforced and Reinforced Plastics and Electrical Insulating Materials," 1985 Annual Book of ASTM Standards, Section 8: 397-409, (1985): Philadelphia.
2. Griffith, A.A. "The Theory of Rupture and Flow in Solids," Philosophical Transactions of the Royal Society of London, V A221: 163-197 (1921).
3. Griffith, A.A. "The Theory of Rupture," Proceedings of the First International Conference on Applied Mechanics: 55-63 (1924)
4. Irwin, G.R. "Fracture Dynamics," Fracturing of Metals: 147-166, American Society for Metals Publication (1948).
5. Broek, David. Elementary Engineering Fracture Mechanics (Fourth Revised Edition). The Netherlands: Martinus Nijhoff Pub. (1986).
6. Atkins, A.G. and Mai, Y.W. Elastic and Plastic Fracture. West Sussex: Ellis Horwood Limited, 1985.
7. Lowden, R.A. and others. "Characterization of Fiber-Matrix Interfaces in Ceramic Composites," Whisker- and Fiber-Toughened Ceramics (Proceeding of an International Conference), Oak Ridge, TN. 7-9 June 1988. 253-264. ASM International, 1988.
8. Agarwal, B.D. and Broutman, L.J. Analysis and Performance of Fiber Composites, New York: John Wiley & Sons, Inc., 1980.
9. Giare, G.S. "Fracture Toughness of Unidirectional Fiber Reinforced Composites in Mode II," Engineering Fracture Mechanics, Vol. 20, No. 1: 11-21 (1984).
10. Kageyama, K., Yanagisawa, N., and Kikuchi, M., "Characterization of Mode II Interlaminar Crack Growth Based on Analytical Compliance Method," ICCM Proceedings of the Seventh International Conference on Composite Materials, Vol 2: 535-540 (1989)

11. Briggs, A. and Davidge, R.W. "Fabrication, Properties, and Applications of Borosilicate Glass Reinforced with Continuous Silicon Carbide Fibers," Whisker- and Fiber-Toughened Ceramics (Proceeding of an International Conference), Oak Ridge, TN. 7-9 June 1988. 253-264. ASM International, 1988.
12. Carlsson, L.A., Gillespie, J.W., and Trethewey, B.R. "Mode II Interlaminar Fracture of Graphite/Epoxy and Graphite/PEEK" Journal of Reinforced Plastics and Composites, Vol 5 (July 1986)
13. Mall, S. and Kochnar, N.K. "Finite-Element Analysis of End-Notch Flexure specimens." Journal of Composites Technology & Research, Vol. 8, No. 2, (Summer 1986).
14. Vozzola, Robert P. Fracture Toughness Testing of a Ceramic Matrix Composite. MS Thesis, AFIT/GAE/AA/87D-24, School of Engineering, Air Force Institute of Technology (AU), Wright-Patterson AFB, OH. (Dec. 1987).
15. Mol, John H. Fracture Toughness Testing of a Ceramic Matrix Composite. MS Thesis, AFIT/GAE/AA/87D-24, School of Engineering, Air Force Institute of Technology (AU), Wright-Patterson AFB, OH. (Dec. 1987)
16. Hoobler, Michael A. Effect of Elevated Temperatures and Thermal Cycling on Ceramic Composite Materials. MS Thesis, AFIT/GAE/ENY/89D-14, School of Engineering, Air Force Institute of Technology (AU), Wright-Patterson AFB, OH. (Dec. 1989).
17. Mate Laser Interferometer Technical Reference Manual Version 2.12 University of Dayton research Institute, Dayton OH (1985)
18. Hartman, George. Test Engineer. Personal Interviews. Metals and Ceramics Division, WRDC/MLLN, Wright-Patterson AFB, OH. 22 Mar. - 15 Nov. 1990.
19. Anderson, Jay. Technician. Personal Interviews. Department of Aeronautical Engineering, Air Force Institute of Technology (AU), Wright-Patterson AFB, OH. 15 Dec 89 - 15 Nov. 1990.
20. Zawada, Larry P., Ceramic Engineer. Personal interviews. Metals and Ceramics Division, WRDC/MLLN, Wright-Patterson AFB, OH. 22 Mar. - 15 Nov. 1990.

21. John, Reji, Research Engineer. Personal Interviews. Metals and Ceramics Division, WRDC/MLLN, Wright-Patterson AFB, OH. 19 Mar. - 15 Nov. 1990

22. Carlsson, L.A., Gillespie, J.W., and Pipes, R.B. "Analysis and Design of the End Notched Flexure (ENF) Specimen for Mode II Testing. Journal of Composite Materials

VITA

Captain Joseph W. Truskowski was born on 27 December 1958 in Wilkes-Barre, Pennsylvania. He graduated from high school in Nanticoke, Pennsylvania in 1976 and enlisted in the United States Air Force (USAF). In January 1978, he received an ROTC scholarship and attended Lehigh University in Bethlehem, Pennsylvania. Upon graduation in January 1982 with the degree of Bachelor of Science in Mechanical Engineering, he received his commission into the USAF. He was assigned to Wright-Patterson AFB where he served as a project engineer in the Engineering Directorate of the Aeronautical Systems Division. He was collocated to the Propulsion System Program Office in 1984 where he was responsible for the development and installation of the test stands for the F101-GE-102 engines used on the B-1 aircraft. In April 1986 he was assigned to the Air Force Weapons Laboratory as a lead engineer in the Advanced Weapons Office where he worked on Strategic Defense Initiative programs. He was selected to attend the Air Force Institute of Technology and entered with class GAE-90D in May 1989.

December 1990

Master's Thesis

FRACTURE TOUGHNESS OF UNIDIRECTIONAL FIBER
REINFORCED CERAMIC COMPOSITES IN MODE II
UTILIZING LASER INTERFEROMETRY

Joseph W. Truskowski, Capt, USAF

Air Force Institute of Technology
WPAFB, OH 45433-6583

AFIT/GAE/ENY/90D-31

Dr. Ted Nicholas
WRDC/MLLN
WPAFB, OH 45433

Approved for public release;
distribution unlimited

A laser interferometry technique to measure crack opening displacement was developed and applied to end notched flexure specimens of a Corning Glass Works 1723 glass matrix with silicon-carbide fibers. The laser interferometer displacement gauge monitored the crack opening displacement (COD) at the location of a support while specimens were subjected to Mode II (forward shear) cracking at room temperature via three point bend tests on a standard Instron Compression machine.

Vertical displacement was measured at the center of the test specimen using a linear variable differential transformer. Load verses displacement curves were generated for both the LVDT displacement and the COD. The COD curve showed a marked improvement in determining the onset of crack growth. From the enhanced critical load determination, the materials fracture toughness in Mode II, G_{IIC} , was calculated for varying crack lengths. The calculations provided estimates with a variance of only 10% from the mean thus illustrating the utility of this procedure.

ceramic, composite, fiber, forward shear,
interferometry

110

Unclassified

Unclassified

Unclassified

UL